Identification of the Gene Signature that Constitutes Pathologic Pathways by Comprehensive Gene Expression Analyses

January 2024

Yuumi HARADA

Identification of the Gene Signature that Constitutes Pathologic Pathways by Comprehensive Gene Expression Analyses

A Dissertation Submitted to
the Graduate School of Science and Technology,
University of Tsukuba
in Partial Fulfillment of Requirements
for the Degree of Doctor of Philosophy in Science

Doctoral Program in Biology,
Degree Programs in Life and Earth Sciences

Yuumi HARADA

Table of Contents

Abstract

In recent times, the significant advancement of comprehensive gene expression technologies has led to a shift in the validation of disease-causing genes and the elucidation of disease mechanisms. Disease-causing genes were identified and validated by measuring the expression of specific genes. More recently, comprehensive gene expression analyses at the level of gene signatures, which represent a collection of multiple gene groups, became applicable for identifying and validating disease-causing genes. In these situations, I successfully combined RNA-sequencing (RNA-seq) and single-cell RNA-sequencing (scRNA-seq) with in vitro experiments to clarify gene signatures controlled by specific genes that could cause and associate diseases. The results allowed me to identify key gene signatures that constitute disease-causing pathways and explore their potential as drug targets. In the first study, I elucidated how the TREM2 gene, a risk factor for Alzheimer's disease (AD), contributes to the disease. By comparing the gene signatures of activated TREM2 in iPS-microglia treated with an anti-TREM2 agonist antibody and the gene signatures extracted from microglia of AD patients using single-nucleus RNA-sequencing (snRNA-seq), I revealed that TREM2 activation is reduced in AD microglia compared to healthy individuals and further declines with disease progression. These results suggested that controlling AD progression is achievable through an anti-TREM2 agonist antibody due to the decreased TREM2 activation in AD patients' microglia. In the second study, I comprehensively elucidated

the signaling mechanism of the TNFR2 gene, which is involved in the proliferation of regulatory T cells (Treg). Through RNA-seq and scRNA-seq analyses, the comparison between the gene signatures of TNFR2-activated Treg and that of Treg in cancer demonstrates that TNFR2 signaling induces Treg proliferation by coordinating multiple pathways simultaneously. Indeed, high expression of TNFR2 gene and upregulation of the aforementioned pathways were observed in cancer Treg, possibly aiding in the evasion of immune surveillance on cancer cells. Thus, I propose TNFR2 signaling as a potential target for suppressing cancer Treg. I regard comprehensive gene expression analyses as a powerful research method that allows identifying gene signatures constituting disease-causing pathways and increasing the success rate of drug development. I also discuss a few points to consider when one carries out the research method proposed here.

Abbreviations

Ab	antibody
AD	Alzheimer's disease
Ampli-seq	amplicon sequencing
bcl	binary base call
BLI	biolayer interferometry
CERAD	Consortium to Establish a Registry for Alzheimer's Disease
cIAP	cellular inhibitor of apoptosis protein
cogdx	clinical consensus diagnosis of cognitive status at the time of death
CSF	cerebrospinal fluid
CRC	colorectal cancer
DEG	differentially expressed gene
EDTA	ethylenediaminetetraacetic acid
EZH2	enhancer of zeste homolog 2
FACS	fluorescence-activated cell sorting
FCM	flow cytometry
FDR	false discovery rate
FOXP3	forkhead box P3
GO	gene ontology
GSEA	gene set enrichment analysis
HC	healthy control
HCC	hepatocellular carcinoma
HPC	hematopoietic progenitor cell
iHPC	iPSC-derived hematopoietic progenitor cell
IκBα	the nuclear factor of the κ light polypeptide gene enhancer in the

	B-cells inhibitor α
iMG	iPS-derivedmicroglia-like cell
IL-2	interleukin-2
iPS	induced pluripotent stem cell
iPSC	iPS cells
KO	knockout
mAb	monoclonal antibody
MCI	mild cognitive impairment
MMSE	Mini-Mental State Examination
NES	normalized enrichment scores
NFAT	nuclear factor of activated T cells
NF-κB	nuclear factor κ B
NIK	NF-κB inducing kinase
NSCLC	non-small cell lung cancer
PBMC	human peripheral blood mononuclear cell
PBS	phosphate-buffered saline
PC	principal component
PCA	principal component analysis
PCR	polymerase chain reaction
RNA-seq	RNA-sequencing
ROSMAP	Religious Orders Study and Rush Memory and Aging Project
scRNA-seq	single-cell RNA-seq
signed P value	−log10 P value with the sign of the log-scaled fold change
snRNA-seq	single-nucleus RNA-seq
sTREM2	soluble form of TREM2

TNFR2	tumor necrosis factor receptor 2
TRAF2	TNF receptor-associated factor 2
Tregs	regulatory T cells
TREM2	triggering receptor expressed on myeloid cells 2
UMAP	uniform manifold approximation and projection
UMI	unique molecular identifier

General Introduction

Molecular biology began with the elucidation of the structure of DNA by J. Watson and F. Crick in 1953 and has made remarkable progress since the completion of the Human Genome Project in 2003 [1]. The expression levels of individual genes were measured using real-time PCR technology from the 1990s and early 2000s. Then, semi-comprehensive gene expression using Microarray emerged in the late 2000s [2]. In the 2010s, RNA-seq technology using next-generation sequencers emerged and overcame the weaknesses of Microarray in comprehensiveness and quantitation, and by the 2020s, comprehensive gene expression analysis by RNA-seq became mainstream [3]. In addition, single-cell RNA-seq (scRNA-seq) and single-nucleus RNA-seq (snRNA-seq) technologies, which enable comprehensive gene expression analysis at the single-cell level, have gained popularity [4].

With the advance in sequence technology in recent years, two academic fields have been formed: omics, which systematically collects vast amounts of biological data, and bioinformatics, which handles and analyzes omics data efficiently by applying data processing techniques/technologies established in informatics [5]. Before the current high-speed and cost-efficient sequence technology developed, the gene expression of a single or a set of genes was often measured to examine the molecular background of a biological phenomenon of interest. Nevertheless, the current sequence technology enables us to measure the expression of all the genes in a genome. By comparing two

genome-wide expression data generated under different biological conditions, we capture changes in the expression of a large number of genes and define a gene signature as a set of multiple genes that have a specific function among the set of altered genes, and a gene signatures as a set of gene signature that refer to all altered genes. The detailed examination of the content of the gene signatures identified is anticipated to provide keys to understanding the biological phenomenon of interest [6-8]. For instance, disease research, such as searching for disease-causing genes and elucidating disease mechanisms, has shifted from the investigation focusing on specific disease-causing genes to identifying and interpreting gene signatures derived from comparative analyses of genome-wide gene expression data [9-13]. Furthermore, the pathways comprising the gene signatures related to disease may include the ones that tightly associate with the pathogenesis.

In this study, I conducted genome-wide gene expression analyses to clarify the gene signatures regulated by disease-causing genes. Further, I explored the correlation between a disease and the gene signature identified. First, I focused on TREM2, a prominent etiologic gene in Alzheimer's disease (AD). In Chapter 1, I identified the gene signatures from the microglia cells in which TREM2 was up-regulated and compared it with the gene signatures retrieved from the comparison between the brain samples from healthy controls and AD patients. Second, I investigated TNFR2 involved in the proliferation of

cancer-enhancing cells, Tregs. In Chapter 2, the gene signatures were obtained by analyzing the Treg cells with enhanced TNFR2 expression and were then compared with the gene signatures from the Treg cells isolated from cancer and other tissues in the same patients. The two works successfully provided clues to the candidate genes for future drug targets.

Chapter 1: Reduced TREM2 activation in microglia of patients with Alzheimer's disease

Abstract

Loss-of-function variants of triggering receptor expressed on myeloid cells 2 (TREM2) increase the risk of developing Alzheimer's disease (AD). The mechanism through which TREM2 contributes to the disease (TREM2 activation vs inactivation) is largely unknown. Here, I analyzed changes in a gene set downstream of TREM2 to determine whether TREM2 signaling is modified by AD progression. I generated an anti-human TREM2 agonistic antibody and defined TREM2 activation in terms of the downstream expression changes induced by this antibody in microglia developed from human induced pluripotent stem cells (iPSC). Differentially expressed genes (DEGs) following TREM2 activation were compared with the gene set extracted from microglial single nuclear RNA sequencing data of patients with AD, using gene set enrichment analysis. I isolated an anti-TREM2-specific agonistic antibody, Hyb87, from anti-human TREM2 antibodies generated using binding and agonism assays, which helped me identify 300 upregulated and 251 downregulated DEGs. Pathway enrichment analysis suggested that TREM2 activation may be associated with Th2-related pathways. TREM2 activation was lower in AD microglia than in microglia from healthy subjects or patients with mild cognitive impairment. TREM2 activation also showed a significant negative correlation with disease progression. Pathway enrichment analysis of DEGs controlled by TREM2 activity indicated that TREM2 activation in AD may lead to anti-apoptotic signaling,

immune response, and cytoskeletal changes in the microglia. I showed that TREM2 activation decreases with AD progression, in support of a protective role of TREM2 activation in AD. In addition, the agonistic anti-TREM2 antibody can be used to identify TREM2 activation state in AD microglia.

Introduction

Alzheimer's disease, the most common cause of dementia, is characterized by cognitive decline and memory deficits. According to the World Health Organization, more than 30 million people suffer from AD worldwide. Despite the high prevalence of the disease, disease-modifying agents that can slow or stop neurodegeneration are not known, and the unmet therapeutic requirements for AD are immense. Currently, the available therapies for AD, such as acetylcholinesterase inhibitors and/or a non-competitive N-methyl-D-aspartate (NMDA) receptor antagonist, provide only symptomatic relief and do not restrict or halt disease progression [14].

Human genetic studies have indicated that loss-of-function of the triggering receptor expressed on myeloid cells 2 (TREM2) correlates with an increased risk of AD [15,16]. Furthermore, as the ε4 allele of apolipoprotein E—a TREM2 ligand—is the dominant genetic risk factor for late-onset AD (LOAD) [17], and TYROBP—a TREM2 adaptor protein—has been identified as the key regulator of LOAD using an integrative network-based approach [18], TREM2 has emerged as an important signaling molecule in AD. TREM2 risk variants are associated with neuropathology [16]. The R47H mutation—a rare TREM2 loss-of-function variant—impairs TREM2 ligand recognition [19–22] and

alters its glycosylation pattern, leading to its instability on the cell surface and degradation in the lysosomes [23,24], and attenuation of downstream signaling [19,22]. In AD and mild cognitive impairment (MCI), TREM2 R47H carriers exhibit substantial gray matter loss in the orbitofrontal cortex and the anterior cingulate cortex, with relative sparing of the parietal lobes [25]. Furthermore, R47H carriers with LOAD have increased neuritic plaque and neurofibrillary tangle densities [26]. Even cognitively normal elderly people with R47H are known to have poorer cognitive function than non-carriers2. A brain-imaging volumetric study of individuals with a risk allele near R47H revealed that the mutation carriers lose brain volume at a significantly faster rate than the non-carriers [27]. These findings prompted the scientific community to verify whether TREM2 activation could be a therapeutic option for AD [28], and ameliorate AD disease pathology in several mice models. TREM2 activation of microglia reduces extracellular amyloid plaques and increases the number of microglia surrounding the plaques in multiple mouse AD models, including the APP/PS1 model with lentiviral TREM2 over-expression [29] and the 5xFAD model with microglial TREM2 over-expression [30]. Furthermore, TREM2 over-expression attenuates neuronal loss and promotes behavioral improvement in 5xFAD and APP/PS1 models [29,30]. Similar findings have been reported in studies based on mutant tau mice models. TREM2 over-expression reduces tau phosphorylation and inflammatory cytokine production, and improves neuronal survival and spatial memory function in the tau P301S mouse model [31]. Recent studies have reported the protective functions of TREM2 in AD preclinical models using anti-TREM2 antibodies (Abs) [32,33]. These studies have highlighted the importance of TREM2 in AD onset and progression and

indicated that TREM2 activation may provide a therapeutic option for patients with AD. TREM2 expression in AD brain tissues has been examined in several reports. However, findings are divided on whether TREM2 expression is altered in the AD tissues. One study found that TREM2 mRNA expression increased in the hippocampus of patients with AD [34]. However, other studies have shown downregulation or no significant changes in TREM2 expression in the hippocampus samples from AD patients at protein and/or mRNA levels [35–37]. TREM2 expression was higher in the temporal cortex of patients with AD than in the corresponding tissues of non-AD donors at mRNA and/or protein levels [38,39]. In the frontal cortex, TREM2 expression was significantly elevated at the protein level in AD patients but not at the mRNA level. A recent report indicated that TREM2 is upregulated in the microglia of the dorsolateral prefrontal cortexes of patients with AD [40]. Considering the supporting genetic evidence that TREM2 loss-of-function mutation increases the risk of AD, it is highly important to decipher if TREM2 upregulation is associated with enhanced TREM2 signaling, thereby retarding the disease progression. Another notable feature of TREM2 is the presence of a soluble form (sTREM2). The membrane protein TREM2 is cleaved by the proteases ADAM10 and ADAM17 to release sTREM2 in response to various stimuli [41,42]. sTREM2 has been used as a microglial activation marker, and its levels were found to be high in the cerebrospinal fluid (CSF) of patients with AD; moreover, it correlates positively with total and phosphorylated tau levels [43–45]. Although reports have shown that sTREM2 is produced following TREM2 over-expression and that sTREM2 levels depend on TYROBP [41,46], whether sTREM2 levels reflect TREM2 activation in the disease

remains unclear. sTREM2 levels in AD may indicate TREM2 upregulation, change in activity, or expression of the responsible proteases. However, considering that the rarely occurring R47H loss-of-function mutant produces sTREM2 more efficiently than the common variant of TREM2 [47], sTREM2 levels may not necessarily reflect the activation status of TREM2. Therefore, further studies are necessary to understand TREM2 activation status in the AD brain and elucidate the mechanism through which changes in TREM2 signaling contribute to AD.

In this study, I used a gene set acting downstream of TREM2 and aimed to investigate whether the TREM2 signal is modulated with AD progression. I further analyzed the potential of using TREM2 activation as a therapeutic option for AD.

Materials and Methods

Generation of anti-TREM2 monoclonal antibody (mAb)

All animal-related research protocols used in this study were approved by the Takeda Institutional Animal Care and Use Committee. Five CD2F1 mice (6 weeks old, female; The Jackson Laboratory, Bar Harbor, ME, USA) and five Trianni IgH kappa mice (6 weeks old, female; Trianni, Inc., San Francisco, CA, USA) were housed in the animal facilities of Takeda California and maintained under regular specific pathogen-free conditions. Following 1 week of acclimatization, the mice were immunized subcutaneously into the hock with 5 μg human TREM2-Fc (R&D Systems, Minneapolis, MN, USA) emulsified with TiterMax Gold adjuvant (TiterMax, Norcross, GA, USA) as part of the first immunization. For the second through the ninth immunizations, the mice were injected subcutaneously into the hock twice weekly with 3 μg human TREM2-Fc

using ODN-1826 (InvivoGen, San Diego, CA, USA) and alum adjuvant. On the day of the third immunization, the mice were intraperitoneally injected with 100 μg anti-mCD40 Ab (BioXcell, West Lebanon, NH, USA). Three days after the final boost, the popliteal and inguinal lymph nodes were isolated from each mouse, and the lymphocytes were fused with P3U1 mouse myeloma cells (ATCC, Manassas, VA, USA) in a 2:1 ratio and subjected to electrofusion using a Legacy ECM 2001 electrocell fusion and electroporation system (BTX, Holliston, MA, USA) to generate hybridomas. The fused cells were seeded in a semi-solid selective culture media containing hypoxanthine-aminopterin-thymidine, and the grown hybridoma clones were manually transferred to 96-well plates. Hybridomas secreting anti-TREM2 mAbs were screened using enzyme-linked immunosorbent assay (ELISA). First, the human TREM2-Fc protein was coated on a 96-well ELISA plate and then incubated with hybridoma culture supernatant and goat anti-mouse IgG (H+L) conjugated with horseradish peroxidase (HRP) (Jackson ImmunoResearch Laboratories, Inc., West Grove, PA, USA). The plates were washed with phosphate-buffered saline (PBS) containing 0.05% Tween-20 after each incubation step. The TMB HRP substrate (Bio-Rad, Hercules, CA, USA) was added to each well and incubated for 5 min. The reaction was stopped using 1 M H_2SO_4 and the absorbance at 450 nm was measured using an EnVision plate reader (PerkinElmer, Waltham, MA, USA). The Hyb87 hybridomas were expanded in Ab expression medium, which was a mixture of Iscove's modified Eagle medium and Ham's F-12 nutrient medium (FujiFilm Wako Pure Chemical, Osaka, Japan) supplemented with MEM non-essential amino acid solution, sodium pyruvate, L-alanyl-L-glutamine, 100 U/mL of penicillin and streptomycin (FujiFilm Wako Pure Chemical), and 10% ultra-low IgG fetal bovine serum (Thermo Fisher Scientific, Waltham, MA, USA). Hyb87 was purified from the culture supernatant using Ab-Capcher ExTra (ProteNova, Higashikagawa, Japan).

Determination of Ab binding to TREM2 on cells

Expi293 cells

We tested the specificity of Hyb87 binding to TREM2 using flow cytometry (FCM). Briefly, a vector expressing human TREM2 and the NeoFection reagent (Astec Co. Ltd., Kasuya, Japan) were mixed at 1:1 ratio in OptiMEM I (Thermo Fisher Scientific). After 15 min, the mixture was added to Expi293 cells (Thermo Fisher Scientific) at a density of 1×10^6 cells/mL. One day after transfection, the cells were reacted with Hyb87 or control IgG (R&D Systems), followed by incubation with anti-mouse IgG-Alexa Fluor 488 (Thermo Fisher Scientific). Cell surface fluorescence was detected using BD Accuri C6 Plus (BD Biosciences, San Jose, CA, USA) and analyzed using the FlowJo software (Becton Dickinson, Ashland, OR, USA).

THP-1 cells

Similarly, I tested the specificity of Hyb87 using the human monocytic THP-1 cells (ATCC) and *TREM2* knockout (KO) THP-1 cells following the Expi293 procedures. *TREM2* KO THP-1 cells were established as mentioned below. The Fc receptor blocking reagent (BD Biosciences) was used during Ab incubation with THP-1 cells or *TREM2* KO THP-1 cells. In brief, duplex RNA was prepared by annealing equimolar amounts of crRNA (5'-ACCCAGGGTATCGTCTGTGATGG-3'or 5'-CACAGTGTTCCAGGGCGTGGCGG-3') and tracrRNA at 95□C for 5 min and cooling to room temperature. To form the ribonucleoprotein (RNP) complex, Cas9 was added to

the duplex RNA and incubated for 15 min at room temperature. The THP-1 cells were simultaneously transfected with both complexes using the Neon transfection system (Thermo Fisher Scientific) and seeded at a density of 2×10^5 cells/well in THP-1 culture medium supplemented with 1 μM RS-1 and 0.1 μM SCR7 (Xcess Biosciences, Chicago, IL, USA) in a 24-well plate. Seven days following the transfection, the cells were sub-cloned using limiting dilution method at 0.3 or 1 cell/well. Genomic DNA was extracted from the outgrown cells using the SimplePrep reagent for DNA (Takara Bio, Kusatsu, Japan) and sequenced using the BigDye Terminator v3.1 cycle sequencing kit (Thermo Fisher Scientific). I selected clone17 with a frameshift mutation in the *TREM2* exon as *TREM2* KO THP-1 and used it for FCM.

Determination of Ab affinity

The kinetic analysis of the affinity of Ab to TREM2 was performed using bio-layer interferometry with an Octet Red96e system (Molecular Devices, Sunnyvale, CA, USA). First, Hyb87 was captured on anti-mouse Fc Octet biosensors (Molecular Devices) for 120 s. The biosensors were reacted with serially diluted recombinant human TREM2-His (R&D Systems) for 120 s, followed by dissociation in PBS for 180 s. The kinetics of the Ab was analyzed with a sensorgram aligned at the beginning of the association step after background subtraction. The sensorgram was analyzed using a 1:1 Langmuir fitting model.

Nuclear factor of activated T cells (NFAT) assay

TREM2 activation was detected as described below. Hyb87 or control IgG (10 μg/mL) was immobilized on a 96-well plate (Corning, New York, NY, USA, #3912) overnight at 4°C. One million THP-1 or *TREM2* KO THP-1 cells were transfected with 5 μg of the luciferase reporter plasmid driven by the NFAT response element using the Neon transfection system (Thermo Fisher Scientific) according to the manufacturer's instructions. In total, 30,000 transfected cells were seeded on the Ab-immobilized plate. After 3 h, luciferase activity was detected with NanoGlo reagent (Promega, Madison, WI, USA) using an EnVision plate reader (PerkinElmer).

Treatment of induced pluripotent stem cell (iPS-)-derived microglia-like cells (iMGs) with Hyb87

Culture of human iPSCs

All human cell protocols used in this study were approved by the Takeda Institutional Ethical Committee and followed the guidelines of the Declaration of Helsinki. Human iPSCs (Clone XCL-1, XCell Science, Novato, CA, USA) were cultured on laminin-coated plates in StemFit (Ajinomoto Healthy Supply Co., Inc, Tokyo, Japan) containing penicillin and streptomycin. The cells were passaged every 6 to 7 days using 0.5 mM EDTA, seeded at a density of 2.0×10^4 cells/well on a 6-well plate and maintained in the presence of 10 μM Y-27632 (FujiFilm Wako Pure Chemical). The culture medium was replaced with StemFit containing penicillin and streptomycin in the absence of Y-27632, 24 h after passaging.

Differentiation of iPSCs to hematopoietic progenitor cells (HPCs)

iPSC-derived hematopoietic progenitors (iHPCs) were generated using defined conditions with several modifications to previously published protocols [48,49]. Briefly, 0.5-1.0 × 10^5 cells were plated per well in a tissue culture-treated 6-well plate (day 0). The cells were cultured in 2 mL StemFit containing Y-27632 for 24 h under normoxic conditions.

Day 1: The medium was changed to basal medium [50] supplemented with 50 ng/mL FGF2, 50 ng/mL BMP4, 12.5 ng/mL activin-A, 10 μM Y-27632, and 2 mM LiCl. The cells were then placed under hypoxic cell culture conditions of 5% O_2 and 5% CO_2 for 2 days.

Day 3: The cells were further maintained in basal medium supplemented with 50 ng/mL each of FGF2 and VEGF under hypoxic conditions.

Day 5: The medium was changed to basal medium containing 50 ng/mL FGF2, 50 ng/mL VEGF, 50 ng/mL TPO, 10 ng/mL SCF, 50 ng/mL IL-6, and 10 ng/mL IL-3. The cells were placed under normoxic conditions.

Day 7 and day 9: The medium was changed to the one used on day 5.

Differentiation of iHPCs to iMGs

iMGs were differentiated from iPSCs via embryoid bodies and HPCs using defined conditions with several modifications to a previously published protocol [50].

Day 11: iHPCs were washed using iMG basal differentiation medium [50]. After

centrifugation, the iHPCs were gently suspended in iMG complete differentiation medium containing 25 ng/mL M-CSF, 100 ng/mL IL-34, and 50 ng/mL TGF-β and seeded at a density of 2×10^5 cells per well on 6-well plates. One milliliter iMG complete differentiation medium was added every 2 days.

Day 23 and day 37: The cells were collected as iMGs and seeded in a 1:1 mixture of conditioned medium and iMG complete differentiation medium [50]. The cells were supplemented with 1 mL iMG complete differentiation medium every two days.

The reagents used in this experiment were purchased from Thermo Fisher Scientific (BMP4, activin-A, VEGF, TPO, IL-6, SCF, and IL-3) or PeproTech (FGF2, M-CSF, and TGF-β).

Treatment of iMGs with Hyb87

iMGs were collected on day 39 and seeded on a 24-well non-tissue culture-treated plate (Corning) coated with 10 μg/mL Hyb87 or control mouse IgG. After 6 h, the cells were harvested for RNA isolation.

AmpliSeq analysis

AmpliSeq libraries were constructed for iMGs and sequenced in biological triplicates using the Ion Proton platform (Thermo Fisher Scientific) according to the manufacturer's instructions. Briefly, 10 ng of total RNA was reverse transcribed using the SuperScript VILO cDNA synthesis kit (Thermo Fisher Scientific), followed by library generation using the Ion AmpliSeq transcriptome human gene expression kit. The libraries were

diluted to 45 pM and pooled equally with 9□10 individual samples per pool. The pooled libraries were multiplexed and clonally amplified using the Ion Chef System, and subsequently, sequenced on Ion PI chips using an Ion Proton sequencing system. Data were first analyzed using the Torrent Suite and the ampliSeqRNA analysis plugin was used to generate count data. Principal component analysis (PCA) was performed using the "prcomp" function of stats package in R [51]. Tukey's honest significant difference test was conducted to compare the first principal component (PC1) in each group using "Tukey HSD" of stats package in R. Visualization of the scatter plot and boxplot was performed using the ggplot2 package in R. All the AmpliSeq data were deposited in the Gene Expression Omnibus (GEO) repository at http://www.ncbi.nlm.nih.gov/geo (accession number: GSE159333).

Identification of differentially expressed genes (DEGs) induced by TREM2 activation

The DEGs representing TREM2 activation (TREM2 DEGs) were identified based on the gene-wise negative binomial generalized linear model with the quasi-likelihood method using the edgeR package in R [52,53]. The criteria for the significance of DEGs were set at false discovery rate-adjusted (FDR-adjusted) P value < 0.05 and absolute fold change > 1.5. Volcano plots of the DEG analysis were drawn using EnhancedVolcano package in R. TREM2 DEGs were defined as genes common between DEGs from Hyb87 vs. PBS and Hyb87 vs. control IgG, and those with the same direction of expression change in the DEGs.

Pathway enrichment analysis

Pathway enrichment analyses of TREM2 DEGs were conducted using the Cortellis MetaCore software (Clarivate, Philadelphia, PA, USA) using "Enrichment Analysis" workflow (default setting).

GSEA

The Religious Order Study and Rush Memory and Aging Project (ROSMAP) data (syn18485175), the single-cell expression profile of human dorsolateral prefrontal cortex derived from 75,060 cells of 48 individuals [54], was downloaded from AD Knowledge Portal (https://adknowledgeportal.synapse.org/Explore/Studies?Study=syn18485175). The data included quality-filtered single-nucleus RNA-sequenced read counts of 17,926 genes of the human reference genome 38 (GRCh38) and the clustering results of the reads to each cell type. The reads from microglial cells were extracted and genes with less than three aligned reads were removed, resulting in a total of 13,039 genes. PCA was performed on log-normalized read counts, and three individuals whose PC1 or second principal component (PC2) were outside of more than three standard deviations from that of the other samples were removed. Healthy controls (HC) and patients with AD in the original report [41] were re-classified into HC, MCI, and AD using Mini-Mental State Examination (MMSE) (HC, $\geq$ 29; MCI, 24 to 28; AD, $\leq$ 23) [55] or clinical consensus diagnosis of cognitive status (cogdx: HC, 1; MCI, 2 or 3; AD, 4 or 5) [54].

I compared the expression of genes across HC, MCI, and AD using DESeq2 [56] in Seurat [57]. Finally, I multiplied the $-\log_{10}$ P value with the sign of the log-scale fold change

(signed P value) for GSEA. I also quantile-normalized the read counts on each gene and conducted linear regression on cognitive, MMSE, Consortium to Establish a Registry for Alzheimer's Disease (CERAD), and Braak scores with covariates of sex, years of education, and age. The CERAD score decreased with the progress of the neuritic plaques, whereas Braak or MMSE scores increased with the deterioration of neurofibrillary tangles or cognitive decline, respectively. To interpret the CERAD GSEA result in the same correlation direction as the MMSE and Braak GSEA results, I calculated the correlations between each gene and CERAD score and converted them to the signed P values by reversing the positive and negative direction.

Another single-nucleus RNA-seq (snRNA-seq) dataset generated using ROSMAP data (syn21125841) [50] was analyzed for a replication study. Data included the number of aligned reads per gene in each cell, which were quantified using Cell Ranger Single-Cell Software Suite (10x Genomics, Pleasanton, CA, USA). Data of 19 individuals which did not overlap with that of ROSMAP syn18485175 data [54] and had the common variant, TREM2, were downloaded from AD Knowledge Portal (https://adknowledgeportal.synapse.org/Explore/Studies?Study=syn21670836). The 19 individual datasets comprised ten patients with AD and nine HCs. The clustering of the cells was conducted using the R package, Seurat [57]. The cells with a high ratio of mitochondrial reads (> 5%), abnormally high or low number of unique molecular identifiers (< 400 or > 40,000, respectively), or an abnormally high or low number of detected genes (> 9,000 or < 200, respectively) were filtered out—resulting in a remainder of 42,087 cells. Next, the read counts for each gene were divided by the total counts in

the cell and log-normalized following multiplication of 10,000. Then, 20,000 features (genes) that were highly variable among the cells were selected using FindVariableFeature in Seurat package [57].

The cells were clustered using shared nearest neighbor modularity optimization using 1 to 20 PCs after the dimension reduction analysis. Then, the clusters were identified as one of the following cell types via the mean expression level of the marker genes selected by the Allen Institute for Brain Science [58]: *GAD1* (interneuron), *SLC17A7* (excitatory neuron), *TYROBP* (microglia), *AQP4* (astrocyte), *PDGFRA* (oligodendrocyte precursor), *OPALIN* (oligodendrocyte), and *NOSTRIN* (endothelial cell). As a result, 2,200 cells were identified as microglia. The reads in the microglia were summed per individual, and genes with less than three reads in total were removed. The gene expression was then compared between AD and HC groups using DESeq2 [56]. The results of each gene were used for GSEA.

GSEA was conducted between TREM2 DEGs and genes extracted from the above-mentioned data sets using the GSEA_R package in R. The criterion for the significance of GSEA was set at FDR-adjusted q-value < 0.05. The datasets generated and analyzed during the current study are available in the GEO repository, https://www.ncbi.nlm.nih.gov/geo/query/acc.cgi?acc=GSE159333

Results

Generation and characterization of agonistic anti-TREM2 mAb, Hyb87

I attempted to obtain an anti-TREM2 agonistic Ab. I used hybridoma techniques

following the immunization of mice with TREM2-Fc protein. The culture supernatant of the hybridomas was screened using ELISA to identify the clone secreting suitable mAbs, and my results showed that the anti-TREM2 Ab clone, Hyb87, bound to human TREM2. I further characterized Hyb87 using multiple assays. First, I tested the binding of Hyb87 to TREM2, both exogenously and endogenously expressed in cells. I prepared Expi293 cells transfected with the human TREM2 expression plasmid. Although the fluorescence intensity of the control IgG did not increase in parental or human TREM2-over-expressing Expi293 cells in FCM, that of Hyb87 did when human TREM2 was expressed (Fig. 1A). I further confirmed the binding of Hyb87 to endogenous TREM2. I used human monocytic THP-1 cells for TREM2 expression [59]. As shown in Fig. 1B, fluorescence intensity was detected in THP-1 cells after adding Hyb87. To further verify the specific binding of Hyb87, I established *TREM2* KO THP-1 cells and observed that Hyb87 binding was lost in these cells (Fig. 1B). These results indicated that Hyb87 bound specifically to human TREM2 on the cell surface. The affinity of Hyb87 to TREM2 was then determined using bio-layer interferometry (BLI). The Ab was immobilized onto the sensor chip as a ligand, and TREM2-His was applied as an analyte. According to an analysis using a Langmuir fitting model, the K_D value of Hyb87 to human TREM2 was 1.07×10^{-9} M. The K_a of the Ab was determined to be 2.32×10^{5} (1/M/s) and the K_d was 2.48×10^{-4} (1/s) (Fig. 1C).

I investigated whether Hyb87 activated TREM2. A previous study reported that TREM2 activation increases intracellular Ca^{2+} concentration and can be detected using the NFAT reporter [60,61]. Hence, I used the NFAT reporter system in this study. THP-1 cells were

transiently transfected with the reporter plasmid and then allowed to react with Hyb87. Compared to the PBS-treated group, Hyb87 increased NFAT activity by 10.4-fold, whereas the increase by control IgG was 1.8-fold (Fig. 1D). This indicated that Hyb87 activated TREM2. Furthermore, I observed a slight increase in NFAT reporter activity by control IgG. I believe that the increment in NFAT activity by the control IgG was a consequence of the binding of the control IgG to the Fc receptor [62]. Meanwhile, NFAT reporter activity by Hyb87 was not significantly different than that by control IgG in *TREM2* KO THP-1 cells (Fig. 1D), suggesting that NFAT activity by Hyb87 in the THP-1 cells was mediated through TREM2.

Isolation of TREM2 DEGs from iMG

I investigated how TREM2 activation changed in the microglia of patients with AD. I assessed the changes in the expression of genes downstream of TREM2 to understand TREM2 activation in AD. I consistently used human data, as significant differences in the transcriptional signatures of human AD and the 5xFAD mouse model have been reported [40]. To determine gene expression changes downstream of TREM2, iMG cells were treated with Hyb87, PBS, or the control IgG, and subjected to transcriptome analysis using the AmpliSeq approach. In PCA of the iMG AmpliSeq data, the variance of PC1 and PC2 was found to be 29.7% and 15.9 %, respectively (Fig. 2A). In the PC1 that explained the maximum variabilities, Hyb87 differed significantly from the PBS control and IgG, indicating that Hyb87-induced changes in the expression of specific genes could be detected. Next, I isolated DEGs in response to Hyb87 treatment (vs. PBS or vs. control

IgG; Table 1). I observed significant changes in gene expression after Hyb87 treatment as per the following criteria: FDR-adjusted P value < 0.05 and absolute fold change > 1.5, which involved 1,274 genes in Hyb87 vs. PBS and 710 genes in Hyb87 vs. control IgG (Fig. 2B, C, and Table 1). In contrast, the DEGs from the control IgG (vs. PBS) comprised as few as 81 genes (Table 1). To exclude gene expression changes due to IgG via Fc receptors, I attempted to define TREM2 DEGs that overlapped in the direction of altered expression between Hyb87 vs. PBS and Hyb87 vs. the control IgG. This allowed me to define TREM2 activation for 551 genes (Fig. 2C and Table 2) consisting of 300 upregulated (TREM2 up) and 251 downregulated (TREM2 down) DEGs (Fig. 2B and Table 1). The TREM2 DEGs were applied to pathway enrichment analysis using MetaCore. TREM2 up showed enrichment in "Immune response_TSLP signaling" (P = 3.0E-7), "Th2 cytokine-induced alternative activation of alveolar macrophages in asthma" (P = 1.1E-06), and "Immune response_IL-4-induced regulators of cell growth, survival, differentiation, and metabolism" (P = 1.2E-06). TREM2 down was associated with "Development_NOTCH-induced EMT" (P = 1.3E-06), "Eosinophil granule protein release in asthma" (P = 2.0E-05), and "Signal transduction_Cyclic AMP signaling" (P = 4.6E-05) (Fig. 2D, E, and Table 3).

Reduction in TREM2 activation with disease progression in patients with AD

Next, I investigated how TREM2 is activated in patients with AD by comparing the TREM2 DEGs with the transcriptome data of microglia from these patients. I used GSEA to determine statistically significant and consistent differences between gene sets from

two biological states [63, 64]. I separately used TREM2 up (300 upregulated genes) and TREM2 down (251 downregulated genes) to clarify the direction of gene expression regulated by TREM2 activation. I selected snRNA-seq data of patients with AD for comparison, for the following reasons: The microglial population that expresses TREM2 exclusively consisted of only 5-10% brain cells; TREM2 DEGs were from iMG, but not limited to microglia. Therefore, single-cell-derived RNA-seq data was ideal for my study, as gene expression changes in microglia may not be detected in the bulk RNA-seq data of tissues consisting of a mixed cell population. I performed GSEA using TREM2 DEGs in two ways: (1) Statistical analysis using DEGs among divided populations; (2) Correlation analysis using AD disease scores obtained from CERAD, Braak, and MMSE. First, I excluded three out of the 48 individuals using PCA, which suggested low data quality, and then I classified 45 individuals into three populations of HC, MCI, or AD using two clinical scores; MMSE of HC (≥ 29), MCI (24-28), and AD (≤ 23), or cogdx of HC (value 1), MCI (value 2, 3), and AD (value 4, 5), leading to six HC, 17 MCI, and 22 AD individuals determined using MMSE, or 13 HC, 10 MCI, and 21 AD individuals determined using cogdx (Table 4), after assessing the quality using PCA and excluding one individual from cogdx classification due to the possibility of other diseases. Next, I calculated the statistical values and signed P value in each population by comparing HC with MCI, HC with AD, or MCI with AD. GSEA was then conducted using these signed P values as the score on the side of the molecular profile data and TREM2 up or down as the data on the dataset side. Intriguingly, I observed that TREM2 up was significantly lower in AD microglia than in HC or MCI microglia when each population was defined

using both MMSE and cogdx (Fig. 3A–D and Table 5). Furthermore, no significant enrichment was observed when I compared HC and MCI microglia. These findings clearly showed that TREM2 activation was lost in AD. However, TREM2 down was significantly associated only with cogdx AD vs. MCI, which meant that TREM2 down was significantly lower in AD microglia than in MCI microglia.

I speculated that the fluctuation range of the fold change was significantly lower in TREM2 down than in TREM2 up, as absolute values of mean fold change were 1.09 in TREM2 up and 0.98 in TREM2 down, with P = 0.03. Second, the relationship between CERAD-, Braak-, or MMSE-correlated microglia genes and TREM2 DEGs (TREM2 up or TREM2 down) was investigated using GSEA to determine whether TREM2 activation changed with the progression of AD. Toward this, I used GSEA to compare TREM2 DEGs with genes that correlated with CERAD, Braak, or MMSE scores, which represented the semi-quantitative measure of neuritic plaques, neurofibrillary tangles, and cognitive function, respectively. TREM2 up showed a significant correlation with CERAD (FDR q-value = 0.009) and Braak-correlated genes (FDR q-value = 0), but not with MMSE-correlated genes (FDR q-value = 0.562) (Fig. 3E–F and Table 6). Furthermore, TREM2 down was not significantly associated with any of the scores tested. Collectively, these results suggested that TREM2 activation decreased with the progression of AD pathology.

Based on these findings, genes enriched in GSEA between TREM2 up and the core enrichment genes in AD (vs. HC) that regulated TREM2 activation in AD were applied to pathway enrichment using MetaCore. Interestingly, the following were selected as the

common pathways: “Apoptosis and survival_anti-apoptotic TNFs/NF-kB/IAP pathway” (P = 1.0E-6 on cogdx; P = 2.9E-7 on MMSE), “Immune response_IFN-α/β signaling via JAK/STAT” (P = 3.4E-5 on cogdx; P = 1.0E-5 on MMSE), and “Immune response_BAFF-induced non-canonical NF-kB signaling” (P = 1.1E-4 on cogdx; P = 4.3E-5 on MMSE). In contrast, pathway enrichment analysis with genes from GSEA and Braak or CERAD indicated “Development_regulation of cytoskeleton proteins in oligodendrocyte differentiation and myelination” (P = 1.8E-6 on Braak; P = 5.6E-5 on CERAD), “Inhibition of remyelination in multiple sclerosis: regulation of cytoskeleton proteins” (P = 1.6E-5 on Braak; P = 1.7E-5 on CERAD), and “Cell adhesion_gap junctions” (P = 3.3E-6 on Braak; P = 3.6E-6 on CERAD) as the common pathways (Fig. 3G, H, and Table 7).

I investigated whether TREM2 expression differed between AD, MCI, and HC, or whether TREM2 expression correlated with CERAD or Braak scores. My results showed that TREM2 expression did not differ significantly between AD, MCI, and HC, and did not show any correlation with the scores (FDR-adjusted P value > 0.85; Tables 8 and 9).

I analyzed another snRNA-seq dataset, ROSMAP data (syn21125841) [40], to replicate my observations. Nineteen individuals were classified into three populations of HC, MCI, or AD using two clinical scores; MMSE or cogdx. Three HC, five MCI, and 11 AD individuals were determined using MMSE, or nine HC, and ten AD individuals were determined using cogdx. (Table 10). I calculated the signed P value from the snRNA-seq data between HC and AD microglia and performed GSEA using TREM2 up for

replication. My results showed that TREM2 up was significantly lower in AD microglia than that in HC microglia (Fig. 4a and b).

Discussion

In this study, I generated an agonistic anti-TREM2 mAb, Hyb87, and utilized it as a tool for activating TREM2. Further, I defined TREM2 activation by assessing changes in the expression of downstream genes. Previous studies used anti-TREM2 Ab as a TREM2 activation tool in various types of cells, including the microglia, dendritic cells, macrophages, osteoclasts, and astrocytes [32,33,50,65–71]. However, in these studies, the Abs were used to visualize signals and/or assess the cellular functions of activated TREM2 in terms of intracellular Ca^{2+} mobilization, ERK phosphorylation, SYK phosphorylation, apoptotic cell death, the formation of $TRACP^{+}$ osteoclasts, migration of osteoclasts, pro- and anti-inflammatory responses, phagocytosis, cell survival, migration, and amyloidogenesis, but not for defining TREM2 activation, as performed in this study. I used Hyb87 to activate TREM2 in iMG cells and identified TREM2 DEGs after comparison with control IgG stimulation (Fig. 2A–C). I observed a slight increase in the NFAT signal by the control IgG (Fig. 1D). The control IgG-mediated responses were possibly due to Fc receptor engagement. A previous report showed that NFAT, as well as other transcription factors, transmit signals downstream of the Fc receptor [62]. Fc receptor engagement and TREM2 increase the expression levels of some of the cell surface molecules, including CD86, CD40, or CCR7 [60]. TREM2 induces signaling downstream of the Fc receptor, suggesting that the DEGs shared between TREM2 and

control IgG treatment, which were not included in my TREM2 DEGs, may primarily be a part of TREM2 DEGs. Wang et al. demonstrated that mutations abolishing IgG binding to the Fc receptor in the agonistic anti-TREM2 mAb, marginally affect its pro-survival effect on macrophages, suggesting that the Ab-mediated TREM2 activation is largely independent of the IgG-mediated cross-linking of Fc receptors [32]. This finding strongly supports my definition of TREM2 DEGs.

The pathway enrichment analysis of TREM2 up showed type2 immune response as represented by the Th2 type cytokine pathways, including TSLP and IL-4 (Fig. 2D and Table 3). My findings agree with those of the previous studies, wherein TREM2 was reported to enhance Th2 cytokine production [46,67,72]. Th2 cytokines also inhibit $A\beta_{1-42}$-induced pro-inflammatory cytokines, including IL-6 and IL-1β, in microglia and THP-1 cells [73]. IL-4 induces the uptake and degradation of $A\beta_{1-42}$ [74]. Intracerebral microinjection of IL-4 and IL-13 reduces Aβ accumulation in APP23 mice via microglial activation [75]. Thus, the TREM2 signal may modulate Th2 type cytokine pathways in Aβ clearance.

I successfully showed low TREM2 activation in microglia of patients with AD and that TREM2 activation decreased with the progression of neuritic plaques and neurofibrillary tangles, represented by CERAD and Braak scores, respectively. My findings indicated TREM2-mediated regulation of AD pathology via controlling microglial functions and corroborated a previous finding that the TREM2 loss-of-function variant R47H is associated with increased density of neuritic plaques and neurofibrillary tangles in multiple brain regions [26]. R47H is associated with amyloid compaction and increased

tau hyperphosphorylation around amyloid deposits [76]. In my analysis, TREM2 activation was not associated with the cognition score, MMSE my . A report examining the association of MMSE and R47H variant revealed no significant difference in the annual rate of MMSE decline between patients with AD carrying a TREM2 common variant and an R47H variant, although the number of participants was small [77]. Further, the R47H risk variant did not significantly affect cognitive performance in a longitudinal study [78]. Out of the 45 donors in the dataset that I used in the evaluation study (Fig. 3), 29 were registered as harboring a TREM2 common variant. On the other hand, the TREM2 sequences of the remaining 16 donors were not available. Therefore, I cannot rule out the possibility that the 16 donors possessed the R47H variant that affected my analysis in elucidating TREM2 activation. However, my replication study recapitulated the results of the evaluation study (Fig. S1), and the dataset used in the replication study comprised TREM2 common variant carriers alone. This indicates that TREM2 signal is low in the microglia of patients with AD regardless of the R47H variant.

I speculated that lower TREM2 activation in the microglia of patients with AD could be caused by proteases. Several proteases, including ADAM10, ADAM17, or meprin β, are known to reduce the levels of membrane-bound TREM2 [41,42,79]. The ADAM17-mediated shedding of the membrane-bound TREM2 is triggered by pro-inflammatory stimulation, such as lipopolysaccharide, TNFα or IFNγ [80]. The reduction of the membrane-bound TREM2 levels by ADAM10 or meprin β has been shown to inhibit TREM2-mediated phagocytosis [79]. Another study reported that γ-secretase degrades the C-terminal fragment of TREM2 and that impaired γ-secretase activity leads to an

accumulation of the C-terminal fragment of TREM2, thereby trapping its adaptor protein—TYROBP to reduce TREM2 signaling [81,82].

My GSEA data showed that TREM2 activation was not significantly different in MCI (vs. HC), suggesting that TREM2 activation could be maintained in the microglia of patients with MCI. As discussed earlier, the function of TREM2 could be affected by proteases that behave differently in MCI and AD microenvironments. Interestingly, a previous report showed that the levels of active form of γ-secretase activating protein reduced in the frontal cortex of severe AD subjects, but not in that of MCI subjects [83]. This difference in protease regulation could contribute to the varying amounts of membrane-bound TREM2 capable of transmitting TREM2 signal in the microglia of patients with MCI and AD. Previously, Jiang et al. reported that TREM2 failed to improve Aβ pathology when the lentiviral over-expression of TREM2 was tried in 18-month-old APP/PS1 mice [84], whereas its over-expression improved Aβ pathology in 7-month-old APP/PS1 mice [29]. This suggests that the TREM2 signal is no longer viable once AD has been established. However, further studies are required to understand how TREM2 activation changes with disease progression.

In the present study, the TREM2 expression levels alone showed no correlation with the clinical scores from the snRNA-seq data used. Although some previous studies reported TREM2 expression changes in AD brains due to aging [34–40], the direction of alteration of TREM2 expression levels is not unilateral. For example, in the hippocampus of patients with AD, TREM2 mRNA has been reported to be higher than that of controls [34], but different groups exhibit either downregulation of TREM2 or no alteration at protein

and/or mRNA levels [35–37]. Although extensive efforts are required to address this discrepancy, some reasons for it may be as follows. TREM2 is mainly expressed in microglia in the brain. Differences in the population size of microglia could lead to changes in the relative expression of TREM2. Additionally, the use of different internal controls for normalization may lead to difficulty in the interpretation of TREM2 expression. The expression level of a molecule is typically normalized with an internal control, such as *GAPDH*, *ACTB*, or *HPRT*. In practice, TREM2 mRNA has been differently normalized in previous studies: with *GAPDH* [35,37], a combination of *ACTB* and *HPRT* [34], or a combination of *GAPDH* and *HPRT* [38]. Moreover, patient demographics may have been different in those studies or sample storage conditions could have affected sample quality. However, none of those studies reported an association of TREM2 expression with its activation.

In previous reports, the sTREM2 level was investigated in CSF to determine its association with AD. Interestingly, a few studies revealed that sTREM2 level in the CSF of patients with AD is associated with hallmarks of AD, such as $A\beta_{1\text{-}42}$ [85], total tau, and phosphorylated tau in CSF [30–32]. However, whether sTREM2 levels reflect TREM2 activation remains unknown. The levels of TREM2 proteases, ADAM10 and ADAM17, are altered in AD CSF or brain [86–89]. Hence, the usability of sTREM2 for TREM2 activation warrants further investigation.

The brain snRNA-seq data of 5xFAD mice and human patients with AD elucidated distinct AD gene signatures between human and mouse microglia [40]. Notably, the human brain shows more qualitative changes in the number of microglia than that of mice,

and the signature of human microglia in AD is different from that of disease-associated microglia in the 5xFAD model. This finding prompted me to use human cell and tissue data instead of mouse data. The study reported higher expression of the transcription factor IRF8 in AD, indicating that IRF8 may be a major driver of human microglia signature in AD. In my study, *IRF8* was significantly downregulated in response to Hyb87 vs. PBS (FDR-adjusted P = 2.6E-5 and $\log_2$ fold change = −0.54 for IRF8), indicating that Hyb87 could reverse the IRF8-signature in human AD microglia. Pathway enrichment data with genes enriched in GSEA between TREM2 up and core enrichment genes in AD (vs. HC) yielded the anti-apoptotic pathway as the top hit. This corroborated anti-apoptotic function of TREM2 in microglia from 5xFAD mice crossed with *TREM2* KO mice[6] or in microglial BV-2 cells [90]. In addition to the pathway enrichment data, some of the genes were enriched in GSEA function in microglia and could control microglial fate downstream of TREM2.

Genes such as heparin-binding epidermal growth factor-like growth factor (*HBEGF*), baculoviral IAP repeat-containing 3 (*BIRC3*), BTG anti-proliferation factor 1 (*BTG1*), CD300 molecule-like family member B (*CD300LB*), IL3 receptor subunit α (*IL3RA*), and platelet-derived growth factor-α (*PDGFA*) were upregulated in response to Hyb87 treatment. Thus, TREM2 activation might efficiently combat AD by orchestrating the expression of the microglial genes involved in microglial fate. HBEGF is a potent stimulator of cell proliferation and migration and plays diverse physiological roles, including wound healing and cardiac development [91]. Previous reports suggest the involvement of HBEGF in microglia and AD. HBEGF signaling stimulates cell

proliferation and phagocytosis of microglia [92]. Furthermore, a trans-ethnic meta-analysis of a genome-wide association study identified an intergenic single nucleotide polymorphism between *HBEGF* and *PFDN1* as an AD susceptibility locus [93]. Study of *Hbgef* KO also showed that HBEGF regulates $A\beta_{1-42}$ and phosphorylated tau levels [94], as well as neurogenesis and cognitive function [95]. BIRC3, also known as cIAP2, is an IAP family protein that regulates apoptosis by blocking caspase activation and inflammation via innate immune receptors [96]. In microglia, BIRC3 acts as a switch between pro-inflammatory activation and cell death by regulating caspase-3 processing [97]. BIRC3 confers resistance to cell death in microglia subjected to chronic inflammatory stress [98]. BTG1 plays an important role in cell growth and differentiation [99]. In microglia, it regulates microglial apoptosis by functioning as a sensitizer in activation-induced cell death [100]. CD300LB is an activator of the CD300 family of myeloid immunoglobulin receptors. Interestingly, CD300LB shares similarity with TREM2, as it associates with DAP12 and recognizes phosphatidylserine as a ligand on the outer plasma membrane of apoptotic cells, thereby regulating the efferocytosis and phagocytosis of apoptotic cells [101,102]. Induction of CD300LB by TREM2 activation indicated that TREM2 may mobilize functionally similar molecules to enhance its effects. IL3RA transduces the IL3 signal. Different groups have demonstrated IL3 induced microglial proliferation using a neutralizing anti-IL3 Ab [103] and its dependence on JAK2 [104]. PDGFA plays physiological roles via PDGFR-α during gastrulation and in the development of multiple tissues, including the lungs, intestine, and central nervous system [105]. A recent report revealed that PDGFA also exerts proliferative effects on the

microglial cells [106]. To validate my speculation, further research is needed for elucidation of the role of TREM2 in AD microglia.

In this study, I focused on microglial data. Interestingly, although peripheral monocytes do not generally express TREM2, its expression was upregulated in monocytes from patients with AD [60,107], thereby potentially corroborating the upregulated TREM2 expression in the microglia of patients with AD [39,40]. Monocyte population and functions have also been reported to change in peripheral blood of patients with AD. Previous studies on peripheral immune cells of patients with AD demonstrated an increase in the population of activated monocytes [108,109], suggesting its pro-inflammatory nature [109,110]. If such monocytic changes correlate with TREM2 activation status in the microglia, they may act as a potential biomarker for microglial TREM2 activation in AD, which can be determined in a less invasive approach. However, further investigations are required to validate these speculations.

Conclusions

My results show that low TREM2 activation in patients with AD and the agonistic anti-TREM2 mAb may render microglia resistant to AD progression. Furthermore, my study outcomes provide evidence that agonistic anti-TREM2 mAb is a powerful tool to identify TREM2 activation in the microglia of patients with AD.

Figures and Tables

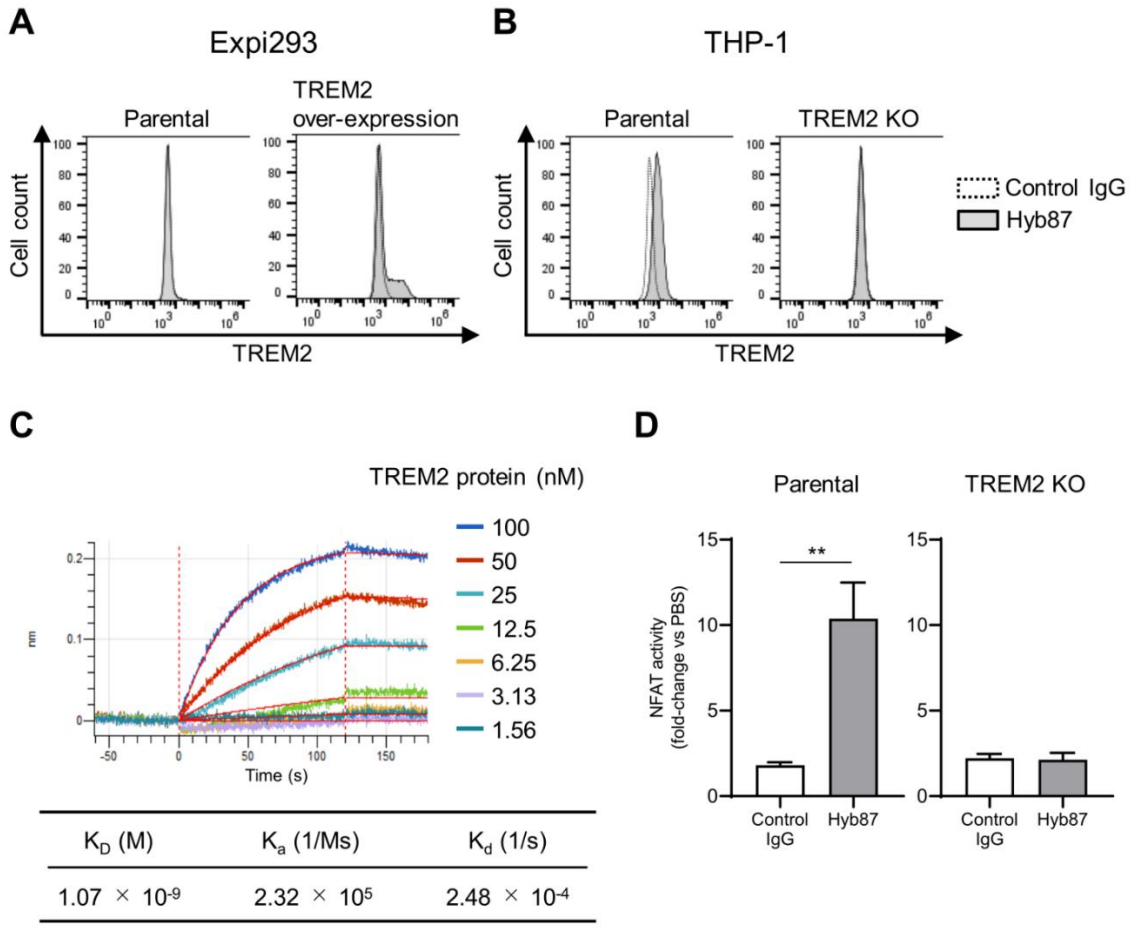

K_D (M)	K_a (1/Ms)	K_d (1/s)
1.07×10^{-9}	2.32×10^{5}	2.48×10^{-4}

Figure 1 Binding and agonist activities of Hyb87 toward TREM2. **A, B** Binding of Hyb87 to TREM2 in cells was determined using FCM. Cells were incubated with Hyb87, followed by incubation with Alexa488-labeled anti-mouse IgG Ab. **A** Parental and human TREM2-transfected Expi293 cells. **B** THP-1 cells and *TREM2* KO THP-1 cells. Control IgG, dashed line; Hyb87, gray histogram. **C** Analysis of Hyb87 affinity to TREM2. BLI was used to determine the affinity of Hyb87 to TREM2. The vertical axis indicates the BLI signal response (nm), and the horizontal line indicates the time after analyte (TREM2 protein) loading. Kinetic parameters were analyzed using a 1:1 Langmuir fitting model. Association (K_a) and dissociation (K_d) constants were calculated and used to determine the K_D value (K_d/K_a). **D** NFAT response of Hyb87. THP-1 cells and *TREM2* KO THP-1 cells transiently transfected with a NFAT-luc plasmid were incubated on a Hyb87-coated plate. Data points represent the mean + SD of values acquired in triplicate. ** for P value < 0.005 vs. control IgG-treated group by Student's *t*-test. All data are representative of at least two independent experiments. TREM2, triggering receptor expressed on myeloid cells 2; FCM, flow cytometry; Ab, antibody; BLI, bio-layer interferometry; NFAT, nuclear factor of activated T cells.

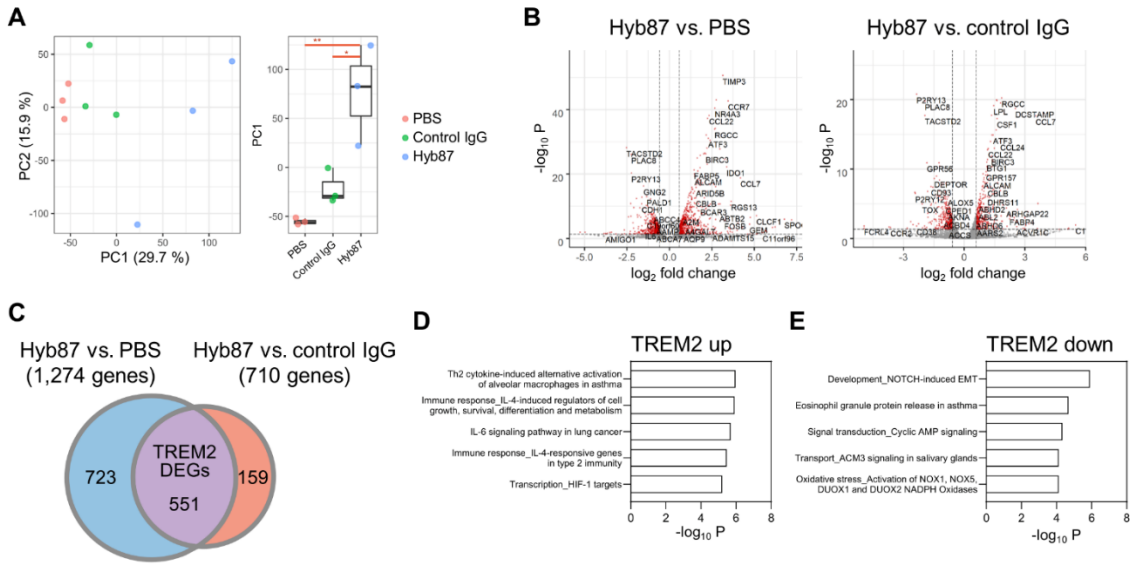

Figure 2 Identification of TREM2 DEGs from iMG. **A** PCA and boxplot analysis of the PC1 distribution of the iMG transcriptome data from PBS, control IgG, and Hyb87 treatment groups. Each group had three replicates. Percentages with each axis represent the variance of the data captured by each PC. * or ** for boxplot indicates P value calculated using Tukey's honest significant difference test between groups. * for P value < 0.05 and ** for P value < 0.01. **B** Volcano plots depicting the results of differential gene expression analysis between Hyb87 and PBS treatment or between Hyb87 and control IgG treatment. The criteria for significance were set at FDR-adjusted P value < 0.05 and absolute fold change > 1.5. DEGs that satisfy the criteria are shown in red. **C** Venn diagram showing TREM2 DEGs. Genes that overlapped between those from Hyb87 treatment vs. PBS and from Hyb87 treatment vs. control IgG treatment were defined as TREM2 DEGs. Considering the direction of expression alteration, the TREM2 DEGs comprised genes, the expression of which changed in the same direction in Hyb87 treatment (vs. PBS and vs. control IgG). **D, E** Top five significant pathways in pathway enrichment analysis using TREM2 up (**D**) and TREM2 down (**E**). TREM2, triggering receptor expressed on myeloid cells 2; DEG, differentially expressed genes; iMG, induced pluripotent stem cell-derived microglia-like cells; PCA, principal component analysis; PBS, phosphate-buffered saline; FDR, false discovery rate.

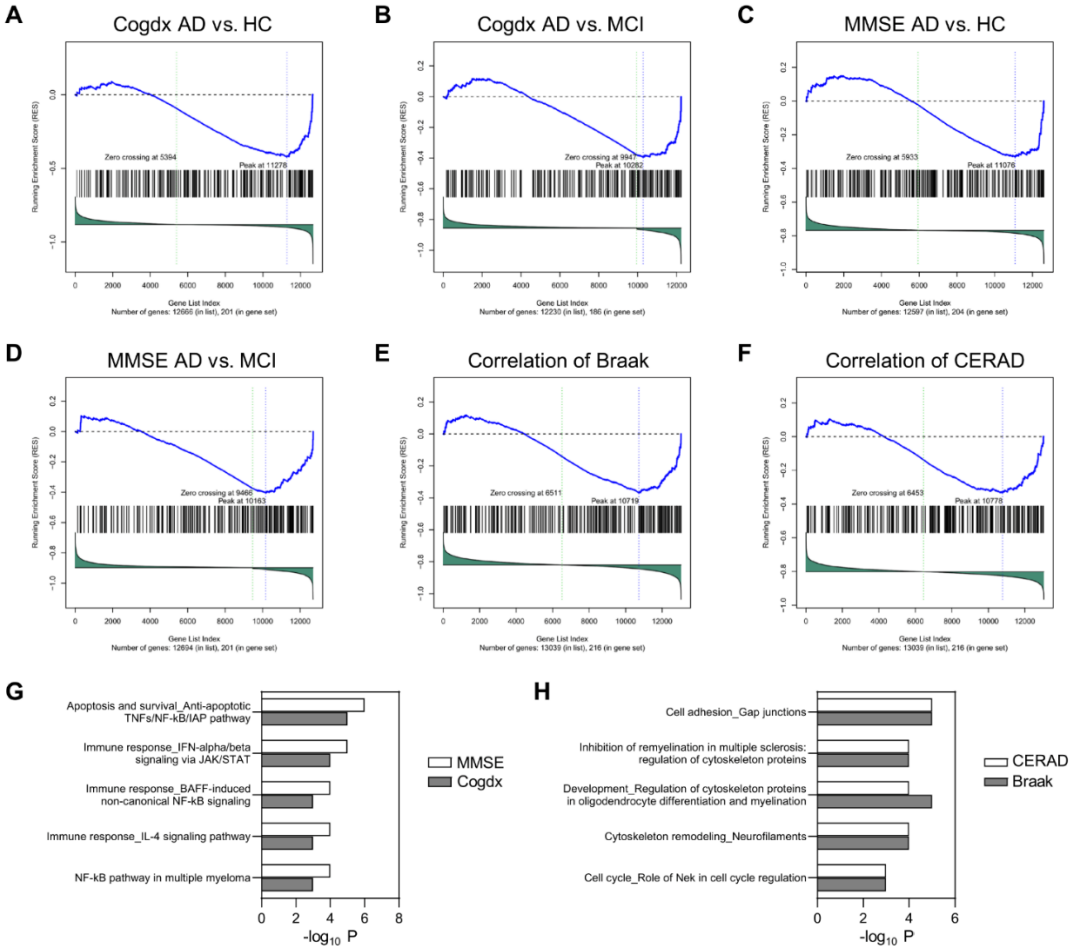

Figure 3 Reduction in TREM2 activation in AD microglia. **A-F** GSEA enrichment plots* of ROSMAP syn18485175 data (samples from 45 individuals were used: six HC, 17 MCI, and 22 AD individuals classified by MMSE or 13 HC, 10 MCI, and 21 AD individuals classified by cogdx) that were significantly enriched. The vertical axis shows all genes arranged in the order of signed P value. The horizontal axis indicates the enrichment score of each gene. **G, H** Top five significant pathways in pathway enrichment analysis using genes enriched in GSEA between TREM2 up and DEGs in AD (vs. HC) (**G**) and between TREM2 up and Braak or CERAD (**H**). TREM2, triggering receptor expressed on myeloid cells 2; AD, Alzheimer's disease; GSEA, gene set enrichment analysis; DEG, differentially expressed genes; CERAD, Consortium to Establish a Registry for Alzheimer's Disease; ROSMAP, Religious order Study and the Memory and Aging Project.

*GSEA enrichment plots indicate that: The lower part of the plot shows the fold change of the referenced gene set (in this case, the AD gene set) and is ordered by fold change score; the middle part of the plot (like a barcode) shows where the gene set (in this case, the TREM2 activated microglia gene set) is enriched where in the reference gene set; the upper part of the plot shows the enrichment score (ES) of the gene set under analysis, and the score at the peak of the plot (the score farthest from 0) is the ES of the gene set. The positive ES peak (ES peak greater than 0) indicates the positive correlation, while the negative ES peak (ES peak less than 0) indicates the negative correlation.

A

Dataset	NES	FDR q-value
syn21125841 AD vs. HC	-1.2498	0.039

B

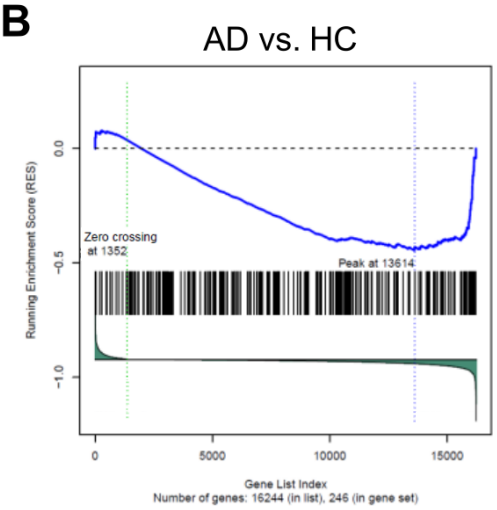

Figure 4. Reduction in TREM2 activation in AD microglia (replication study)

A GSEA normalized enrichment scores (NES) and FDR q-value. **B** GSEA enrichment plots of the replication data set (ROSMAP syn21125841 data: samples from 19 individuals were classified into three HC, five MCI, and 11 AD by MMSE, or nine HC and 10 AD by cogdx) that was significantly enriched. The vertical axis shows all genes arranged in the order of signed P value. The horizontal axis indicates the enrichment score of each gene.

Table 1. DEGs of Hyb87 (vs. PBS or control IgG)

Gene	log_2FC	P value	FDR-adjusted P value
CCR7	2.071967	1.16E-23	2.04E-19
TIMP3	1.545119	2.62E-22	2.31E-18
CCL4	-1.345	2.32E-17	1.36E-13
CXCR4	1.435716	9.08E-17	3.99E-13
NR4A3	1.312751	2.16E-16	7.59E-13
CCL22	1.145776	8.92E-16	2.61E-12
DUSP5	1.148727	5.15E-14	1.29E-10
HNRNPC	-0.97935	1.66E-12	3.66E-09
IL1B	-1.03171	6.28E-11	1.23E-07
IRF4	1.061496	1.21E-10	2.12E-07
CRLF2	1.124942	3.80E-10	6.08E-07
GPR183	0.861224	2.48E-09	3.64E-06
LPL	0.789109	5.26E-09	7.12E-06
BMP6	1.77063	7.92E-09	9.28E-06
RGS1	0.765801	7.82E-09	9.28E-06
BCL2L11	1.103587	2.13E-08	2.34E-05
EGR2	0.869803	3.53E-08	3.65E-05
IDO1	1.724228	4.34E-08	4.01E-05
AVPI1	1.099792	4.32E-08	4.01E-05
TGFA	1.385466	4.92E-08	4.33E-05
ATF3	0.86758	5.73E-08	4.80E-05
TP53I13	-0.95667	6.22E-08	4.97E-05
CCL8	-1.46184	9.52E-08	7.27E-05
MTSS1	0.812631	2.20E-07	0.000161
NR4A2	1.128576	2.76E-07	0.000194
CCL24	1.187412	5.69E-07	0.000384
BTG1	0.701546	6.10E-07	0.000397
GADD45B	0.779982	7.18E-07	0.000451
BIRC3	0.800397	9.43E-07	0.00054
EDNRA	-0.79408	9.33E-07	0.00054
IGFBP3	-0.71547	9.51E-07	0.00054
SDS	0.791525	1.16E-06	0.000639
VEGFA	0.777951	1.43E-06	0.000764
IL8	-0.71003	1.71E-06	0.000884
ARID5B	0.78693	1.94E-06	0.000974
NR4A1	1.401836	2.49E-06	0.001218
RGS13	2.456661	2.59E-06	0.001229
LINC00597	-1.17488	2.95E-06	0.001357
CCL3L3	-0.77501	3.09E-06	0.001357
KLHL24	0.741195	3.07E-06	0.001357
GLUL	0.625998	5.33E-06	0.002287
IL18R1	-0.81536	5.53E-06	0.002314
GIMAP2	0.879867	5.79E-06	0.002336
RGCC	0.80885	5.85E-06	0.002336
GIMAP6	0.833009	5.99E-06	0.002339
NFKBIZ	-0.64207	7.87E-06	0.00301
PMP22	0.642112	8.52E-06	0.003187
FZD1	-0.76655	8.89E-06	0.003256
TNFAIP3	-0.60947	1.04E-05	0.003723
CD44	-1.11131	1.24E-05	0.00436
TRAPPC11	-0.79314	1.42E-05	0.00489
FCAMR	-1.15809	1.70E-05	0.005758
MATK	0.810322	2.05E-05	0.006394
EDN1	-0.73941	2.05E-05	0.006394
LOC595101	-0.73507	2.00E-05	0.006394
GRASP	0.687493	2.01E-05	0.006394
CCL20	-0.64986	2.07E-05	0.006394
SLC7A8	0.590146	2.89E-05	0.008773
C6orf223	1.384672	3.34E-05	0.009966
IL1A	-0.72215	3.83E-05	0.011035
FOXO3	0.651878	3.90E-05	0.011061
SNORA28	-0.63988	4.12E-05	0.011505
NCAM1	0.558271	5.16E-05	0.013968
NUAK1	0.737988	6.56E-05	0.017054
SRGAP2	-0.7262	6.60E-05	0.017054
GPR157	0.583998	6.41E-05	0.017054
HTRA4	1.134858	7.10E-05	0.018017
ADORA3	0.554279	7.17E-05	0.018017
CCL3	-0.66841	7.63E-05	0.018904
LOC100303749	-1.12677	8.28E-05	0.020225
DPY19L4	-0.87198	9.48E-05	0.022218
APPL2	0.580223	9.45E-05	0.022218
FRAT1	1.263783	9.94E-05	0.022985
FOXO1	0.969337	0.000102	0.023158
SNORA46	-0.62939	0.000104	0.023158
SLC29A3	0.581412	0.000103	0.023158
RCSD1	0.598558	0.000113	0.024428
RASGRP1	-0.67503	0.000145	0.030622
EIF2C1	0.575658	0.000178	0.035903
ABTB2	1.845003	0.000186	0.037079
SLC2A6	-0.58148	0.000198	0.038662
DRAM1	-0.56865	0.000208	0.040119
SATB1	0.574013	0.000211	0.040365
GATSL2	1.352565	0.000223	0.042131
C17orf103	1.047523	0.000243	0.045027
ALAD	0.645072	0.000243	0.045027
CENPV	1.620224	0.00025	0.045732
MREG	0.603646	0.000253	0.045732
ATRX	-0.57791	0.000255	0.045732
TNFAIP6	-0.59163	0.000282	0.049573
IRS2	0.92132	0.000285	0.049608

Table 2. TREM2 DEGs (1/10)

Gene	Hyb87 vs. PBS			Hyb87 vs. control IgG		
	log_2FC	P value	FDR-adjusted P value	log_2FC	P value	FDR-adjusted P value
AARS2	0.678936	0.000515	0.007997	0.626018	0.001052	0.022418
ABCB1	1.594127	8.71E-05	0.001969	1.097794	0.002668	0.044055
ABHD11	-0.69441	0.005487	0.047904	-0.77782	0.001432	0.028316
ABHD2	0.913806	1.07E-11	1.59E-09	0.709984	6.33E-08	9.34E-06
ABHD6	0.993414	8.71E-11	1.12E-08	0.594339	4.56E-05	0.002015
ABTB2	2.958083	7.77E-11	1.00E-08	1.11308	0.000836	0.018889
ACAD11	0.770594	3.06E-05	0.000814	0.733622	5.25E-05	0.002246
ACBD4	-1.03825	3.38E-05	0.000884	-1.02027	3.46E-05	0.001662
ACCS	-0.84124	0.001049	0.01379	-0.7519	0.002858	0.046388
ACO1	0.734748	6.83E-07	3.04E-05	0.714499	1.12E-06	9.97E-05
ACOT9	0.620892	1.65E-05	0.00048	0.604775	2.41E-05	0.00124
ACP6	-0.75401	0.001039	0.013689	-0.82589	0.000275	0.007977
ACPP	-0.64516	0.000291	0.005134	-0.66721	0.000152	0.00503
ADAM19	0.837569	8.84E-09	7.00E-07	0.67671	2.15E-06	0.000171
ADAMTS10	-1.04985	1.49E-07	8.29E-06	-0.64909	0.000944	0.020781
ADCK2	-0.75855	4.83E-06	0.000167	-0.66869	4.54E-05	0.002009
ADD2	1.220102	1.65E-07	9.08E-06	0.699303	0.001156	0.023942
AGRN	0.764304	4.12E-05	0.001043	0.719482	8.04E-05	0.003134
AHNAK	0.968346	1.16E-08	8.92E-07	0.811596	8.65E-07	7.96E-05
AK4	1.297972	1.37E-05	0.000411	0.890674	0.001188	0.024409
AKNA	-0.86173	1.89E-07	1.01E-05	-0.79375	1.27E-06	0.000113
AKT1S1	0.905996	8.45E-07	3.67E-05	0.900484	6.92E-07	6.69E-05
ALCAM	1.485524	7.55E-23	4.58E-20	0.962777	7.29E-12	3.05E-09
ALOX5	-0.95268	9.76E-12	1.47E-09	-0.80567	4.76E-09	9.74E-07
ANKRD23	-0.87196	0.000712	0.010256	-0.85483	0.000704	0.016735
ANKRD28	0.794594	1.74E-05	0.000507	0.683873	0.000142	0.004792
ANKRD33B	1.172116	2.43E-06	9.22E-05	1.152835	1.92E-06	0.000156
ANTXR2	1.165132	5.19E-11	6.76E-09	0.70393	2.19E-05	0.001155
AP1S3	1.383863	1.28E-08	9.78E-07	1.189905	2.41E-07	2.87E-05
APAF1	-0.99631	1.28E-09	1.28E-07	-0.7177	7.69E-06	0.000499
APBB1IP	-0.73164	8.62E-07	3.71E-05	-0.6562	8.19E-06	0.000524
APEX1	-1.07532	3.57E-10	4.02E-08	-0.89106	1.23E-07	1.61E-05
AQP9	0.843237	0.002069	0.023365	1.436268	4.87E-07	4.89E-05
ARAP2	1.161799	1.30E-11	1.90E-09	1.128087	2.43E-11	9.09E-09
ARHGAP10	0.868109	1.17E-09	1.19E-07	0.655973	2.34E-06	0.000182
ARHGAP15	-1.26624	2.98E-10	3.38E-08	-1.23172	5.32E-10	1.44E-07
ARHGAP22	1.536658	0.000107	0.002347	2.082124	3.66E-07	3.88E-05
ARHGAP9	-1.05222	2.30E-10	2.68E-08	-0.88616	5.81E-08	8.81E-06
ARID4B	0.662711	2.49E-05	0.000688	0.588286	0.000145	0.00489
ARID5B	1.564844	3.62E-19	1.48E-16	0.777914	6.30E-07	6.15E-05
ARNTL2	1.610864	1.56E-12	2.67E-10	1.078001	2.56E-07	3.00E-05
ARV1	-0.97702	9.35E-06	0.0003	-0.94821	1.31E-05	0.00077
ATF3	2.287533	4.46E-35	7.83E-32	1.419953	1.00E-18	1.17E-15
ATM	-0.94666	4.80E-06	0.000167	-0.86848	2.09E-05	0.001116
ATP10A	-0.74842	0.000941	0.012735	-0.73456	0.000942	0.020761
ATP1B3	0.813066	7.30E-10	7.69E-08	0.641395	7.06E-07	6.75E-05
ATP2A3	-1.46407	1.95E-12	3.21E-10	-1.20524	3.31E-09	7.37E-07
ATP6V1B2	0.620607	1.43E-06	5.73E-05	0.636685	7.78E-07	7.31E-05
AVPI1	1.953837	1.14E-20	5.72E-18	0.854045	1.57E-06	0.000134
AXIN2	1.866793	2.40E-07	1.24E-05	1.103108	0.000469	0.012137
B3GALNT1	-1.14051	7.51E-06	0.000245	-1.14645	4.74E-06	0.000332
B3GNTL1	-0.83504	0.000462	0.007366	-0.82434	0.000438	0.011489
BASP1	1.142756	6.17E-09	5.18E-07	0.717432	9.50E-05	0.003522
BAZ1B	-0.7453	6.98E-05	0.001653	-0.6007	0.001179	0.024328
BCAP31	0.654293	0.002414	0.026084	0.671756	0.001459	0.028667
BCAR3	1.815312	5.81E-13	1.10E-10	1.090348	9.54E-07	8.69E-05

Table 2. TREM2 DEGs (2/10)

Gene	Hyb87 vs. PBS			Hyb87 vs. control IgG		
	log_2FC	P value	FDR-adjusted P value	log_2FC	P value	FDR-adjusted P value
BCL2L11	1.751835	6.79E-18	2.59E-15	0.648249	0.000203	0.006311
BIRC3	2.134204	5.38E-30	5.56E-27	1.333807	1.57E-15	1.32E-12
BMP6	2.719963	1.97E-19	8.46E-17	0.949333	2.38E-05	0.001226
BRCA1	-1.40577	4.89E-08	3.06E-06	-0.76575	0.002716	0.044715
BTG1	1.812673	1.68E-29	1.56E-26	1.111127	1.49E-14	1.01E-11
C11orf84	-0.97229	4.46E-06	0.000157	-0.80883	0.00011	0.003897
C11orf96	5.491615	0.001084	0.014133	5.491615	0.000428	0.011275
C12orf75	-1.13963	1.26E-06	5.14E-05	-1.00997	1.30E-05	0.000766
C15orf38	-0.77905	1.92E-05	0.000546	-0.71711	6.93E-05	0.002795
C15orf48	0.762135	8.28E-08	5.02E-06	0.749469	1.26E-07	1.64E-05
C16orf45	0.772412	3.18E-05	0.000841	0.612166	0.000693	0.016526
C17orf96	1.415739	1.02E-09	1.04E-07	1.036952	1.77E-06	0.000147
C19orf35	-0.69703	0.002154	0.024142	-1.01799	4.78E-06	0.000332
C19orf60	-1.33229	2.20E-08	1.53E-06	-0.98824	2.48E-05	0.001262
C1orf162	-0.87909	0.002258	0.024841	-0.8931	0.00135	0.026971
C1RL	-0.64021	0.000914	0.012481	-0.66593	0.000497	0.012672
C6orf223	2.405711	9.83E-14	2.11E-11	1.021039	7.59E-05	0.003018
CABLES1	-1.02485	1.30E-06	5.28E-05	-0.93315	7.45E-06	0.000487
CACNB3	1.477825	1.39E-05	0.000416	1.299457	4.39E-05	0.001953
CALCRL	1.184105	5.51E-07	2.53E-05	0.739947	0.000677	0.016257
CARD9	-0.67148	2.46E-05	0.000682	-0.63321	6.12E-05	0.002527
CBFA2T3	-0.64657	0.000269	0.004857	-0.64381	0.000242	0.007298
CBLB	1.552928	8.00E-16	2.38E-13	1.150538	1.48E-10	4.40E-08
CBX5	-0.72117	2.41E-06	9.17E-05	-0.5901	9.56E-05	0.00353
CCDC68	1.713803	1.22E-08	9.38E-07	1.398949	4.44E-07	4.58E-05
CCDC85B	-1.09124	3.84E-07	1.87E-05	-1.06017	5.96E-07	5.85E-05
CCL1	1.553035	3.78E-08	2.43E-06	1.842772	1.06E-10	3.37E-08
CCL22	2.328392	1.73E-42	6.09E-39	1.182616	1.18E-16	1.09E-13
CCL24	2.964714	1.36E-31	1.70E-28	1.777302	1.03E-17	1.06E-14
CCL7	4.182746	2.58E-22	1.51E-19	3.530185	1.33E-21	2.13E-18
CCNA1	1.79587	0.002173	0.024293	1.68881	0.002043	0.036613
CCND3	-0.74944	3.17E-07	1.59E-05	-0.73562	4.54E-07	4.61E-05
CCNJL	1.479306	2.99E-08	2.01E-06	0.950669	0.000112	0.003985
CCR1	-0.74484	4.52E-06	0.000159	-0.74617	3.81E-06	0.000276
CCR7	3.45875	3.38E-47	1.98E-43	1.386783	5.47E-15	4.18E-12
CD101	-0.69991	1.89E-06	7.39E-05	-0.63879	1.17E-05	0.000699
CD109	0.790779	8.61E-09	6.88E-07	0.711663	1.61E-07	2.06E-05
CD1A	-0.84499	3.57E-09	3.17E-07	-0.75239	1.08E-07	1.47E-05
CD1B	1.505634	7.06E-09	5.80E-07	0.983886	3.52E-05	0.001664
CD244	-0.60316	0.002728	0.028511	-0.71334	0.000303	0.008584
CD28	-0.9393	3.53E-07	1.74E-05	-0.70833	9.51E-05	0.003522
CD300A	-0.80704	1.48E-08	1.09E-06	-0.68929	9.63E-07	8.73E-05
CD300LB	1.039153	2.18E-09	2.10E-07	0.715138	1.56E-05	0.000875
CD38	-2.66341	0.000107	0.002348	-2.34767	0.000667	0.016038
CD3EAP	-1.10285	3.60E-06	0.00013	-0.89918	0.000127	0.004386
CD47	-0.80879	1.23E-06	5.03E-05	-0.67085	4.72E-05	0.002064
CD83	0.753089	5.25E-08	3.26E-06	0.740821	8.12E-08	1.15E-05
CD93	-1.25124	1.06E-06	4.41E-05	-1.63763	1.10E-10	3.39E-08
CDH1	-1.64122	7.62E-14	1.75E-11	-1.25445	4.49E-09	9.39E-07
CDH20	-2.1501	2.61E-07	1.34E-05	-1.79664	1.53E-05	0.000858
CDK14	1.034444	3.98E-10	4.43E-08	0.6437	4.11E-05	0.001863
CHST11	0.847015	2.15E-10	2.56E-08	0.653469	5.38E-07	5.31E-05
CHST7	1.194629	1.18E-12	2.12E-10	0.809275	3.62E-07	3.88E-05
CISH	1.516252	1.32E-08	1.00E-06	1.076896	1.01E-05	0.000625
CLCF1	5.120227	7.62E-10	7.97E-08	1.878247	8.77E-05	0.003336
CLN8	0.802398	1.85E-08	1.31E-06	0.671084	1.75E-06	0.000146
CMPK2	-1.10012	0.003083	0.031369	-1.37892	8.47E-05	0.003265

Table 2. TREM2 DEGs (3/10)

Gene	Hyb87 vs. PBS			Hyb87 vs. control IgG		
	log_2FC	P value	FDR-adjusted P value	log_2FC	P value	FDR-adjusted P value
COL6A1	1.363504	1.34E-18	5.37E-16	1.114367	7.45E-14	4.36E-11
COL6A2	1.136013	9.08E-14	2.04E-11	1.062741	1.48E-12	7.24E-10
COQ2	-0.85475	2.07E-06	8.00E-05	-0.72195	4.76E-05	0.002075
COX18	-1.06705	3.29E-08	2.16E-06	-0.82561	1.36E-05	0.000785
CPEB2	1.193797	8.10E-07	3.54E-05	0.971634	2.20E-05	0.001155
CPED1	-0.94092	6.93E-08	4.25E-06	-0.919	1.04E-07	1.42E-05
CRLF2	2.700651	2.61E-38	6.54E-35	1.575709	1.64E-19	2.21E-16
CSF1	1.67582	7.21E-22	4.09E-19	1.624429	3.58E-21	5.25E-18
CTDNEP1	-0.78523	3.35E-06	0.000122	-0.6424	0.000122	0.004266
CTGF	2.979976	9.16E-14	2.04E-11	1.774783	1.86E-08	3.20E-06
CTSO	-0.94521	4.83E-06	0.000167	-0.78447	0.00012	0.004234
CXCL5	1.709894	1.99E-06	7.73E-05	1.190042	0.000175	0.005623
CXCR2	-1.2529	1.54E-12	2.66E-10	-1.13988	6.72E-11	2.27E-08
CXCR4	2.207914	6.80E-32	9.20E-29	0.772198	4.46E-07	4.58E-05
CYCSP52	1.270041	1.27E-11	1.88E-09	0.791327	5.88E-06	0.0004
CYP27A1	1.00015	1.87E-12	3.10E-10	0.735004	9.23E-08	1.29E-05
CYP51A1	0.731477	1.53E-07	8.44E-06	0.591146	1.50E-05	0.000849
CYSLTR1	-0.91342	7.90E-09	6.40E-07	-0.86953	2.96E-08	4.96E-06
CYSLTR2	-1.56993	0.000628	0.009289	-1.3992	0.001907	0.035187
DCSTAMP	3.251019	3.27E-28	2.73E-25	2.517492	8.09E-23	1.78E-19
DDX60L	0.74519	2.70E-05	0.000732	0.625756	0.000291	0.008314
DENND1C	-0.98108	1.52E-07	8.40E-06	-0.74558	4.89E-05	0.002111
DENND3	-0.871	9.67E-08	5.72E-06	-0.93076	1.13E-08	2.09E-06
DEPTOR	-1.17422	4.88E-08	3.06E-06	-1.47556	5.24E-12	2.30E-09
DFNB31	1.736877	2.11E-11	2.92E-09	1.026097	7.57E-06	0.000493
DHFR	-0.63398	0.000223	0.004175	-0.73554	1.68E-05	0.00093
DHRS11	1.340098	4.81E-11	6.36E-09	1.150221	3.96E-09	8.38E-07
DHRS3	1.701684	7.12E-14	1.67E-11	1.03738	2.87E-07	3.26E-05
DIXDC1	1.146603	0.001722	0.020404	1.474623	5.59E-05	0.002363
DMPK	-1.69571	3.02E-09	2.78E-07	-1.24884	1.02E-05	0.000625
DNAJB5	0.857709	2.68E-06	0.000101	0.787393	1.07E-05	0.000654
DOT1L	1.469943	6.92E-18	2.59E-15	1.153202	1.37E-12	6.89E-10
DPCD	-1.281	4.29E-07	2.03E-05	-1.07724	1.61E-05	0.000901
DPF3	-1.1529	0.000978	0.013075	-1.11088	0.001139	0.023724
DPH1	-0.67155	0.000631	0.009334	-0.5929	0.002237	0.039173
DPP4	2.677921	2.50E-05	0.000688	1.601624	0.001284	0.025973
DSG2	2.100859	4.77E-06	0.000166	1.442504	0.000325	0.009046
DUSP1	1.02315	1.44E-11	2.08E-09	0.594821	3.83E-05	0.001769
DUSP5	2.757872	1.10E-47	9.71E-44	1.609145	2.85E-24	1.25E-20
ECE1	1.62227	0.002372	0.025752	3.636717	5.99E-08	9.00E-06
EFCAB11	-1.00685	0.002676	0.028101	-1.08017	0.000935	0.020634
EGR1	2.327614	3.22E-13	6.58E-11	1.22653	2.79E-06	0.000217
EGR2	2.018585	5.03E-30	5.53E-27	1.148782	1.16E-13	6.40E-11
EGR3	2.055356	8.32E-16	2.44E-13	1.406665	4.29E-10	1.20E-07
ELOVL7	1.807386	6.30E-08	3.89E-06	1.106479	0.000135	0.004583
EML1	-1.43448	0.002039	0.023106	-1.38565	0.00224	0.039173
EMP1	1.322249	9.07E-16	2.61E-13	0.928122	1.94E-09	4.49E-07
EMR3	-1.15376	0.000144	0.002937	-1.09799	0.000206	0.00637
ENO2	1.266124	6.01E-06	0.000202	0.768919	0.002468	0.041877
ENO3	1.238734	6.33E-12	9.76E-10	0.649478	9.88E-05	0.003611
EPHA2	-0.73698	5.27E-05	0.001286	-0.7702	1.95E-05	0.001056
ETFB	-0.99094	9.83E-09	7.71E-07	-1.00153	5.90E-09	1.18E-06
EVI2B	-0.99728	5.48E-09	4.66E-07	-0.81094	1.46E-06	0.000126
FABP4	4.761956	3.46E-09	3.11E-07	2.2321	9.66E-06	0.000604
FABP5	1.441464	7.15E-25	5.03E-22	0.925182	9.41E-13	4.86E-10
FADS3	0.99642	5.14E-10	5.58E-08	0.798115	2.86E-07	3.26E-05
FAM105A	-0.79997	3.24E-08	2.14E-06	-0.58754	3.55E-05	0.00167
FAM136A	-0.91818	4.09E-07	1.95E-05	-0.67311	0.00016	0.005229

Table 2. TREM2 DEGs (4/10)

Gene	Hyb87 vs. PBS			Hyb87 vs. control IgG		
	log_2FC	P value	FDR-adjusted P value	log_2FC	P value	FDR-adjusted P value
FAM167A	-1.18988	0.000412	0.006779	-1.04579	0.00157	0.030464
FAM195A	0.764307	0.000231	0.004288	0.706143	0.000487	0.012534
FAM20A	1.064331	1.94E-11	2.73E-09	0.590535	8.73E-05	0.003336
FAM40B	2.015263	3.46E-06	0.000125	1.094713	0.002659	0.043974
FAM69A	1.657251	1.01E-06	4.23E-05	1.121187	0.000238	0.007215
FAT1	1.332338	0.00015	0.003048	1.221659	0.000261	0.007751
FCAMR	-2.29587	6.13E-14	1.46E-11	-1.13778	0.000151	0.004996
FCRL4	-4.9812	0.000799	0.011206	-4.94614	0.000654	0.015845
FFAR2	-1.15183	3.44E-08	2.24E-06	-0.60999	0.002959	0.047807
FHDC1	-1.56496	0.00036	0.006121	-1.40844	0.001146	0.023798
FLJ41200	-1.08132	2.25E-09	2.15E-07	-0.80778	5.12E-06	0.000352
FNIP2	0.989375	7.99E-12	1.22E-09	0.607227	1.09E-05	0.000665
FOSL2	1.280777	1.28E-12	2.25E-10	1.035584	2.30E-09	5.26E-07
FOXO1	2.158921	7.19E-18	2.63E-15	1.189584	2.52E-08	4.26E-06
FPR1	-1.1659	1.71E-10	2.08E-08	-0.9722	5.79E-08	8.81E-06
FYN	0.695993	1.19E-06	4.87E-05	0.613998	1.44E-05	0.000819
GADD45B	1.802035	1.46E-25	1.07E-22	1.022053	2.08E-11	8.14E-09
GADD45G	0.83929	1.37E-05	0.000411	0.685376	0.000237	0.007191
GAL	4.038182	4.31E-07	2.04E-05	3.135845	1.68E-06	0.00014
GAL3ST4	-0.82807	3.89E-07	1.88E-05	-1.10118	2.19E-11	8.37E-09
GAPT	-0.97818	2.06E-08	1.45E-06	-0.64374	0.000163	0.0053
GCNT2	-1.70539	0.000143	0.002932	-1.66856	0.00015	0.004995
GEM	4.718891	8.13E-07	3.55E-05	2.984891	1.99E-05	0.00107
GFI1	1.814146	0.000669	0.009759	2.249483	3.02E-05	0.001465
GGPS1	-0.63486	0.001008	0.013379	-0.70321	0.000231	0.007032
GHRL	-1.11637	4.03E-07	1.94E-05	-0.75528	0.000498	0.012672
GJA1	2.087373	4.90E-13	9.59E-11	1.584274	1.13E-09	2.83E-07
GLA	1.038689	9.61E-14	2.11E-11	0.796144	3.95E-09	8.38E-07
GNA13	1.10061	5.51E-16	1.67E-13	0.78822	1.54E-09	3.66E-07
GNAI1	-1.06475	1.08E-07	6.31E-06	-1.1271	1.56E-08	2.77E-06
GNG2	-1.52795	1.19E-19	5.23E-17	-1.24689	2.00E-14	1.26E-11
GNPTAB	1.252126	1.83E-17	6.43E-15	0.880059	3.29E-10	9.34E-08
GPC4	0.986297	6.00E-10	6.43E-08	0.650926	1.98E-05	0.001069
GPD1	1.840573	0.000167	0.003298	1.448283	0.001003	0.021753
GPR137B	1.051289	7.68E-14	1.75E-11	0.762677	1.84E-08	3.20E-06
GPR157	1.665881	1.50E-24	1.01E-21	1.081883	4.43E-13	2.36E-10
GPR183	2.158299	3.51E-36	6.86E-33	1.297074	9.25E-18	1.02E-14
GPR56	-1.9556	1.50E-15	4.18E-13	-1.84423	1.97E-14	1.26E-11
GPRC5C	-1.13993	1.47E-07	8.23E-06	-0.92725	1.40E-05	0.000802
GREM1	5.658393	0.000176	0.003455	2.975063	0.002117	0.037701
GSTO1	1.057339	1.33E-09	1.33E-07	0.749456	7.04E-06	0.000464
GUCY1A2	1.854428	1.87E-06	7.34E-05	1.203369	0.000491	0.01261
HBEGF	1.03832	4.53E-13	9.05E-11	0.629072	4.05E-06	0.000291
HDGFRP3	0.865593	4.02E-08	2.57E-06	0.809656	1.93E-07	2.46E-05
HEATR8	-1.0547	0.000661	0.009669	-0.93421	0.002151	0.03812
HES4	2.071816	5.28E-05	0.001286	1.84938	8.39E-05	0.003242
HFE	-0.65001	0.000382	0.006385	-0.5899	0.001119	0.023432
HINT2	-0.59634	0.000565	0.008611	-0.61932	0.000311	0.008747
HIVEP2	0.836352	0.000198	0.003778	0.935007	2.44E-05	0.001253
HLX	0.690035	9.87E-06	0.000313	0.807344	2.64E-07	3.07E-05
HN1	-0.5872	0.000276	0.004961	-0.60677	0.000167	0.005402
HNRNPUL1	-0.62012	4.80E-05	0.001186	-0.59956	8.00E-05	0.003134
HOMER1	0.669106	0.000499	0.007794	0.624705	0.00089	0.019855
HOMER2	2.877319	9.79E-14	2.11E-11	1.757961	3.13E-08	5.20E-06
HOXB6	-1.35997	0.000274	0.004926	-1.49042	3.69E-05	0.001724
HPGD	-1.11948	1.30E-06	5.28E-05	-0.9312	4.38E-05	0.001953
HSD3B7	1.492208	2.52E-10	2.91E-08	0.875097	3.50E-05	0.001664
HSPA7	-0.58721	7.09E-05	0.001669	-0.85398	1.14E-08	2.09E-06

Table 2. TREM2 DEGs (5/10)

Gene	Hyb87 vs. PBS			Hyb87 vs. control IgG		
	log_2FC	P value	FDR-adjusted P value	log_2FC	P value	FDR-adjusted P value
HTR7	-1.07108	0.000683	0.009932	-1.04318	0.000734	0.017168
HTRA4	2.587009	3.28E-20	1.56E-17	1.452151	2.78E-10	8.00E-08
HVCN1	-0.66984	6.89E-06	0.000228	-0.71326	1.60E-06	0.000136
IARS	0.831357	2.75E-09	2.54E-07	0.798314	8.87E-09	1.69E-06
ICT1	-0.63479	0.000622	0.009214	-0.59543	0.001183	0.024348
IDO1	3.371157	8.45E-26	6.46E-23	1.646929	2.50E-11	9.16E-09
IFITM1	-0.83906	8.09E-05	0.001856	-0.82513	8.49E-05	0.003265
IGSF3	1.02044	3.78E-08	2.43E-06	0.685137	0.000106	0.003788
IL1R2	1.497748	1.33E-10	1.65E-08	1.093987	3.66E-07	3.88E-05
IL1RN	0.781246	1.74E-08	1.26E-06	0.911543	7.98E-11	2.65E-08
IL27RA	0.92509	2.67E-07	1.36E-05	0.653752	0.000149	0.004982
IL3RA	1.199856	5.95E-09	5.03E-07	0.600859	0.001458	0.028663
IL7R	1.636633	1.16E-28	1.02E-25	1.348578	8.93E-22	1.74E-18
ILDR2	-1.02028	8.78E-05	0.001973	-1.3142	2.54E-07	3.00E-05
INSIG1	0.665795	4.13E-06	0.000147	0.741537	3.14E-07	3.54E-05
IRF4	2.080963	2.89E-30	3.39E-27	1.019466	3.61E-11	1.27E-08
ITGA4	-0.72131	2.80E-07	1.42E-05	-0.60684	1.25E-05	0.000743
ITGB1BP2	-1.78781	6.96E-10	7.42E-08	-1.41089	8.41E-07	7.78E-05
ITGB3	1.917049	1.58E-10	1.94E-08	1.090682	2.71E-05	0.00135
ITGB8	1.435409	2.54E-10	2.91E-08	1.564729	4.08E-12	1.84E-09
JAK1	0.940333	1.63E-12	2.72E-10	0.658386	3.16E-07	3.54E-05
KCNE1L	2.121521	1.96E-10	2.36E-08	1.061147	0.000108	0.003852
KCNH2	5.111255	0.005343	0.047036	5.111255	0.002614	0.043641
KIAA1467	0.729229	0.000323	0.005612	0.590922	0.002543	0.042777
KIAA1598	0.625359	8.68E-06	0.000282	0.614394	1.13E-05	0.000685
KIFC1	-1.38969	2.27E-07	1.19E-05	-1.18151	8.15E-06	0.000523
KLRC4	-1.08265	1.22E-05	0.000375	-1.25915	2.05E-07	2.59E-05
LAD1	1.78559	1.64E-21	9.00E-19	1.481391	9.92E-17	9.68E-14
LAG3	-1.84657	3.89E-05	0.000994	-1.61344	0.000281	0.008086
LAMC1	0.872577	4.26E-09	3.71E-07	0.65089	6.75E-06	0.00045
LAMP3	1.322578	3.48E-19	1.46E-16	0.978656	3.86E-12	1.78E-09
LAT	1.396787	9.66E-08	5.72E-06	0.879922	0.0002	0.006254
LDB1	-0.829	6.64E-07	2.97E-05	-0.79724	1.50E-06	0.000129
LDHAL6B	1.020593	2.91E-06	0.000108	0.83403	6.48E-05	0.002638
LDLR	0.902188	5.93E-07	2.71E-05	0.721177	3.51E-05	0.001664
LDLRAD4	-0.97074	1.75E-07	9.52E-06	-0.82733	6.46E-06	0.000433
LEPROTL1	-0.71437	3.24E-05	0.000853	-0.64565	0.000149	0.004982
LGALS12	-1.73769	1.59E-12	2.68E-10	-1.55224	1.37E-10	4.15E-08
LGALS3	1.000246	9.00E-12	1.36E-09	0.804864	1.98E-08	3.38E-06
LINC00152	1.452354	1.37E-05	0.000411	0.938939	0.00167	0.032035
LINC00623	-0.85186	0.000172	0.003394	-0.73599	0.000998	0.02167
LIPN	1.419103	9.20E-07	3.93E-05	0.872255	0.000802	0.018271
LMO7	-0.96386	4.08E-07	1.95E-05	-0.69927	0.000185	0.005859
LMTK2	-0.86342	6.30E-07	2.83E-05	-0.70568	3.59E-05	0.001681
LOC440905	-1.04575	0.003653	0.035458	-1.05044	0.002768	0.045365
LOC730101	1.765865	2.69E-07	1.37E-05	1.333826	2.17E-05	0.001155
LOX	3.417947	0.000362	0.006145	3.185272	0.000259	0.00773
LPL	2.240047	1.98E-41	5.79E-38	1.450938	2.89E-23	7.25E-20
LRMP	-0.6885	2.76E-05	0.000745	-0.83966	3.27E-07	3.62E-05
LRRC37A6P	-0.86655	3.49E-05	0.000905	-0.99851	1.40E-06	0.000122
LRRC4	-0.85732	9.22E-06	0.000297	-0.85862	6.99E-06	0.000462
LTB	-1.62417	5.25E-16	1.62E-13	-1.37479	2.14E-12	1.02E-09
MAN1A1	0.705662	1.96E-06	7.64E-05	0.598347	4.05E-05	0.001851
MAOA	0.757506	3.37E-07	1.67E-05	0.646098	9.92E-06	0.000614
MAP2K3	0.811414	7.00E-08	4.27E-06	0.622213	2.20E-05	0.001155
MAP3K14	1.221237	5.98E-13	1.12E-10	0.673025	2.03E-05	0.001089
MAP4K4	1.304754	3.98E-11	5.31E-09	0.734904	5.38E-05	0.002288
MAPK13	0.927275	2.18E-10	2.57E-08	0.683564	1.39E-06	0.000122

Table 2. TREM2 DEGs (6/10)

Gene	Hyb87 vs. PBS			Hyb87 vs. control IgG		
	log_2FC	P value	FDR-adjusted P value	log_2FC	P value	FDR-adjusted P value
MAPK8IP2	1.065326	0.001984	0.022686	1.547783	1.13E-05	0.000685
MATK	2.212029	1.07E-26	8.53E-24	1.401707	1.00E-14	7.05E-12
MCAM	1.849673	8.71E-05	0.001969	1.409934	0.000765	0.017733
MCF2L	-1.18606	4.77E-05	0.001181	-1.38241	1.38E-06	0.000122
MCOLN3	0.762099	8.79E-05	0.001973	0.671277	0.000388	0.01042
MEF2B	-1.01511	0.000318	0.005529	-0.82548	0.003008	0.0481
METTL1	1.3541	5.31E-13	1.03E-10	0.904854	2.35E-07	2.83E-05
METTL14	-1.41197	5.55E-07	2.54E-05	-1.12056	5.76E-05	0.002399
MFGE8	1.270327	3.44E-09	3.10E-07	0.621289	0.001539	0.029958
MFI2	0.930181	1.84E-05	0.000527	0.806675	0.000126	0.004372
MGST1	0.94308	5.09E-07	2.36E-05	0.754511	2.37E-05	0.001224
MICALL2	1.336554	5.05E-05	0.00124	1.028592	0.000769	0.017786
MIR155HG	1.353777	8.84E-06	0.000285	1.229973	2.29E-05	0.001194
MITF	0.738675	4.96E-07	2.31E-05	0.780125	1.01E-07	1.39E-05
MLEC	-0.82141	8.16E-08	4.96E-06	-0.69927	3.75E-06	0.000273
MMD	-0.88849	1.69E-08	1.22E-06	-0.60544	8.51E-05	0.003268
MMP10	6.22042	8.10E-06	0.000264	3.029631	0.000307	0.008654
MMP15	-1.4462	1.16E-10	1.46E-08	-1.24653	1.58E-08	2.79E-06
MMP19	1.121156	8.45E-10	8.74E-08	0.887056	4.65E-07	4.70E-05
MPI	-0.58533	0.001964	0.022554	-0.67198	0.000335	0.009265
MPZL3	-0.80232	8.63E-05	0.001958	-0.92955	4.41E-06	0.000311
MREG	2.393957	2.25E-34	3.59E-31	1.790311	9.61E-24	2.82E-20
MS4A6A	-0.83784	5.58E-10	6.02E-08	-0.90242	3.13E-11	1.12E-08
MSTO2P	-1.37454	7.54E-05	0.001755	-1.24802	0.000256	0.00767
MT1H	-2.3111	0.000396	0.006559	-2.05456	0.001487	0.029104
MTMR9LP	-1.01905	0.000147	0.002992	-0.92235	0.000488	0.01254
MTPAP	-0.65842	0.00033	0.005676	-0.58699	0.001198	0.02454
MYBPH	1.11826	3.95E-06	0.000142	0.914207	8.02E-05	0.003134
MYCBP	-1.04859	1.17E-07	6.73E-06	-0.75542	0.000102	0.003697
MYLK4	-1.37978	0.003005	0.030781	-1.37492	0.002362	0.040578
MYO1E	0.892888	1.33E-11	1.93E-09	0.647323	4.41E-07	4.58E-05
MYO5C	-1.62705	3.16E-06	0.000116	-1.42691	3.51E-05	0.001664
N4BP2L1	0.936653	2.43E-05	0.000675	0.775364	0.000282	0.00809
NAPSB	-0.8271	9.33E-06	0.0003	-0.83114	5.98E-06	0.000405
NCAM1	1.274306	8.49E-18	3.05E-15	0.716036	2.28E-07	2.76E-05
NCCRP1	2.111259	5.04E-12	7.85E-10	1.783187	4.52E-10	1.24E-07
NDFIP2	0.962055	8.25E-07	3.59E-05	0.706566	0.00016	0.005229
NDUFA11	-0.99563	1.45E-08	1.07E-06	-0.8881	3.28E-07	3.62E-05
NFAM1	-0.92352	4.75E-09	4.09E-07	-0.91547	5.33E-09	1.08E-06
NFATC2	-0.98547	1.23E-07	7.02E-06	-0.93214	4.49E-07	4.59E-05
NFE2L1	-0.77092	4.86E-07	2.27E-05	-0.67849	7.92E-06	0.000512
NMB	0.960181	0.004369	0.04032	1.004745	0.002056	0.036742
NOP9	-0.67999	0.000879	0.012118	-0.84599	2.85E-05	0.001399
NOTCH3	0.994516	2.14E-08	1.50E-06	0.730824	1.93E-05	0.001047
NR4A3	2.677025	7.81E-45	3.43E-41	1.364275	9.18E-19	1.15E-15
NREP	-1.01441	1.50E-05	0.000444	-1.03226	6.69E-06	0.000447
NRIP3	1.46097	3.28E-14	8.13E-12	1.52147	1.84E-15	1.47E-12
NRP2	0.971675	4.65E-12	7.30E-10	0.940941	1.61E-11	6.43E-09
NSUN4	-0.62092	0.003024	0.030906	-0.76856	0.000196	0.006162
NUAK2	2.401826	5.46E-09	4.66E-07	1.07491	0.001192	0.024459
O3FAR1	-0.59761	0.000306	0.00536	-0.90682	4.72E-08	7.41E-06
OBSL1	-1.12588	3.65E-05	0.000939	-1.16454	1.30E-05	0.000766
OLFM1	-2.27536	1.39E-09	1.38E-07	-1.34273	0.000503	0.012756
OMA1	-0.7577	4.58E-05	0.001146	-0.61361	0.000818	0.018571
OPHN1	-0.95592	1.77E-05	0.000513	-1.04791	1.94E-06	0.000157
OSCAR	-0.9856	3.89E-05	0.000994	-1.01478	1.73E-05	0.000954
OTUD7B	0.897348	1.52E-05	0.00045	0.59299	0.002567	0.043026
OXNAD1	-1.12809	6.50E-05	0.001555	-1.09929	7.69E-05	0.003045

Table 2. TREM2 DEGs (7/10)

Gene	Hyb87 vs. PBS			Hyb87 vs. control IgG		
	log_2FC	P value	FDR-adjusted P value	log_2FC	P value	FDR-adjusted P value
P2RX7	0.616932	9.42E-05	0.002093	0.73502	3.45E-06	0.000254
P2RY10	0.999477	6.24E-09	5.20E-07	0.671109	4.07E-05	0.001854
P2RY12	-1.67018	0.000123	0.002605	-2.42162	1.33E-09	3.25E-07
P2RY13	-2.24641	7.68E-24	5.00E-21	-2.3478	8.71E-26	1.53E-21
PALD1	-1.33953	3.35E-16	1.05E-13	-1.21313	6.08E-14	3.68E-11
PAQR5	1.674903	1.68E-11	2.38E-09	1.390129	1.50E-09	3.61E-07
PAQR7	-0.75779	0.000684	0.009932	-0.74258	0.000726	0.017042
PARM1	-0.92734	9.07E-11	1.15E-08	-0.7017	5.27E-07	5.24E-05
PCDHGB7	-1.00697	7.10E-09	5.80E-07	-0.76792	6.80E-06	0.000451
PCDHGC3	-0.8974	0.004456	0.040885	-0.98342	0.001271	0.025778
PCYOX1L	-0.88879	6.78E-08	4.17E-06	-0.75752	3.06E-06	0.000234
PDE1B	-0.77319	2.32E-05	0.00065	-0.6922	0.000126	0.004372
PDE7A	0.756091	4.30E-06	0.000153	0.61125	0.000136	0.004619
PDGFA	0.68403	0.000101	0.002237	0.958027	8.38E-08	1.18E-05
PDLIM4	1.20078	2.34E-07	1.22E-05	1.107594	8.09E-07	7.57E-05
PELI3	1.180298	1.60E-05	0.000468	0.737163	0.003162	0.049989
PFKP	1.802524	6.96E-20	3.14E-17	1.369095	8.17E-14	4.63E-11
PHF16	1.40985	8.52E-10	8.76E-08	0.888179	2.52E-05	0.001268
PIK3R3	1.176189	1.34E-08	1.01E-06	0.756563	9.26E-05	0.00347
PIM1	1.081229	2.73E-11	3.72E-09	0.679648	9.86E-06	0.000612
PIM2	0.772548	2.81E-07	1.42E-05	0.795151	1.13E-07	1.50E-05
PIM3	1.033572	2.02E-11	2.82E-09	0.754879	3.65E-07	3.88E-05
PLA2G7	0.92062	2.96E-11	4.01E-09	0.614773	4.62E-06	0.000325
PLAC8	-2.25181	7.97E-30	7.78E-27	-1.9372	4.34E-24	1.53E-20
PLAUR	0.637268	5.00E-07	2.32E-05	0.696748	4.54E-08	7.19E-06
PLCD3	1.072448	3.96E-05	0.00101	0.759246	0.001966	0.035786
PLCL1	1.2043	2.50E-12	3.96E-10	0.842468	2.38E-07	2.84E-05
PLEK2	-1.00256	4.33E-06	0.000154	-0.68094	0.001552	0.030189
PLEKHA5	1.231389	1.43E-08	1.07E-06	0.852988	2.52E-05	0.001268
PLEKHA7	-0.78248	0.000556	0.008492	-1.13821	3.31E-07	3.62E-05
PLXNA3	0.812849	1.84E-07	9.90E-06	0.706478	4.13E-06	0.000295
POLD4	-0.7357	4.07E-07	1.95E-05	-0.68328	2.20E-06	0.000174
POLR2J2	-0.84272	0.005207	0.046189	-0.97863	0.000828	0.018736
POPDC3	2.714808	1.85E-08	1.31E-06	1.482371	0.000123	0.004311
POR	0.894007	9.65E-08	5.72E-06	0.597833	0.000201	0.00626
PPARG	1.399579	1.81E-07	9.77E-06	0.985433	4.86E-05	0.002109
PPM1K	1.317698	1.20E-12	2.14E-10	0.760753	9.14E-06	0.000574
PPP1R14C	1.027593	3.27E-05	0.000859	0.902876	0.00013	0.004428
PQLC3	-0.61424	0.000949	0.01282	-0.62209	0.000729	0.017058
PRAM1	-0.87319	6.37E-07	2.86E-05	-1.00013	1.02E-08	1.93E-06
PRKACA	-1.09137	8.91E-11	1.14E-08	-0.65491	5.72E-05	0.002391
PRMT7	-0.76698	0.000357	0.006088	-0.75223	0.000381	0.010243
PSD4	-0.91594	6.74E-05	0.001604	-0.70609	0.001816	0.033899
PSMB8	-0.97783	8.76E-06	0.000284	-0.81736	0.000162	0.005268
PTPLAD2	-0.60361	0.002089	0.023542	-0.71135	0.000224	0.006816
PTRF	1.786351	8.78E-21	4.54E-18	1.188062	6.39E-12	2.74E-09
PYCARD	-1.03619	5.07E-10	5.54E-08	-0.97593	3.51E-09	7.71E-07
RAB38	1.528936	9.12E-05	0.002035	1.314142	0.000273	0.007962
RAB3IL1	-0.79637	7.33E-06	0.00024	-1.22435	9.43E-12	3.85E-09
RAD51B	-3.65917	0.001878	0.021875	-3.70875	0.001066	0.022643
RAE1	-0.75023	2.47E-05	0.000684	-0.68673	9.61E-05	0.00354
RAI14	3.570621	0.000502	0.007817	3.025517	0.000565	0.014084
RALA	0.753826	0.001419	0.017535	0.899156	0.00012	0.004222
RAPGEF1	1.220329	2.69E-08	1.82E-06	1.2729	3.74E-09	8.11E-07
RARRES2	1.67727	3.13E-08	2.09E-06	0.841744	0.001815	0.033899
RASAL3	-0.68695	6.16E-06	0.000206	-0.68415	5.89E-06	0.0004
RASGRP4	-1.05971	4.36E-08	2.76E-06	-0.90438	2.11E-06	0.000169
RCN3	-0.98594	1.27E-07	7.23E-06	-0.76965	2.73E-05	0.001354

Table 2. TREM2 DEGs (8/10)

Gene	Hyb87 vs. PBS			Hyb87 vs. control IgG		
	log_2FC	P value	FDR-adjusted P value	log_2FC	P value	FDR-adjusted P value
REG4	-1.14869	0.002041	0.023106	-1.24813	0.000545	0.01365
REL	1.091454	8.59E-15	2.25E-12	0.883107	1.08E-10	3.38E-08
RERE	-0.99183	5.63E-06	0.000191	-0.71137	0.000956	0.021002
RGCC	2.656203	5.67E-38	1.24E-34	1.847352	6.23E-25	5.48E-21
RGS13	3.628101	1.20E-14	3.11E-12	1.17144	0.000101	0.003697
RGS14	-0.67849	0.001338	0.01675	-1.08167	2.20E-07	2.70E-05
RHOJ	-2.10985	0.003655	0.035458	-2.64072	0.000103	0.003726
RIPK2	0.780045	1.38E-06	5.55E-05	0.666509	2.49E-05	0.001262
RMI2	-0.83479	0.000371	0.006248	-0.89671	9.80E-05	0.003589
RNASET2	-0.70548	5.63E-06	0.000191	-0.63946	3.43E-05	0.001652
RNF219	-0.64713	0.001417	0.017535	-0.59441	0.00298	0.047976
ROGDI	-0.78098	0.002808	0.029163	-0.80519	0.001622	0.031264
RSAD2	2.29009	7.59E-05	0.001763	1.446054	0.00251	0.042382
RUFY4	-1.27277	6.41E-06	0.000213	-1.14068	3.91E-05	0.001797
RXRA	-1.00114	2.15E-10	2.56E-08	-1.04069	4.44E-11	1.53E-08
RYR1	-2.42385	2.05E-09	1.98E-07	-2.44152	8.98E-10	2.29E-07
S100Z	-2.10653	1.36E-12	2.37E-10	-1.8094	6.19E-10	1.62E-07
SATB1	1.394734	2.52E-17	8.69E-15	0.820722	6.95E-08	1.01E-05
SDC1	1.59147	3.44E-06	0.000125	1.006512	0.001038	0.02228
SDS	1.595642	3.58E-20	1.65E-17	0.804117	2.11E-07	2.63E-05
SEC14L2	5.697793	0.000278	0.004963	3.007259	0.002988	0.047976
SEMA3C	2.158466	2.36E-12	3.78E-10	1.024375	3.33E-05	0.001609
SEMA4C	-0.66264	1.60E-06	6.33E-05	-0.76036	4.38E-08	7.07E-06
SEMA4D	-0.7105	2.16E-05	0.000612	-0.83358	6.43E-07	6.25E-05
SERPINE1	2.32073	3.60E-13	7.27E-11	1.438145	1.04E-07	1.42E-05
SERPING1	-0.58627	0.004386	0.040434	-0.62607	0.002034	0.036568
SESN3	-0.73327	0.000483	0.007614	-0.74833	0.000275	0.007977
SGMS2	1.052244	0.000951	0.012829	1.101817	0.000315	0.008793
SH3BP5	0.612159	0.004801	0.043329	0.760298	0.000395	0.010531
SH3D19	1.499088	5.79E-14	1.39E-11	0.888302	1.01E-06	9.05E-05
SH3D21	1.027066	1.93E-07	1.03E-05	0.693367	0.00021	0.006447
SH3RF1	-1.1814	1.22E-07	7.01E-06	-0.82988	0.000159	0.005218
SIDT2	-0.81046	1.23E-06	5.03E-05	-0.78361	2.17E-06	0.000172
SIGLEC10	-0.6194	0.000108	0.002358	-0.79173	7.44E-07	7.03E-05
SIRPB2	-0.67437	0.000607	0.009054	-0.68393	0.000416	0.011023
SLC12A9	-0.74873	6.70E-06	0.000223	-0.89463	7.31E-08	1.05E-05
SLC1A4	-0.73779	1.40E-06	5.63E-05	-0.65665	1.50E-05	0.000849
SLC20A2	-0.75268	0.000388	0.006448	-0.72573	0.000523	0.013174
SLC25A23	-0.64541	3.49E-05	0.000905	-0.61112	7.68E-05	0.003045
SLC26A11	1.112548	3.92E-11	5.26E-09	0.737704	3.46E-06	0.000254
SLC29A1	-0.58897	3.98E-05	0.001014	-0.63775	8.48E-06	0.00054
SLC35E3	0.832359	2.29E-06	8.77E-05	0.659376	0.000109	0.003879
SLC41A2	1.278019	2.97E-16	9.49E-14	0.952834	1.69E-10	4.95E-08
SLC44A1	0.927917	3.12E-09	2.86E-07	0.886582	1.05E-08	1.96E-06
SLC46A3	-0.64945	0.000117	0.002512	-0.86025	3.51E-07	3.81E-05
SLC5A3	0.909141	3.36E-07	1.67E-05	0.73514	2.20E-05	0.001155
SLC7A11	1.330262	1.39E-18	5.42E-16	1.150711	5.77E-15	4.22E-12
SLC7A5	-0.85549	3.25E-08	2.14E-06	-0.70055	4.39E-06	0.000311
SLC7A7	-0.62963	1.05E-05	0.000329	-0.73738	2.82E-07	3.24E-05
SLC9A3R2	-1.46194	0.000127	0.00266	-1.18903	0.001689	0.032281
SLCO4A1	0.805608	0.001794	0.021079	0.743542	0.002834	0.046175
SLCO4C1	-1.39367	1.42E-09	1.40E-07	-1.3405	3.01E-09	6.78E-07
SLFN13	-1.82643	5.83E-06	0.000197	-1.27448	0.001673	0.032035
SMAD3	-1.28811	6.18E-09	5.18E-07	-0.83513	0.000122	0.004266
SMIM3	0.977782	1.12E-07	6.49E-06	0.669803	0.00014	0.004736
SNX25	0.605548	0.002054	0.02322	0.701481	0.000312	0.008747
SOD2	0.698159	8.50E-08	5.10E-06	0.740971	1.51E-08	2.71E-06
SPATS2	0.632253	0.000211	0.003993	0.610463	0.000279	0.008064

Table 2. TREM2 DEGs (9/10)

Gene	Hyb87 vs. PBS			Hyb87 vs. control IgG		
	log_2FC	P value	FDR-adjusted P value	log_2FC	P value	FDR-adjusted P value
SPHK1	1.310071	2.00E-15	5.40E-13	0.967957	5.90E-10	1.57E-07
SPOCD1	6.768394	1.45E-08	1.07E-06	2.444419	5.23E-05	0.002246
SPTBN1	-0.76953	8.70E-07	3.74E-05	-0.63299	4.19E-05	0.001886
SRFBP1	-0.93338	1.43E-07	7.99E-06	-0.6761	0.000105	0.003771
SRSF3	-1.05005	2.29E-10	2.68E-08	-0.77144	1.83E-06	0.00015
ST14	-0.87991	8.74E-09	6.95E-07	-0.94277	6.76E-10	1.75E-07
ST3GAL6	1.780098	2.55E-09	2.40E-07	1.418888	2.21E-07	2.70E-05
STAC3	-1.26637	2.12E-05	0.0006	-0.94956	0.001295	0.026118
STARD10	-0.66637	0.000175	0.003445	-0.59126	0.000774	0.017804
STAT4	1.392584	3.68E-08	2.38E-06	0.776719	0.000655	0.015845
STK10	-0.72891	2.32E-06	8.83E-05	-0.6655	1.37E-05	0.00079
STX4	0.592317	1.20E-05	0.000371	0.643483	2.04E-06	0.000165
SUCLG2	-0.65352	0.0005	0.007804	-0.6588	0.000393	0.010501
SUMF1	-0.62682	9.94E-05	0.002197	-0.65	4.88E-05	0.002111
SUSD3	-0.7682	1.55E-06	6.19E-05	-0.83885	1.41E-07	1.82E-05
SYNGAP1	0.666051	0.000273	0.004913	0.789094	1.50E-05	0.000849
SYTL1	-1.8963	4.39E-10	4.85E-08	-1.61892	6.82E-08	9.99E-06
TAC1	3.590437	2.15E-13	4.51E-11	1.903326	1.13E-07	1.50E-05
TACSTD2	-2.54122	4.45E-32	6.52E-29	-1.93803	1.05E-21	1.84E-18
TBC1D14	-0.5898	0.000265	0.004809	-0.77837	1.65E-06	0.000138
TBC1D22A	-0.62512	0.000277	0.004963	-0.62848	0.000232	0.007032
TBC1D8	1.211237	1.71E-16	5.55E-14	0.672309	9.85E-07	8.88E-05
TBX3	0.67429	0.00017	0.003356	0.659835	0.000196	0.006162
TCP11L2	1.219118	8.59E-13	1.57E-10	0.745829	2.85E-06	0.000221
TDP2	0.670348	4.60E-06	0.000161	0.633157	1.32E-05	0.000774
TES	-0.66292	4.72E-05	0.001171	-0.59188	0.000246	0.007415
TESK2	1.429673	7.29E-13	1.35E-10	0.845621	3.15E-06	0.000235
TFPI	1.257634	1.86E-13	3.94E-11	0.935949	8.19E-09	1.58E-06
TFPI2	7.190562	2.49E-08	1.70E-06	2.111071	0.000748	0.017395
TFRC	1.46328	1.39E-23	8.75E-21	1.146415	1.92E-16	1.69E-13
TGFA	2.361948	3.13E-20	1.53E-17	0.976482	1.78E-06	0.000147
TGFBI	1.137023	1.15E-16	3.83E-14	0.743494	1.28E-08	2.33E-06
TGM2	1.481905	1.04E-15	2.94E-13	0.991355	6.53E-09	1.28E-06
TIMP3	3.140087	1.50E-55	2.64E-51	1.594968	1.85E-24	1.09E-20
TJP2	0.937184	9.74E-07	4.10E-05	0.668409	0.000264	0.007783
TK2	-0.71295	1.88E-06	7.39E-05	-0.61246	3.49E-05	0.001664
TLCD2	-1.22403	1.24E-06	5.04E-05	-1.01252	4.66E-05	0.002054
TLE1	1.69552	2.43E-08	1.67E-06	1.119197	3.71E-05	0.001731
TLR10	-1.88103	2.63E-09	2.45E-07	-1.64738	1.21E-07	1.60E-05
TM4SF19	1.941344	9.29E-13	1.68E-10	1.465235	1.68E-09	3.94E-07
TMEM154	-1.2252	7.85E-05	0.001814	-1.39211	3.69E-06	0.000269
TMEM158	1.162082	7.12E-07	3.14E-05	0.860682	9.48E-05	0.003522
TMEM169	-0.84033	0.000326	0.005645	-1.0738	3.27E-06	0.000242
TMEM194A	0.749721	1.84E-05	0.000527	1.043902	4.67E-09	9.66E-07
TMEM51	-1.29184	4.91E-13	9.59E-11	-0.95008	4.20E-08	6.84E-06
TMEM92	-1.53401	0.000159	0.003193	-1.80751	3.15E-06	0.000235
TNFRSF12A	0.929378	1.35E-06	5.47E-05	0.690958	0.000166	0.005368
TNFRSF18	1.315637	7.83E-10	8.15E-08	0.764333	0.000116	0.004105
TNFRSF4	0.790729	0.000246	0.004521	0.941734	1.18E-05	0.000703
TNFRSF9	0.647375	1.29E-05	0.00039	0.691085	3.14E-06	0.000235
TNFSF10	-1.4596	2.63E-08	1.79E-06	-1.40741	4.85E-08	7.55E-06
TNFSF13	-0.61649	1.83E-05	0.000527	-0.74328	2.70E-07	3.13E-05
TOMM40L	-0.73445	0.000647	0.009512	-0.99154	2.94E-06	0.000226
TOX	-1.56397	0.000153	0.003087	-2.07806	7.46E-08	1.07E-05
TOX2	-0.91788	4.24E-05	0.001068	-0.99605	6.21E-06	0.000418
TPST2	-0.80052	4.74E-08	2.99E-06	-0.63367	1.14E-05	0.000686
TRAF5	1.762699	3.77E-07	1.84E-05	0.916581	0.002153	0.03812
TRIM22	-0.65226	0.000123	0.002604	-0.66129	9.04E-05	0.003417

Table 2. TREM2 DEGs (10/10)

Gene	Hyb87 vs. PBS			Hyb87 vs. control IgG		
	log_2FC	P value	FDR-adjusted P value	log_2FC	P value	FDR-adjusted P value
TSC22D1	0.729303	1.57E-06	6.25E-05	0.826827	5.60E-08	8.63E-06
TTC39B	0.729287	0.002117	0.023801	1.000866	2.49E-05	0.001262
TUBA4A	1.91624	3.33E-05	0.00087	1.396385	0.000635	0.015507
TUBA8	2.264006	1.08E-06	4.48E-05	1.61576	5.66E-05	0.002372
TUBB6	0.772663	1.10E-06	4.55E-05	0.64767	2.93E-05	0.001432
UCHL1	1.068077	3.00E-05	0.000801	0.993121	6.35E-05	0.002601
UFSP2	-1.07175	1.49E-06	5.94E-05	-0.91708	2.92E-05	0.00143
UPB1	1.507977	0.000215	0.004048	1.815879	8.55E-06	0.000541
UXS1	0.770554	3.87E-07	1.88E-05	0.657729	1.07E-05	0.000654
VASP	-0.6347	4.59E-05	0.001146	-0.62423	5.65E-05	0.002372
VEGFA	1.628075	4.11E-21	2.19E-18	0.850124	3.36E-08	5.53E-06
VSIG4	-0.59139	1.60E-05	0.000468	-0.69792	4.30E-07	4.50E-05
WDFY2	-1.36385	2.63E-13	5.44E-11	-0.93788	2.07E-07	2.60E-05
WDR77	-0.9764	2.54E-08	1.73E-06	-0.8698	5.26E-07	5.24E-05
WDR92	-1.21694	5.45E-05	0.001326	-0.92466	0.001957	0.035786
WNT10B	0.656387	0.004606	0.04198	0.767591	0.000785	0.017983
XIRP1	6.069261	1.28E-05	0.000388	3.38565	0.000155	0.00511
XPO5	-0.81458	0.000123	0.002604	-0.6888	0.001037	0.02228
ZBTB2	-0.68507	0.000752	0.010704	-0.74699	0.0002	0.006252
ZDHHC18	0.93428	3.62E-10	4.06E-08	0.63594	9.72E-06	0.000606
ZMIZ1	1.154419	3.85E-14	9.40E-12	0.669568	3.07E-06	0.000234
ZMYND15	0.962136	1.95E-08	1.38E-06	0.633531	0.000105	0.003771
ZNF462	0.735097	1.77E-05	0.000514	0.660509	8.75E-05	0.003336
ZNF467	-0.88772	2.65E-05	0.000724	-0.76403	0.00024	0.007244
ZNF565	-1.05403	0.000134	0.002776	-0.96527	0.000375	0.010116
ZNF641	-0.75107	1.27E-05	0.000385	-0.62033	0.00026	0.007733
ZNRF1	0.936507	4.28E-07	2.03E-05	0.712081	6.52E-05	0.002647

Table 3. Pathway enrichment analysis of TREM2 DEGs (1/3)

Pathway	Total	P value	FDR-adjusted P value	In Data	Genes
Immune response_TSLP signalling	39	3.02E-07	0.000317	8	IL7RA, p38 MAPK, JAK1, CISH, STAT4, CRLF2, PI3K reg class IA, TSLPR
Th2 cytokine-induced alternative activation of alveolar macrophages in asthma	32	1.07E-06	0.00042	7	TGM2, Galectin-3, IRF4, CXCR4, CCL22, Eotaxin-2, TSLPR
Immune response_IL-4-induced regulators of cell growth, survival, differentiation and metabolism	62	1.2E-06	0.00042	9	PPAR-γ, CISH, FKHR, A-FABP, LPL, EGR2 (Krox20), Cyclin A, GFI-1, ATP6V1B2
IL-6 signaling pathway in lung cancer	35	2.05E-06	0.000538	7	p38 MAPK, JAK1, MEK3(MAP2K3), VEGF-A, MMP-10, ENO2, PI3K reg class IA
Immune response_IL-4-responsive genes in type 2 immunity	70	3.41E-06	0.000716	9	PPAR-γ, c-Rel (NF-kB subunit), FKHR, IL1RN, TFF3, CCL22, CCL1, Eotaxin-2, CCL7
Transcription_HIF-1 targets	95	6.13E-06	0.001023	10	TfR1, TGM2, PAI1, CXCR4, PLAUR (uPAR), MDR1, AK3, CTGF, Lysyl oxidase, VEGF-A
G protein-coupled receptors signaling in lung cancer	76	6.81E-06	0.001023	9	HB-EGF, TGF-α, Galanin, Galpha(q)-specific peptide GPCRs, CXCR4, Galpha(i)-specific peptide GPCRs, VEGF-A, HB-EGF(mature), G-protein α-12 family
Immune response_IL-17 signaling pathways	60	9.16E-06	0.001203	8	p38 MAPK, JAK1, MEK3(MAP2K3), ENA-78, NIK(MAP3K14), PI3K reg class IA, CCL7, GCP2
Putative pathways for stimulation of fat cell differentiation by Bisphenol A	32	1.68E-05	0.001959	6	PPAR-γ, FKHR, A-FABP, LPL, PI3K reg class IA, GPD1
Development_Stimulation of differentiation of mouse embryonic fibroblasts into adipocytes by extracellular factors	71	3.23E-05	0.003249	8	HIVEP2, PPAR-γ, p38 MAPK, FKHR, A-FABP, LPL, Lysyl oxidase, EGR2 (Krox20)
Development_Beta adrenergic receptors in brown adipocyte differentiation	36	3.4E-05	0.003249	6	PPAR-γ, p38 MAPK, MEK3(MAP2K3), A-FABP, LPL, EGR2 (Krox20)
Immune response_Oncostatin M signaling via MAPK	37	4E-05	0.003285	6	PPAR-γ, p38 MAPK, JAK1, MEK3(MAP2K3), EGR1, LDLR
ERBB family and HGF signaling in gastric cancer	54	4.06E-05	0.003285	7	p38 MAPK, HB-EGF, TGF-α, MEK3(MAP2K3), EGR1, VEGF-A, PI3K reg class IA
Immune response_IL-5 signaling via JAK/STAT	56	5.17E-05	0.00372	7	JAK1, Pim-1, CISH, DUSP5, MKP-1, c-IAP2, VEGF-A
Signal transduction_Angiotensin II/AGTR1 signaling via Notch, Beta-catenin and NF-kB pathways	76	5.31E-05	0.00372	8	p38 MAPK, Axin2, NOTCH3 (3ICD), Connexin 43, CTGF, NOTCH3, VEGF-A, NIK(MAP3K14)
Role of activation of WNT signaling in the progression of lung cancer	77	5.84E-05	0.003834	8	p38 MAPK, Axin, Axin2, WNT10B, CD147, NOTCH3, VEGF-A, WNT
HBV-dependent transcription regulation leading to HCC	25	6.31E-05	0.003903	5	PPAR-γ, EGR3, ATF-3, EGR1, EGR2 (Krox20)
Development_NOTCH in inhibition of WNT/Beta-catenin-induced osteogenesis	42	8.39E-05	0.004899	6	PPAR-γ, Axin, TLE1, WNT10B, A-FABP, WNT

Table 3. Pathway enrichment analysis of TREM2 DEGs (2/3)

Pathway	Total	P value	FDR-adjusted P value	In Data	Genes
Neurogenesis_NGF/ TrkA MAPK-mediated signaling	105	9.27E-05	0.005128	9	p38 MAPK, SPHK1, HB-EGF, C3G, MEK3(MAP2K3), EGR1, PLAUR (uPAR), MMP-10, MATK
Vascular endothelial cell damage in SLE	63	0.000111	0.005838	7	p38 MAPK, PAI1, IL1RN, FN14(TNFRSF12A), IL1R2, VEGF-A, CSF1
Immune response_TNF-R2 signaling pathways	45	0.000125	0.006241	6	p38 MAPK, Bim, c-IAP1, c-IAP2, NIK(MAP3K14), PI3K reg class IA
Immune response_CD137 signaling in immune cell	29	0.000133	0.006367	5	p38 MAPK, Bim, CD137(TNFRSF9), MEK3(MAP2K3), NIK(MAP3K14)
Cytoskeleton remodeling_Substance P mediated membrane blebbing					Substance P extracellular region, Tubulin α, G-protein α-12 family, Tubulin (in microtubules)
Cytoskeleton remodeling_Substance P mediated membrane blebbing	16	0.000142	0.006479	4	Substance P extracellular region, Tubulin α, G-protein α-12 family, Tubulin (in microtubules)
Cell adhesion_Gap junctions	30	0.000158	0.006712	5	Tubulin β, Tubulin α, Connexin 43, ZO-2, Tubulin (in microtubules)
Th9 cells in asthma	47	0.00016	0.006712	6	CRLR, IRF4, NIK(MAP3K14), CCL7, TSLPR, OX40(TNFRSF4)
Development_PEDF signaling	49	0.000202	0.008164	6	SOD2, c-IAP1, c-IAP2, VEGF-A, Fra-2, PI3K reg class IA
Normal and pathological TGF-β-mediated regulation of cell proliferation	33	0.000252	0.009794	5	p38 MAPK, PDGF-A, Axin, MEK3(MAP2K3), ITGB3
Immune response_IL-11 signaling via JAK/STAT	34	0.000291	0.010917	5	PPAR-γ, JAK1, Pim-1, A-FABP, Pim-3
Cell adhesion_Plasmin signaling	35	0.000335	0.012123	5	p38 MAPK, TFPI-2, MEK3(MAP2K3), VEGF-A, PI3K reg class IA
Immune response_IL-12-induced IFN-γ production	36	0.000383	0.013009	5	GADD45 γ, STAT4, MEK3(MAP2K3), NIK(MAP3K14), GADD45 β
Tau pathology in Alzheimer disease	55	0.000384	0.013009	6	p38 MAPK, Glypican-4, Syndecan-1, p38δ (MAPK13), Agrin, Tubulin (in microtubules)
Development_Role of G-CSF in hematopoietic stem cell mobilization	21	0.000435	0.013904	4	JAK1, DPP4, CXCR4, GFI-1
Immune response_Generation of memory CD4+ T cells	37	0.000437	0.013904	5	IL7RA, JAK1, FKHR, CCR7, OX40(TNFRSF4)
WNT signaling in proliferative-type melanoma cells	38	0.000496	0.015318	5	Axin, MITF, Axin2, WNT10B, WNT
Role of integrins in eosinophil degranulation in asthma	58	0.000513	0.015318	6	p38 MAPK, Plastin, Galectin-3, Substance P extracellular region, Eotaxin-2, CCL7
Expression targets of Tissue factor signaling in cancer	22	0.000525	0.015318	4	PAI1, PLAUR (uPAR), CTGF, CSF1
Autocrine Somatotropin signaling in breast cancer	39	0.00056	0.015539	5	CISH, MEK3(MAP2K3), EGR1, TFF3, VEGF-A
Development_Regulation of cytoskeleton proteins in oligodendrocyte differentiation and myelination	59	0.000563	0.015539	6	PDGF-A, Tubulin β, Tubulin α, NCAM1, Fyn, Tubulin (in microtubules)

Table 3. Pathway enrichment analysis of TREM2 DEGs (3/3)

Pathway	Total	P value	FDR-adjusted P value	In Data	Genes
Immune response_IL-1 signaling pathway	82	0.000577	0.015539	7	PPAR-γ, SPHK1, MEK3(MAP2K3), EGR1, c-IAP2, NIK(MAP3K14), CCL7
Oxidative stress_ROS-induced cellular signaling	108	0.000615	0.016146	8	TfR1, p38 MAPK, PAI1, IRP1, EGR1, NOTCH3 (3ICD), VEGF-A, NIK(MAP3K14)
Development_WNT/Beta-catenin and NOTCH in induction of osteogenesis	40	0.000632	0.016189	5	PPAR-γ, Axin, WNT10B, A-FABP, WNT
Neuroprotective action of lithium	63	0.000801	0.020037	6	p38 MAPK, Bim, Axin, MEK3(MAP2K3), VEGF-A, WNT
Putative pathways of hormone action in neurofibromatosis type 1	25	0.000871	0.021149	4	EGR3, EGR1, EGR2 (Krox20), PI3K reg class IA
Immune response_IL-7 signaling in B lymphocytes	43	0.000885	0.021149	5	IL7RA, JAK1, Pim-1, FKHR, Fyn
Signal transduction_PDGF signaling via MAPK cascades	65	0.000946	0.022085	6	p38 MAPK, SPHK1, PDGF-A, NOR1, MEK3(MAP2K3), EGR1
T follicular helper cell dysfunction in SLE	90	0.001007	0.022447	7	JAK1, FKHR, IRF4, NIK(MAP3K14), Fyn, ICOS-L, OX40(TNFRSF4)
Pioglitazone and Rosiglitazone in treatment of type 2 diabetes and metabolic syndrome X	26	0.001015	0.022447	4	PPAR-γ, A-FABP, LPL, GPD1
Signal transduction_PDGF signaling via JAK-STAT and reactive oxygen species (ROS)	66	0.001025	0.022447	6	JAK1, PDGF-A, SOD2, EGR1, TM7SF4, CCL7
Differentiation of Th2 cells in asthma	45	0.001092	0.022871	5	JAK1, CCL22, PI3K reg class IA, TSLPR, OX40(TNFRSF4)
Role of DNA methylation in progression of multiple myeloma	45	0.001092	0.022871	5	Bim, JAK1, SOD2, EGR1, WNT

Table 4. Clinical profiles of donors from ROSMAP syn18485175 data

Donor ID	Age at death	MMSE	Braak	CERAD	Cogdx	Classification by MMSE	Classification by cogdx
10101291	83.4	22.0	3	4	2	AD	MCI
10101327	89.7	12.0	5	1	4	AD	AD
10222853	85.8	1.0	5	1	4	AD	AD
10248033	88.5	12.0	3	2	4	AD	AD
10260309	88.4	29.0	3	4	1	HC	HC
10261026	80.9	29.0	3	4	1	HC	HC
10288185	76.9	24.0	2	4	2	MCI	MCI
10514454	79.5	28.0	2	4	1	MCI	HC
10536568	85.0	28.0	1	3	1	MCI	HC
11072071	88.0	27.0	2	4	1	MCI	HC
11159965	86.9	0.0	5	1	4	AD	AD
11200645	83.7	29.0	4	2	1	HC	HC
11302830	85.8	27.0	3	2	4	MCI	AD
11310718	80.5	27.0	5	2	2	MCI	MCI
11336574	89.0	0.0	6	1	4	AD	AD
11342432	90+	29.0	2	4	1	HC	HC
11345331	87.2	2.0	4	1	4	AD	AD
11399321	86.9	25.0	1	4	3	MCI	MCI
11399871	86.1	12.0	3	4	4	AD	AD
11409232	80.1	30.0	3	4	2	HC	MCI
11609672	86.3	27.0	4	2	1	MCI	HC
11630705	83.5	17.0	6	1	4	AD	AD
20104101	90+	0.0	2	3	4	AD	AD
20112377	74.8	8.0	5	1	4	AD	AD
20149910	90+	27.0	4	4	1	MCI	HC
20170043	90+	0.0	5	1	4	AD	AD
20173942	90+	13.0	4	1	4	AD	AD
20179164	83.7	8.0	3	4	6	AD	-
20207013	90+	27.0	1	4	1	MCI	HC
20249897	87.3	25.0	3	4	2	MCI	MCI
20261901	90+	17.0	5	2	4	AD	AD
20275399	87.5	25.0	3	4	5	MCI	AD
20282398	87.4	28.0	3	1	2	MCI	MCI
20956867	79.1	30.0	3	4	1	HC	HC
20963866	83.6	0.0	6	1	4	AD	AD
20977678	90+	1.0	3	4	2	AD	MCI
20978133	87.7	21.0	5	1	4	AD	AD
21126823	90+	27.0	1	4	2	MCI	MCI
21135554	90+	10.0	5	2	4	AD	AD
21142003	88.9	28.0	4	4	1	MCI	HC
21159840	82.7	16.0	5	1	4	AD	AD
21172121	76.1	27.0	5	1	3	MCI	MCI
21189544	90+	3.0	5	1	4	AD	AD
21412626	90+	24.0	3	4	1	MCI	HC
76647134	81.5	0.0	5	1	4	AD	AD

Table 5. Correlation between TREM DEGs and AD vs. HC vs. MCI microglia using GSEA

Dataset	TREM2 DEG	NES	FDR q-value*
Cogdx AD vs. HC	TREM2 Up	−1.638	0
Cogdx AD vs. MCI	TREM2 Up	−1.565	0
MMSE AD vs. HC	TREM2 Up	−1.350	0.001
MMSE AD vs. MCI	TREM2 Up	−1.557	0.002
Cogdx AD vs. MCI	TREM2 Down	1.342	0.019
MMSE AD vs. MCI	TREM2 Down	1.191	0.085
Cogdx MCI vs. HC	TREM2 Down	−1.117	0.265
Cogdx AD vs. HC	TREM2 Down	1.099	0.477
MMSE AD vs. HC	TREM2 Down	1.087	0.514
MMSE MCI vs. HC	TREM2 Up	1.111	0.663
Cogdx MCI vs. HC	TREM2 Up	0.797	0.811
MMSE MCI vs. HC	TREM2 Down	0.823	0.903

GSEA results between TREM DEGs and signed P value of AD vs. HC, MCI vs. HC, and AD vs. MCI in microglia of ROSMAP syn18485175 data.

*FDR q-value indicates FDR-adjusted P value of GSEA

TREM2, triggering receptor expressed on myeloid cells 2; DEG, differentially expressed genes; AD, Alzheimer's disease; HC, healthy control; MCI, mild cognitive impairment; GSEA, gene set enrichment analysis; NES, normalized enrichment scores; FDR, false discovery rate; cogdx, clinical consensus diagnosis of cognitive status at the time of death; MMSE, Mini-Mental State Examination; ROSMAP, Religious order Study and the Memory and Aging Project.

Table 6. Correlation between TREM2 DEGs and clinical scores of AD using GSEA

Dataset	TREM2 DEG	NES	FDR q-value*
Correlation of Braak	TREM2 Up	−1.527	0
Correlation of CERAD	TREM2 Up	−1.458	0.009
Correlation of CERAD	TREM2 Down	−0.957	0.439
Correlation of MMSE	TREM2 Down	0.975	0.472
Correlation of MMSE	TREM2 Up	1.043	0.562
Correlation of Braak	TREM2 Down	0.849	0.788

GSEA results between TREM DEGs and clinical score of AD of ROSMAP syn18485175 data.

*FDR q-value indicates FDR-adjusted P value of GSEA

TREM2, triggering receptor expressed on myeloid cells 2; DEG, differentially expressed genes; AD, Alzheimer's disease; GSEA, gene set enrichment analysis; NES, normalized enrichment scores; FDR, false discovery rate; CERAD, Consortium to Establish a Registry for Alzheimer's Disease; MMSE, Mini-Mental State Examination; ROSMAP, Religious order Study and the Memory and Aging Project.

Table 7. Pathway enrichment analysis of genes enriched in GSEA between TREM2 up and AD microglia (1/4)

Pathway	Total	Cogdx AD vs. HC			MMSE AD vs. HC		
		FDR-adjusted P value	In Data	Genes	FDR-adjusted P value	In Data	Genes
Apoptosis and survival_Anti-apoptotic TNFs/NF-kB/IAP pathway	27	4.618E-04	4	c-IAP1, TRAF5, NIK(MAP3K14), c-IAP2	9.737E-05	4	c-IAP1, TRAF5, NIK(MAP3K14), c-IAP2
Immune response_IFN-α/β signaling via JAK/STAT	64	5.164E-03	4	STAT4, C3G, RSAD2, JAK1	1.670E-03	4	STAT4, C3G, RSAD2, JAK1
CHDI_Correlations from Replication data_Cytoskeleton and adhesion module	64	5.164E-03	4	Fyn, C3G, PLAUR (uPAR), CXCR4	3.752E-03	3	c-IAP1, NIK(MAP3K14), c-IAP2
Immune response_OX40L/ OX40 signaling pathway	69	5.216E-03	4	FKHR, TRAF5, NIK(MAP3K14), CXCR4	3.752E-03	4	Tubulin α, Fra-2, c-Rel (NF-kB subunit), JAK1
G protein-coupled receptors signaling in lung cancer	76	5.920E-03	4	G-protein α-12 family, Galpha(i)-specific peptide GPCRs, Galpha(q)-specific peptide GPCRs, CXCR4	3.752E-03	3	c-IAP1, NIK(MAP3K14), c-IAP2
Chemotaxis_SDF-1/ CXCR4-induced chemotaxis of immune cells	79	5.920E-03	4	Fyn, SFK, G-protein α-13, CXCR4	4.654E-03	3	c-IAP1, TRAF5, NIK(MAP3K14)
Immune response_BAFF-induced non-canonical NF-kB signaling	32	6.276E-03	3	c-IAP1, NIK(MAP3K14), c-IAP2	5.012E-03	3	c-IAP1, NIK(MAP3K14), c-IAP2
T follicular helper cell dysfunction in SLE	90	6.276E-03	4	Fyn, FKHR, JAK1, NIK(MAP3K14)	1.462E-02	3	HB-EGF(mature), HB-EGF, TGF-α
NF-kB pathway in multiple myeloma	35	6.276E-03	3	c-IAP1, NIK(MAP3K14), c-IAP2	5.751E-03	3	Fra-2, c-IAP1, c-IAP2
Immune response_IL-12-induced IFN-γ production	36	6.276E-03	3	STAT4, GADD45 β, NIK(MAP3K14)	5.834E-03	3	c-IAP1, NIK(MAP3K14), c-IAP2
Immune response_IL-4 signaling pathway	94	6.276E-03	4	Tubulin α, FKHR, Fra-2, JAK1	2.588E-02	2	STAT4, NIK(MAP3K14)
Immune response_IL-7 signaling in T lymphocytes	37	6.276E-03	3	Fyn, FKHR, JAK1	1.609E-02	2	TRAF5, NIK(MAP3K14)
Stem cells_Pancreatic cancer stem cells in tumor metastasis	40	7.323E-03	3	Fyn, G-protein α-13, CXCR4	2.997E-02	2	STAT4, JAK1
Apoptosis and survival_Lymphotoxin-β receptor signaling	42	7.869E-03	3	c-IAP1, TRAF5, NIK(MAP3K14)	2.997E-02	2	JAK1, NIK(MAP3K14)
Immune response_IL-7 signaling in B lymphocytes	43	7.880E-03	3	Fyn, FKHR, JAK1	1.697E-02	3	STAT4, JAK1, NIK(MAP3K14)
Immune response_TNF-R2 signaling pathways	45	8.029E-03	3	c-IAP1, NIK(MAP3K14), c-IAP2	2.077E-02	3	RSAD2, JAK1, NIK(MAP3K14)
Apoptosis and survival_IL-17-induced CIKS-independent signaling pathways	46	8.029E-03	3	STAT4, MKP-1, JAK1	2.432E-02	2	STAT4, JAK1
Immune response_Inhibitory action of Lipoxins on pro-inflammatory TNF-α signaling	46	8.029E-03	3	FKHR, JAK1, NIK(MAP3K14)	2.497E-02	2	TRAF5, NIK(MAP3K14)

Table 7. Pathway enrichment analysis of genes enriched in GSEA between TREM2 up and AD microglia (2/4)

Pathway	Total	Cogdx AD vs. HC			MMSE AD vs. HC		
		FDR-adjusted P value	In Data	Genes	FDR-adjusted P value	In Data	Genes
Development_PEDF signaling	49	8.718E-03	3	Fra-2, c-IAP1, c-IAP2	2.497E-02	2	JAK1, c-IAP2
Development_G-CSF signaling	49	8.718E-03	3	JAK1, c-IAP2, CXCR4	2.562E-02	2	c-IAP1, c-IAP2
Signal transduction_NF-kB activation pathways	51	9.348E-03	3	c-IAP1, NIK(MAP3K14), c-IAP2	2.588E-02	2	JAK1, c-IAP2
Immune response_IL-5 signaling via JAK/STAT	56	1.176E-02	3	MKP-1, JAK1, c-IAP2	2.588E-02	2	c-IAP1, c-IAP2
Cytoskeleton remodeling_Substance P mediated membrane blebbing	16	1.923E-02	2	Tubulin α, G-protein α-12 family	2.588E-02	2	JAK1, NIK(MAP3K14)
Stem cells_CD30 signaling in transformed embryonic stem cells	18	2.341E-02	2	TRAF5, NIK(MAP3K14)	2.588E-02	2	c-IAP1, c-IAP2
CHDI_Correlations from Replication data_Causal network (positive correlations)	79	2.820E-02	3	CD83, NIK(MAP3K14), CXCR4	2.588E-02	2	c-IAP1, c-IAP2
Development_Role of G-CSF in hematopoietic stem cell mobilization	21	2.950E-02	2	JAK1, CXCR4	2.588E-02	2	STAT4, JAK1
SLE genetic marker-specific pathways in antigen-presenting cells (APC)	84	3.115E-02	3	STAT4, JAK1, NIK(MAP3K14)	2.653E-02	2	TRAF5, NIK(MAP3K14)
Immune response_IL-2 signaling via JAK/ STAT	25	3.751E-02	2	STAT4, JAK1	2.653E-02	2	c-IAP1, c-IAP2
Development_ERBB-family signaling	39				4.341E-03	3	HB-EGF, TGF-α, NIK(MAP3K14)
Non-genomic signaling of ESR2 (membrane) in lung cancer cells	53				5.949E-03	3	HB-EGF(mature), HB-EGF, TGF-α
Development_EGFR signaling pathway	71				1.297E-02	3	HB-EGF, TGF-α, JAK1
TLR and EGFR-induced inflammatory signaling in normal and asthmatic airway epithelium	22				2.077E-02	2	HB-EGF, TGF-α
Neurogenesis_NGF/ TrkA MAPK-mediated signaling	105				2.497E-02	3	C3G, HB-EGF, PLAUR (uPAR)
Pancreatic cancer cell resistance to Tarceva (erlotinib)	27				2.497E-02	2	HB-EGF, TGF-α
Development_Dopamine-induced transactivation of EGFR in SVZ neural stem cells	31				2.588E-02	2	HB-EGF, TGF-α
Immune response_IL-11 signaling via JAK/STAT	34				2.588E-02	2	JAK1, Pim-3
Plasminogen activators signaling in pancreatic cancer	35				2.588E-02	2	HB-EGF, PLAUR (uPAR)
Cigarette smoke-induced inflammatory signaling in airway epithelial cells	36				2.588E-02	2	HB-EGF, TGF-α
PR action in breast cancer: stimulation of cell growth and proliferation	36				2.588E-02	2	HB-EGF, JAK1

Table 7. Pathway enrichment analysis of genes enriched in GSEA between TREM2 up and AD microglia (3/4)

Pathway	Total	Cogdx AD vs. HC			MMSE AD vs. HC		
		FDR-adjusted P value	In Data	Genes	FDR-adjusted P value	In Data	Genes
Development_Oligodendrocyte differentiation (general schema)	38				2.653E-02	2	HB-EGF, TGF-α
Cell adhesion_PLAU signaling	39				2.653E-02	2	PLAUR (uPAR), JAK1
Immune response_TSLP signalling	39				2.653E-02	2	STAT4, JAK1
Immune response_Th1 and Th2 cell differentiation	40				2.656E-02	2	STAT4, JAK1
The role of UV radiation in melanoma development	40				2.656E-02	2	HB-EGF, TGF-α
Apoptosis and survival_Anti-apoptotic TNFs/NF-kB/Bcl-2 pathway	42				2.791E-02	2	TRAF5, NIK(MAP3K14)
Inhibition of apoptosis in gastric cancer	42				2.791E-02	2	c-IAP1, c-IAP2
Apoptosis and survival_TNFR1 signaling pathway	43				2.796E-02	2	c-IAP1, c-IAP2
Immune response_BAFF-induced canonical NF-kB signaling	43				2.796E-02	2	c-Rel (NF-kB subunit), NIK(MAP3K14)
EGFR signaling in Prostate Cancer	46				2.997E-02	2	HB-EGF, TGF-α
Immune response_Induction of apoptosis and inhibition of proliferation mediated by IFN-γ	47				3.022E-02	2	C3G, JAK1
G-protein signaling_TC21 regulation pathway	25	3.751E-02	2	C3G, G-protein α-12 family			
Immune response_IFN-α/β signaling via PI3K and NF-kB pathways	94	3.856E-02	3	RSAD2, JAK1, NIK(MAP3K14)			
Transcription_HIF-1 targets	95	3.856E-02	3	TfR1, PLAUR (uPAR), CXCR4			
Apoptosis and survival_IL-17-induced CIKS-dependent NF-kB signaling and mRNA stabilization	28	4.059E-02	2	TRAF5, NIK(MAP3K14)			
Development_Role of CNTF and LIF in regulation of oligodendrocyte development	28	4.059E-02	2	JAK1, c-IAP2			
Role of IFN-β in activation of T cell apoptosis in multiple sclerosis	29	4.059E-02	2	c-IAP1, c-IAP2			
Apoptosis and survival_nAChR in apoptosis inhibition and cell cycle progression	29	4.059E-02	2	Fyn, FKHR			
Histone deacetylases in Prostate Cancer	29	4.059E-02	2	Tubulin α, FKHR			
Role of CNTF and LIF in regulation of oligodendrocyte development in multiple sclerosis	30	4.224E-02	2	JAK1, c-IAP2			
Apoptosis and survival_Role of IAP-proteins in apoptosis	31	4.389E-02	2	c-IAP1, c-IAP2			

Table 7. Pathway enrichment analysis of genes enriched in GSEA between TREM2 up and AD microglia (4/4)

Pathway	Total	Cogdx AD vs. HC			MMSE AD vs. HC		
		FDR-adjusted P value	In Data	Genes	FDR-adjusted P value	In Data	Genes
Activation of ACTH production in pituitary gland in major depressive disorder	32	4.439E-02	2	JAK1, NIK(MAP3K14)			
Cytoskeleton remodeling_Reverse signaling by Ephrin-B	32	4.439E-02	2	Tubulin α, CXCR4			
Resistance of pancreatic cancer cells to death receptor signaling	33	4.492E-02	2	c-IAP1, c-IAP2			
SDF-1 axis in endothelial progenitor cell recruitment in healing myocardial infarction	33	4.492E-02	2	FKHR, CXCR4			
Role of Apo-2L(TNFSF10) in Prostate Cancer cell apoptosis	34	4.548E-02	2	c-IAP1, c-IAP2			
G-protein signaling_RhoA regulation pathway	34	4.548E-02	2	Fyn, G-protein α-12 family			
Development_Growth hormone signaling via STATs and PLC/IP3	35	4.708E-02	2	Fyn, C3G			
Immune response_IL-22 signaling pathway	36	4.867E-02	2	STAT4, JAK1			
Immune response_Generation of memory CD4+ T cells	37	5.027E-02	2	FKHR, JAK1			
Development_SDF-1 signaling in hematopoietic stem cell homing	38	5.037E-02	2	C3G, CXCR4			
Apoptosis and survival_APRIL and BAFF signaling	39	5.037E-02	2	TRAF5, NIK(MAP3K14)			
Apoptosis and survival_Ubiquitination and phosphorylation in TNF-α-induced NF-kB signaling	39	5.037E-02	2	c-IAP1, c-IAP2			

Table 8. Comparison of TREM2 expression levels between AD vs. HC vs. MCI microglia

Dataset	FDR-adjusted P value*
MMSE AD vs. HC	1
MMSE AD vs. MCI	1
MMSE MCI vs. HC	1
Cogdx AD vs. HC	1
Cogdx AD vs. MCI	1
Cogdx MCI vs. HC	1

*FDR-adjusted P value from comparison test between AD vs. HC, AD vs. MCI, and MCI vs. HC of ROSMAP syn18485175 data.

Table 9. Correlation between TREM2 expression levels and Braak, CERAD, and MMSE scores in AD microglia

Dataset	FDR-adjusted P value*
Braak	0.865
MMSE	0.852
CERAD	0.905

*FDR-adjusted P value from correlation between TREM2 gene and MMSE, Braak, or CERAD of ROSMAP syn18485175 data.

Table 10. Clinical profiles of donors from ROSMAP syn21125841 data

Donor ID	Age at death	MMSE*	Braak	CERAD	Cogdx	Classification by MMSE	Classification by cogdx
10298957	82.4	10.0	3	2	4	AD	AD
15121461	90+	16.2	5	1	4	AD	AD
15144878	86.2	7.0	5	1	4	AD	AD
15178486	90+	30.0	4	4	1	HC	HC
15179365	83.6	17.0	3	1	4	AD	AD
15196848	90+	28.0	3	4	1	MCI	HC
20240514	89.7	30.0	3	4	1	HC	HC
20280666	90+	27.6	4	4	1	MCI	HC
20371236	90+	14.0	5	1	4	AD	AD
20535564	82.7	0.0	5	1	4	AD	AD
20800682	84.8	30.0	3	4	1	HC	HC
20897173	89.3	21.4	3	4	1	AD	HC
20911508	90+	0.0	5	1	4	AD	AD
20959216	90+	12.0	5	2	4	AD	AD
20963578	81.9	28.0	4	4	1	MCI	HC
21272396	87.2	28.0	1	4	1	MCI	HC
21403995	86.1	15.0	3	1	4	AD	AD
30544882	89.4	13.0	3	2	4	AD	AD
34779151	86.3	25.0	2	4	1	MCI	HC

*Missing items were imputed based on other variables in cases where a participant refused to answer one to four MMSE items or was physically unable to answer one or more items

Chapter 2: TNFR2 pathways are fully active in cancer regulatory T cells

Abstract

Tumor necrosis factor receptor 2 (TNFR2), a membrane-bound tumor necrosis factor receptor expressed by regulatory T cells (Tregs), participates in Treg proliferation. Although a specific TNFR2 pathway has been reported, the signaling mechanism has not been completely elucidated. This study sought to clarify TNFR2 signaling in human Tregs using amplicon sequencing and single-cell RNA-sequencing to assess Tregs treated with a TNFR2 agonist antibody. Pathway enrichment analysis based on differentially expressed genes highlighted tumor necrosis factor α signaling via nuclear factor-κ B, interleukin-2 signal transducer and activator of transcription 5 signaling, interferon-g response, and cell proliferation-related pathways in Tregs after TNFR2 activation. *TNFR2*-high Treg-focused analysis found that these pathways were fully activated in cancer Tregs, showing high TNFR2 expression. Collectively, these findings suggest that TNFR2 orchestrates multiple pathways in cancer Tregs, which could help cancer cells escape immune surveillance, making TNFR2 signaling a potential anticancer therapy target.

Introduction

Regulatory T cells (Tregs) are a subset of T cells that act as negative regulators of cytotoxic T cells immune response [111]. Tregs are required for the maintenance of peripheral tolerance to self and non-toxic antigens; for example, the loss of Tregs can contribute to autoimmune deficiency, polyendocrinopathy, enteropathy, and X-linked diseases [112]. Dysfunction or reduction in the number of Tregs is also observed in

autoimmune diseases such as systemic lupus erythematosus and type-1 diabetes [112]. Conversely, excessive Treg activation is observed in cancer tissues, where it can cause cytotoxic T cells to fail to recognize cancer antigens and lead to cancer growth [113, 114]. These findings suggest that the regulation of Treg function and proliferation could be an effective treatment strategy for autoimmune diseases and cancers.

Proliferation of Tregs is initiated by the activation of, and subsequent signaling via, the T cell receptor by costimulatory receptors such as inducible T cell costimulatory (ICOS), tumor necrosis factor receptor 2 (TNFR2), which is a receptor for TNFα and has anti-inflammatory activities [115], OX40 (TNF receptor superfamily member 4, TNFRSF4), and 4-1BB (TNF receptor superfamily member 9, TNFRSF9) [114]. In Tregs, the role of TNFR2 as a co-stimulator has been evaluated using selective TNFR2 agonist antibodies or TNFR2 ligands [116-119]. Human peripheral blood mononuclear cell (PBMC)-derived Tregs can be expanded via treatment with a TNFR2 agonist antibody [116]. Treatment with a TNFR2-selective ligand increases Treg expansion *in vivo* [118] and improves symptoms in animal models of immunological disease, such as collagen-induced arthritis [119] and graft versus host disease [117]. Conversely, inhibition of TNFR2 signaling using an antagonist antibody, and the subsequently reduced Treg proliferation, reduce cancer growth in a syngeneic mouse model by enhancing immune responses in cancer tissue [120]. These studies support the hypothesis that modulation of TNFR2 has therapeutic potential for autoimmune diseases and cancers.

Several studies have described the mechanisms of TNFR2 stimulation during Treg proliferation by focusing on specific signaling pathways. Upon activation of TNFR2,

TNFR2-associated signaling cascade molecules, including TNF receptor-associated factor 2 (TRAF2), cellular inhibitor of apoptosis protein-1 (cIAP-1), and cIAP-2 interact with the C-terminus of TNFR2 [115]. cIAP1 and cIAP2 activation is an initial step in gene transcription via nuclear factor-κ B (NF-κB) [115]. Additionally, treatment with a mitogen-activated protein kinase (MAPK) inhibitor suppresses TNFR2 signal-induced proliferation of mouse Tregs [121]. Expression of histone methyltransferase and enhancer of zeste homolog 2 (EZH2), which enhances the stability of Tregs, is induced by TNFR2 agonist antibodies [122]. Specifically, TNFR2 agonist antibodies can expand Tregs in human blood and upregulate the expression of various genes, including those encoding adenosine monophosphate kinase and carnitine transferase 1A, which are involved in the Krebs cycle and fatty acid supply [123]. However, none of the studies have comprehensively investigated all TNFR2 signals in Treg.

TNFR2-expressing Tregs have been previously associated with cancer: in ovarian cancer patients, TNFR2 expression is high in Tregs [124] and a correlation has been reported between the number of TNFR2-high Tregs in pleural effusion and the prognosis of lung cancer patients [125]. TNFR2 is also used as a marker of highly suppressive Tregs as TNFR2-high Treg populations showed higher suppressive activity against cytotoxic T cells compared to TNFR2-low Tregs [126]. However, it remains to be elucidated whether TNFR2 signals are active in such TNFR2-expressing Tregs in cancer patients.

In this study, to understand the entire TNFR2 biological pathway, I performed amplicon sequencing (Ampli-seq) analysis to identify highly upregulated pathways in Tregs in response to TNFR2 activation. I further clarified the relationship between TNFR2

expression and Treg gene expression profiles using single-cell RNA-seq analysis. Comparison of my sequencing datasets with public databases allowed me to further characterize the roles of TNFR2 in the functional regulation of cancer Tregs.

Materials and Methods

Isolation and culture of human Tregs

All human cell protocols used in this study were approved by the Takeda Institutional Ethical Committee (Protocol No. CS-00100155) and followed the guidelines of the Declaration of Helsinki. Human peripheral blood samples were collected from healthy volunteers. Whole blood was mixed with phosphate-buffered saline (PBS; FUJIFILM Wako Pure Chemical, Osaka, Japan) containing 2 mM ethylenediaminetetraacetic acid (EDTA; Invitrogen, Waltham, MA, USA) and added to a tube containing Ficoll (GE Healthcare, Tokyo, Japan). After centrifuging at 400 × *g* for 40 min, the PBMC layer (between the PBS and Ficoll layers) was collected and washed twice with 2 mM EDTA-PBS. $CD4^+CD25^+$ Tregs were isolated using Regulatory $CD4^+CD25^+$ T Cell Dynabeads (Thermo Fisher Scientific, Waltham, MA, USA) following the manufacturer's instructions.

The purity of Tregs was monitored by measuring CD4, CD25, and forkhead box P3 (FOXP3) expression by fluorescence-activated cell sorting (FACS) using a Treg detection kit (Miltenyi Biotec, Bergisch Gladbach, Germany). Twenty thousand cells were seeded into a round-bottom 96-well plate and cultured in RPMI-1640 (FUJIFILM Wako Pure Chemical) containing 10% fetal bovine serum and 500 IU/mL interleukin-2 (IL-2; R&D

Systems, Minneapolis, MN, USA) in a humidified CO_2 incubator at 37 °C. Dynabeads Treg expander (Invitrogen) was added at a bead: cell ratio of 1: 2. TNFR2 activation was achieved using an MR2-1 TNFR2 agonist antibody (Hycult Biotech, Uden, Netherlands). As control treatment, mouse IgG_1 (R&D Systems) was used. After 5–7 days of culture, FOXP3 expression was measured by FACS using the Treg detection kit containing anti-FOXP3 antibody (Miltenyi Biotec); cultured cells without anti-FOXP3 antibody staining were used as the negative control. Treg proliferation was determined by measuring the ATP content of each well using CellTiter-Glo (Promega, Madison, WI, USA).

Ampli-seq analysis

Ampli-seq libraries were constructed and sequenced using the Ion Proton platform (Thermo Fisher Scientific) according to the manufacturer's instructions. Briefly, 10 ng total RNA isolated from cultured Tregs were reverse transcribed using the SuperScript VILO cDNA synthesis kit (Thermo Fisher Scientific), followed by library generation using the Ion Ampli-seq transcriptome human gene expression kit (Thermo Fisher Scientific). The libraries were diluted to 45 pM, and equal volumes from five individual samples were combined into a pooled sample. The pooled libraries were multiplexed, clonally amplified using the Ion Chef system (Thermo Fisher Scientific), and sequenced on Ion PI chips using an Ion Proton sequencing system (Thermo Fisher Scientific). The data were first analyzed using Torrent Suite with the Ampli-seqRNA analysis plugin to generate count data. Principal component analysis (PCA) was performed using the "prcomp" function of the stats package in R (R default package). A test for equal means

in a one-way layout was conducted to compare PC1 in each group using the “oneway.test” of stats package in R. Differentially expressed genes (DEGs) were identified based on the gene-wise negative binomial generalized linear model with the quasi-likelihood method using the edgeR package in R [127, 128]. Heatmaps were created using the ComplexHeatmap package in R [129]. All Ampli-seq data were deposited in the Gene Expression Omnibus (GEO) repository at http://www.ncbi.nlm.nih.gov/geo (accession number: GSE185145).

Single-cell RNA-seq analysis

A single-cell RNA-seq library was prepared from cultured Tregs using a Chromium Single Cell 3' Library Kit v2 (10× Genomics, Pleasanton, CA, USA) following the manufacturer’s instructions. The libraries were sequenced using the Illumina HiSeq system at a depth of 100,000 reads per cell to generate binary base call (bcl) files. The initial analysis was carried out using the 10X Genomics Cell Ranger version 3 pipeline. Using the Cell Ranger “count” software, the bcl files were converted to FASTQ format, filtered, and mapped to the GRCh38 reference genome. Mapped reads data were counted and normalized to generate a matrix containing normalized gene counts. Using the Cell Ranger “aggr” software, count data from multiple samples were aggregated, normalized to the same sequencing depth, and recomputed to the feature-barcode matrix. Downstream analysis was conducted primarily using the Seurat version 3 package [57,130] in R. Low-quality cells (< 200 genes/cell and > 10% mitochondrial genes) and doublet cells were excluded using the Seurat and DoubletFinder packages [131],

respectively, in R. Count data were further normalized with the global-scaling normalization method, $\log_e$-transforms, and linear transformation to remove mitochondrial contamination and the Hamming-corrected unique molecular identifier (UMI) count variations using the Seurat function “NormalizeData” and “ScaleData”. The resulting top 2,000 variable genes were used for PCA with the Seurat function "FindVariableFeatures" and "RunPCA". The first nine principal components adopted to visualize the uniform manifold approximation and projection (UMAP) were color-coded by each sample condition using the Seurat function "RunUMAP" and "DimPlot". The gene expression levels of *TNFR2* (Gene symbol: *TNFRSF1B*) in each cell were visualized in UMAP using the Seurat function "FeaturePlot”. The cells were divided into two groups based on *TNFR2* expression level according to the valley of the bimodal distribution (high, ≥ 0; low, < 0 of $\log_e$-normalized expression value). DEGs between the *TNFR2* high and low groups were identified with the non-parametric Wilcoxon rank sum test using the Seurat function "FindMarkers". The P values from the statistical tests were converted into false discovery rate (FDR)-adjusted P values using the "p.adjust" function in the stats (R default) package. Heatmaps were generated using the ComplexHeatmap [129] and RColorBrewer packages [132]. All single-cell RNA-seq data were deposited in the GEO repository at http://www.ncbi.nlm.nih.gov/geo (accession number: GSE185144).

Cancer Treg single-cell RNA-seq data analysis

Single-cell RNA-seq data from patients with hepatocellular carcinoma (HCC) (GSE98638) [133], non-small cell lung cancer (NSCLC) (GSE99254) [134], and

colorectal cancer (CRC) (GSE108989) [135] were downloaded from the GEO repository. The datasets consisted of T cells from cancer patients isolated by FACS analysis into different subtypes: $CD8^+$ T cells ($CD3^+$ and $CD8^+$), T helper cells ($CD3^+$, $CD4^+$, and $CD25^-$), and Tregs ($CD3^+$, $CD4^+$, and $CD25^{high}$), which were profiled by Smart-seq2 and sequenced on the HiSeq system. Counts and annotation data for each cell were downloaded and normalized by the global-scaling normalization method, log_e-transformed, and linearly transformed to remove mitochondrial contamination and UMI count variations using the Seurat functions “NormalizeData” and “ScaleData”.

Statistical analysis was conducted using the non-parametric Wilcoxon rank sum test with the Seurat function "FindMarkers" for each dataset to identify DEGs between cancer and normal Tregs. After normalization of the expression data, the original datasets were collected into clusters that were then used in my analysis: Cancer Treg: Cluster 8 in HCC, Cluster 9 in NSCLC, and Cluster 12 in CRC; Normal Treg: Cluster 7 in HCC, Cluster 8 in NSCLC, and Cluster 10 in CRC. The P values from the statistical tests were converted to FDR-adjusted P values using the "p.adjust" function in the stats (R default) package. Violin plots were constructed using the Seurat function “VlnPlot.”

Pathway enrichment analysis

The DEGs identified from Ampli-seq or single-cell RNA-seq were used for pathway enrichment analysis. Briefly, pathway enrichment analysis was conducted by Fisher’s exact test using the “fisher.test” function of the stats package in R with “hallmark gene sets” from the Molecular Signatures Database [136-138]. The criterion for pathway

enrichment analysis was set at P value < 0.01.

Results

Expansion of human Tregs with TNFR2 agonist antibody treatment

We first confirmed the activity of the TNFR2 agonist antibody (clone MR2-1) by monitoring Treg proliferation. Tregs were isolated from PBMCs of healthy volunteers and stimulated with the TNFR2 agonist antibody in the presence of anti-CD3/CD28. After 7 days of culture, Treg proliferation increased by 57.1% in response to 10 μg/mL TNFR2 agonist antibody when compared to that in the control group. The antibody expanded Tregs in a dose-dependent manner with an EC_{50} value of 45.4 ng/mL, and its maximum effect was observed at ≥ 3 μg/mL (Figure 5A). Therefore, I used 3 μg/mL TNFR2 agonist antibody for subsequent studies. The percentage of FOXP3-positive cells in the TNFR2 agonist antibody treatment group was tested to confirm Treg purity after proliferation. There was 91.0% FOXP3 expression on day 0 before TNFR2 agonist antibody treatment, which was then maintained at 90.9% after TNFR2 agonist antibody treatment (Figure 5B), similar to that after control IgG treatment (87.6%). These results suggested that the Treg purity was maintained after the TNFR2 agonist antibody induced cell expansion. FOXP3 expression was also maintained after TNFR2 agonist antibody treatment as compared to that after control treatment, as demonstrated by measuring a representative sample.

Ampli-seq identification of pathways upregulated by TNFR2 agonist antibody treatment

Ampli-seq analysis was conducted using Tregs treated with the TNFR2 agonist antibody.

I first confirmed the difference between the gene expression profiles of the TNFR2 agonist antibody and control IgG treatment groups using PCA of the Ampli-seq transcriptome data (Figure 6A). The results of the PCA indicated a clear difference between the expression profiles of the TNFR2 agonist antibody and IgG treatment groups, shown by a clear separation in PC1. Next, I extracted the upregulated DEGs between the Tregs treated with TNFR2 agonist antibody or IgG, which were then used in pathway enrichment analysis with the hallmark gene set [138]. Ten pathways were significantly enriched by the upregulated DEGs (Figures. 6B-I): cell proliferation- and cell cycle-related pathways ("E2F targets," "G2M checkpoint," "Myc targets v1," "DNA repair," and "mitotic spindle"); downstream signaling of the cytokine receptor ("TNFα signaling via NFκB," "IFNγ response," and "IL-2 STAT5 signaling"); and "mTORC1" and "androgen response" pathways. Thus, my Ampli-seq findings clearly identified pathways regulated by TNFR2 activation.

Upregulation of NF-κB, IL-2 STAT5, and IFNγ response pathways in Treg with high TNFR2 expression

We next performed single-cell RNA-seq analysis to analyze the TNFR2 pathways in Treg subpopulations. After treatment with the TNFR2 agonist antibody, Tregs were subjected to single-cell RNA-seq. For this analysis, I used non-treatment as a negative control, instead of IgG, and TNFR2 agonist antibody because 1) IgG did not affect the proliferation of Tregs (Figure 5A); 2) Fcγ receptors are not expressed in human Tregs [139], which was confirmed by my Ampli-seq data (data not shown), and therefore, the

TNFR2-independent IgG effect through Fcγ receptors was negligible; and 3) in single-cell RNA-seq analysis, the number of genes detected per cell was generally much lower than that in bulk cell analysis, such as Ampli-seq, suggesting that gene expression could largely affect pathway enrichment data if IgG can cause off-target gene expression changes. My analysis successfully detected the difference in the entire gene expression profiles of *TNFR2*-high and *TNFR2*-low Tregs treated with the TNFR2 agonist antibody, which were visualized by UMAP (Figure 7A) and used to extract upregulated DEGs from *TNFR2*-high Tregs.

To evaluate whether the expression level of *TNFR2* was associated with the pathways identified in my sequencing analyses, I performed pathway enrichment analysis to compare the DEGs between *TNFR2*-high and *TNFR2*-low Tregs (*TNFR2*-high, $\log_e >= 0$; *TNFR2*-low, $\log_e < 0$) (Figure 7B). DEGs from the *TNFR2*-high Treg population showed enrichment in downstream cytokine receptor signaling, such as the "IFNγ response," "TNFα signaling via NFκB," "IFNα response," "IL-2 STAT5 signaling," and "IL-6 JAK-STAT3 signaling" pathways. Additionally, the pathways related to intracellular signaling, such as "mTORC1 signaling," "PI3K AKT mTOR signaling," and, "androgen response" pathways were significantly enriched by DEGs in *TNFR2*-high Tregs.

Upregulation of TNFR2 pathways in cancer Tregs

To evaluate the involvement of TNFR2 signaling in disease conditions, I analyzed transcriptome data from cancer tissues in which cancer-associated Tregs caused cancer

cells to escape immune surveillance [140]. I specifically focused on single-cell RNA-seq data that allowed for cell-type specific analysis and found three single-cell RNA-seq data available for HCC (GSE98638) [133], NSCLC (GSE99254) [134], and CRC (GSE108989) [135]. Each dataset included Tregs isolated from cancer tissues and adjacent normal tissue and peripheral blood. I found that *TNFR2* expression was higher in cancer Tregs than in normal Tregs from HCC (FDR-adjusted P value of 3.1×10^{-30}), NSCLC (FDR-adjusted P value of 7.3×10^{-37}), and CRC (FDR-adjusted P value of 1.9×10^{-60}) (Figures 8A–C). These results revealed that TNFR2 could transform Tregs into cancer Tregs.

Pathway enrichment analysis was performed using DEGs extracted from *TNFR2*-high cancer Tregs that were commonly upregulated in the HCC, NSCLC, and CRC datasets. Similar to the pathway enrichment results from the single-cell RNA-seq analysis of TNFR2 agonist antibody-stimulated Tregs, cell proliferation-related pathways ("Myc targets v1", "G2M checkpoint", "E2F targets", "mitotic spindle", and "DNA repair"), downstream pathways of cytokine receptors ("IFNγ response," "IFNα response," "TNFα signaling via NFκB," "IL-2 STAT5 signaling," "IFNα response," and "IL-6 JAK STAT3 signaling"), cell metabolism pathways ("glycolysis" and "oxidative phosphorylation"), and other intracellular signaling pathways ("mTORC1 signaling," "PI3K AKT mTOR signaling," and "androgen response") were significantly correlated with the upregulated DEGs (Figure 8D). These results suggested that TNFR2 signals were enhanced in *TNFR2*-high cancer Tregs.

Discussion

TNFR2 plays a critical role in regulating Treg function, which in turn, can modulate disease progression. Thus, functional modulation of TNFR2 has been thought to have therapeutic potential for various diseases, including cancers, autoimmune diseases, and neurological diseases, which has been reviewed elsewhere [115]. Moreover, transcriptome analysis identified genes with upregulated expression upon TNFR2 activation in mouse Tregs treated with TNFR2-selective ligand [141]. However, this analysis did not fully characterize how TNFR2 controls cellular signals in Tregs, particularly in TNFR2-high Tregs. Therefore, for a comprehensive understanding of the downstream signaling of TNFR2, in this study, I analyzed Ampli-seq and single-cell RNA-seq data of Tregs treated with a TNFR2 agonist antibody, followed by pathway enrichment analysis, by focusing on *TNFR2*-high Tregs.

In my study, upregulation of "TNFα signaling via the NF-κB" pathway was identified by TNFR2 agonist antibody-treated and *TNFR2*-high Tregs. A previous *in vitro* study showed that phosphorylation of NF-κB and transcriptional activity of NF-κB is enhanced by TNFα stimulation in Tregs [142]. Meanwhile, another report showed that activation of TNFR2 by an agonist activates the degradation of the nuclear factor of the κ light polypeptide gene enhancer in the B-cells inhibitor α (IκBα), indicating activation of the NF-κB pathway in Tregs upon TNFR2 activation [143]. My pathway enrichment data from transcriptome data on TNFR2 agonist antibody-treated Tregs precisely captured TNFR2 activation, consistent with previous findings produced by different methods, as described below. A closer examination of individual genes in the "TNFα signaling via the

NF-κB" pathway showed that the expression levels of *NFKB2* and *RELB* were elevated. TNFR2 is known to activate non-canonical NF-κB signaling via activation of NF-κB inducing kinase (NIK), responsible for processing the C-terminal region of p100, which is encoded by *NFKB2* [144]. The processing of p100 induces translocation of the transcription factor RelB (encoded by *RELB*), followed by induction of target gene transcription by the RelB/p52 transcription factor [144]. My transcriptome data clearly showed activation of the non-canonical NF-κB pathway in Tregs by stimulation with a TNFR2 agonist. Taken together, these findings suggest that TNFR2 activation is likely to promote Treg proliferation through non-canonical NF-κB signaling.

The "IL-2 STAT5 signaling" pathway was also upregulated in TNFR2 agonist antibody-treated and *TNFR2*-high Tregs. The IL-2 receptor is expressed in Tregs and activates STAT5, which then promotes the activation and proliferation of Tregs [145]. Activation of TNFR2 by the TNFR2 agonist antibody enhanced Treg proliferation when combined with IL-2 [116]. In addition to its involvement in proliferation, IL-2 induces FOXP3 expression [146]. Meanwhile, STAT5 functions downstream of IL-2 and enhances transcription of *FOXP3* by binding its promoter region [146]. My *in vitro* data confirmed that the IL-2 signaling pathway was enhanced by the TNFR2 agonist, resulting in Treg proliferation. These results were consistent with previous studies reporting that activation of TNFR2 in mouse Tregs can induce *TNFR2* expression but not *TNFR1* through TNFα-dependent phosphorylation of STAT5 by IL-2 [145], and TNFR2 agonist antibody elevated *STAT5* expression in Tregs [141]. Moreover, my results demonstrated that the "IL-6 JAK STAT3" pathway was activated in *TNFR2*-high Tregs. A previous study

indicated that activation of the STAT3 transcription factor enhances *FOXP3* expression in Tregs [146], suggesting that "IL-2 STAT5 signaling" and "IL-6 JAK STAT3" are likely to regulate Treg proliferation pathways.

My data showed that the "IFNγ response" was upregulated in Tregs treated with the TNFR2 agonist antibody and in *TNFR2*-high Tregs. Interestingly, the TNFR2 agonist antibody decreased the ratio of IFNγ-positive Tregs [147]. Hence, the highlighted IFNγ response pathway in my analysis likely did not increase the abundance of IFNγ-positive Tregs but rather enhanced IFNγ signaling. TNFR2 activates AKT and PI3K [148], which affect the phosphorylation of STAT1 and was consistent with my identification of the "PI3K AKT mTOR signaling" pathway in the *TNFR2*-high Tregs. This "IFNγ response" pathway may also indicate that TNFR2 transmits signals to STAT1 via AKT-PI3K, which agrees with the findings of another study that also showed the IFNγ pathway is involved in the generation of Tregs [149]. Furthermore, the activation of the "IFNα response" pathways could be due to the activation of STAT1 as IFNα induces gene transcription via STAT1 [150]. A previous report showed that IFNα signaling promotes the development of Tregs in the thymus and survival in the peripheral tissues [151]. Hence, activation of the "IFNγ pathway" and "IFNα pathway" could represent one mechanism by which TNFR2 activation stimulates Treg proliferation.

My single-cell RNA-seq analysis highlighted not only the inflammation- and cytokine-related pathways discussed above but also Treg metabolism by TNFR2 signaling. As shown in Figure 7B, "glycolysis" and "oxidative phosphorylation" pathways were pronounced in *TNFR2*-high Tregs. In thymus-derived Tregs, TNFR2 induced glycolysis

through PI3K-mTOR signaling [152] and my data also captured this aspect.

From single-cell RNA-seq analysis of TNFR2 agonist antibody-stimulated Tregs, I identified a total of 32 pathways (Figure 7B). Meanwhile, cancer Tregs had 43 highlighted pathways (Figure 8D). Interestingly, 31 out the 32 pathways from TNFR2 agonist antibody-stimulated Tregs were included in the 43 pathways of cancer Tregs. This finding strongly suggests that TNFR2 signaling is fully active in cancer Tregs. Furthermore, pathway enrichment analysis of cancer Tregs was performed using DEGs extracted that were commonly upregulated in *TNFR2*-high cancer Tregs of HCC, NSCLC, and CRC. This suggests that the upregulation of TNFR2 signaling in cancer Tregs is a common feature in these cancer types. In fact, a previous report showed that the level of TNFR2 expression in Tregs was elevated in ovarian cancer patients, especially in patients with ascites [124]. Meanwhile, another report showed a correlation between the number of TNFR2-high Tregs in pleural effusion and the prognosis of lung cancer patients. The survival rate was significantly lower in patients with TNFR2-high Tregs [125]. Moreover, TNFR2 expression levels in Tregs within the peripheral blood correlate with the clinical pathology of lung cancer patients [153].

Similar analyses will reveal that pronounced TNFR2 signaling also occurs in these cancer types in which the increased number of TNFR2-high Treg is evident or possibly determines the prognosis of patients. Six out of the 11 pathways in cancer Tregs not overlapped with TNFR2 agonist antibody-stimulated Tregs were cell proliferation-related pathways such as: “Myc targets v1,” “G2M checkpoint,” “E2F targets,” “mitotic spindle,” “Myc targets v2,” and “mitogenesis.” I speculate that this is because cancer Tregs could

chronically receive TNFR2 activation stimuli under the cancerous environment that may activate TNFR2-dependent proliferation pathways in cancer Tregs. This phenomenon may occur by the enhanced expression of TNFR2 ligand, TNFα, which was also identified as an upregulated gene in my cancer Treg analysis. Indeed, the expression of TNFα is elevated in human cancer tissues, such as gastric and colorectal cancers, compared to adjacent normal tissues [154]. TNFα is also known to upregulate TNFR2 expression [155]; therefore, TNFR2 signaling may be further enhanced in cancer Tregs. Although pathway enrichment analysis with single-cell RNA-seq data of TNFR2 agonist antibody-stimulated Tregs failed to show the cell proliferation pathways, "G2M checkpoint" and "E2F targets" were top two pathways in the pathway enrichment analysis with Ampli-seq data (Figure 6B). For example, *EZH2* expression was upregulated and included in the "E2F target" and "G2M checkpoint" pathways in the Ampli-seq (Figure 6C and D), and EZH2 expression is reportedly upregulated by TNFR2 stimulation [156] and involved in Treg stability after TNFR2 activation [157]. Taken together, the two pathways "E2F target" and "G2M checkpoint" may capture the proliferative phenotype of *TNFR2*-high Tregs, in response to *in vitro* TNFR2 agonist antibody stimulation, but genes encoding such cell proliferation pathways were not collectively detected upregulated in *TNFR2*-high vs *TNFR2*-low Tregs *in vitro.* However, it is noteworthy that the single-cell RNA-seq identified the larger number pathways compared to the Ampli-seq, implying that the significance of my study that for the first time has fully uncovered TNFR2 signaling in *TNFR2*-high Treg by using single-cell RNA-seq.

Aside from cancer, changes in Treg function or their reduced abundance also represent

features of other diseases. For instance, Treg dysfunction or reduced abundance has been reported in various autoimmune diseases, including systemic lupus erythematosus and type-1 diabetes [112]. Moreover, recent studies have demonstrated an altered Treg population in neurodegenerative diseases such as Alzheimer's disease and Parkinson's disease [158]. By completely identifying all TNFR2 pathways, the determination of whether TNFR2 is active or inactive in Tregs in the above-mentioned diseases will become possible. In addition, the overall proportion of TNFR2-high Tregs may serve as a diagnostic marker as well as a marker of TNFR2 therapy efficacy. However, these postulations must be confirmed by analyzing TNFR2 expression profiles and investigating the proportion of *TNFR2*-low and *TNFR2*-high populations in these diseases. In addition, recent single-cell RNA-seq studies based on clinical samples from cancer patients identified Treg subtypes by their gene expression profiles and function [134-136, 159]. Thus, by increasing the size of patient cohort and analyzing the detailed relationship between TNFR2 expression levels and Treg subsets in the future studies, it may be possible to characterize the specific Treg subsets more deeply responsible for TNFR2 signaling.

Thus, my results provide evidence that TNFR2 signaling is activated in TNFR2-high cancer Tregs and that TNFR2-activated Tregs may help cancer cells escape immune surveillance, making TNFR2 signaling a potential anticancer therapy.

Figures and Tables

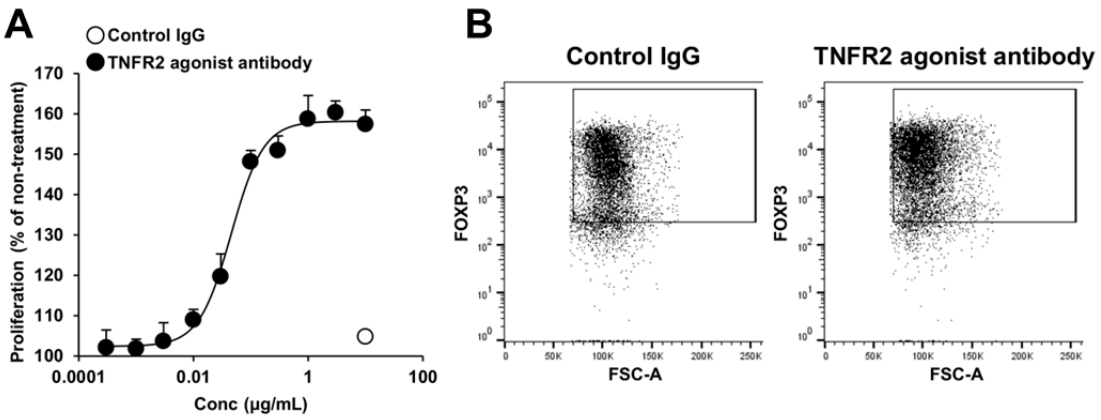

Figure 5. Treg expansion by treatment with TNFR2 agonist antibody

A Treg expansion by TNFR2 agonist antibody treatment. Tregs were isolated from healthy donor PBMCs and cultured in the presence of the control IgG or TNFR2 agonist antibody for 7 d. Treg proliferation in response to the control IgG or TNFR2 was detected by measuring ATP content and calculated as a percentage of the non-treatment group. Data points represent the mean + standard deviation, acquired in triplicate. **B** FOXP3 protein expression in Tregs treated with the control IgG or TNFR2 agonist antibody. FOXP3 expression was measured by FACS. Data was obtained from a representative sample from each group. All data are representative of at least two independent experiments.

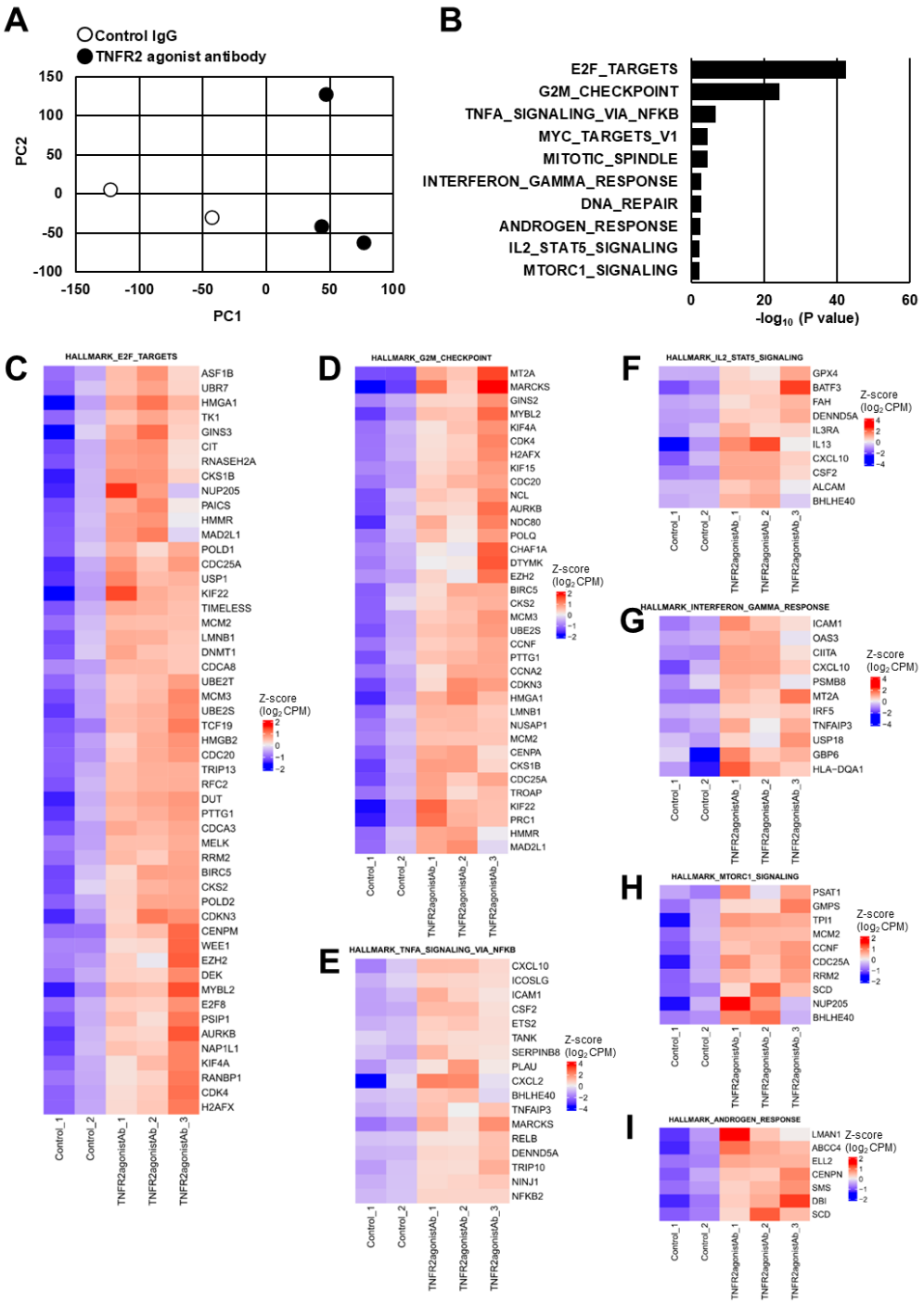

Figure 6. Pathway enrichment analysis using Ampli-seq transcriptome data from Tregs treated with the TNFR2 agonist antibody Ampli-seq analysis was performed using Tregs treated with a TNFR2 agonist antibody

A A scatter plot of the first and second principal components in the PCA. **B** Enriched pathways of the upregulated DEGs identified in Tregs treated with the TNFR2 agonist antibody. Significantly enriched pathways with a P value < 0.01 are shown. Bars indicate the -log$_{10}$ (P value) in each pathway. **C-I** Heatmaps of individual DEG expression values associated with each pathway. These pathways included **C** E2F Target, **D** G2M checkpoint, **E** TNFα signaling via NF-κB, **F** IL-2 STAT5 signaling, **G** IFNγ response, **H** mTORC1 signaling, and **I** androgen response. The expression levels for each gene are shown as z-scaling log$_2$ counts per million (CPM) values in the heatmaps.

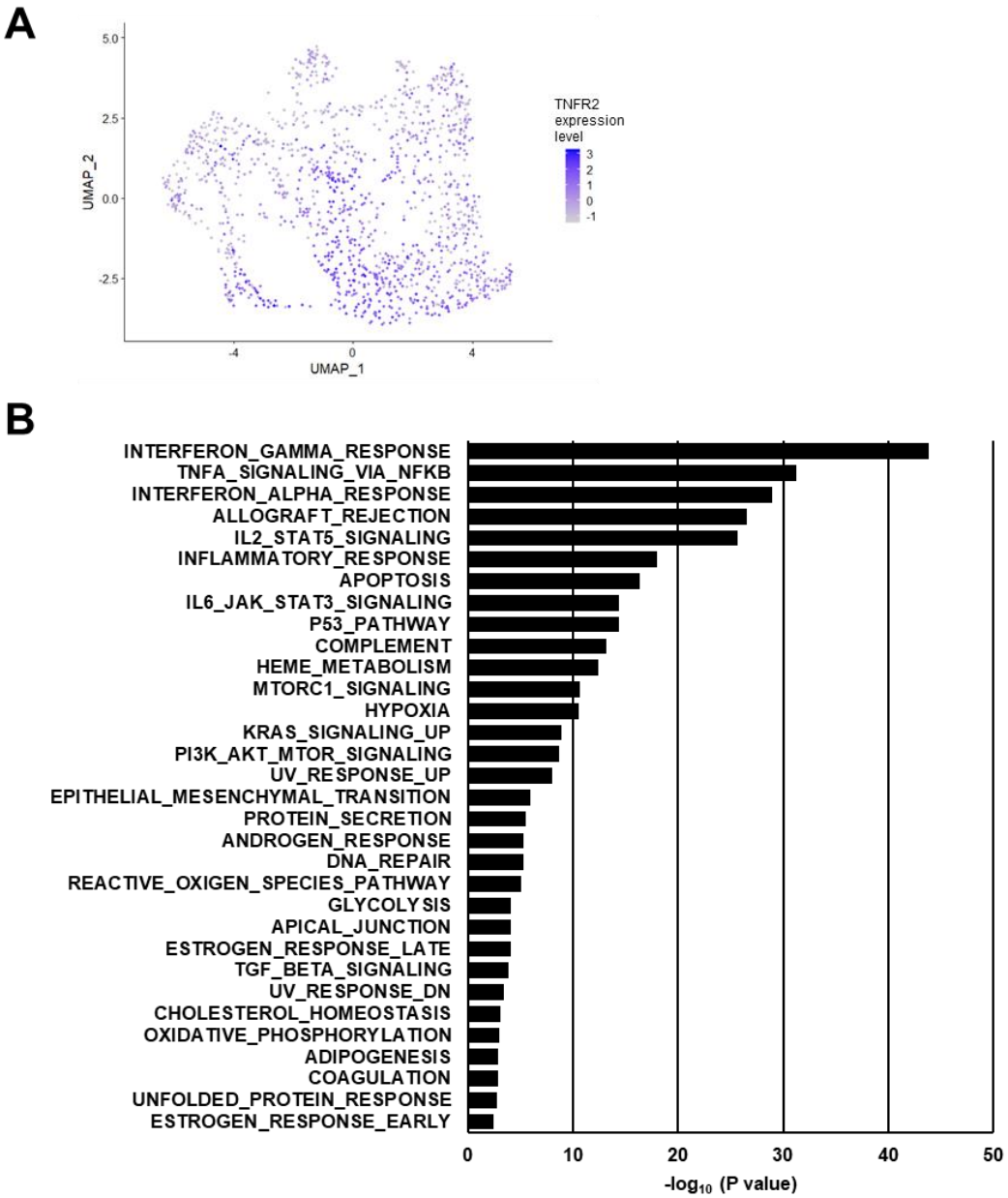

Figure 7. Pathway enrichment analysis using single-cell RNA-seq transcriptome data from Tregs treated with the TNFR2 agonist antibody

A Log_e-normalized *TNFR2* expression levels are shown in the UMAP plot. **B** Pathway enrichment of DEGs between *TNFR2*-high and *TNFR2*-low Tregs. Significantly enriched pathways with a P value < 0.01 are shown. Bars indicate the $-log_{10}$ (P value) for each pathway.

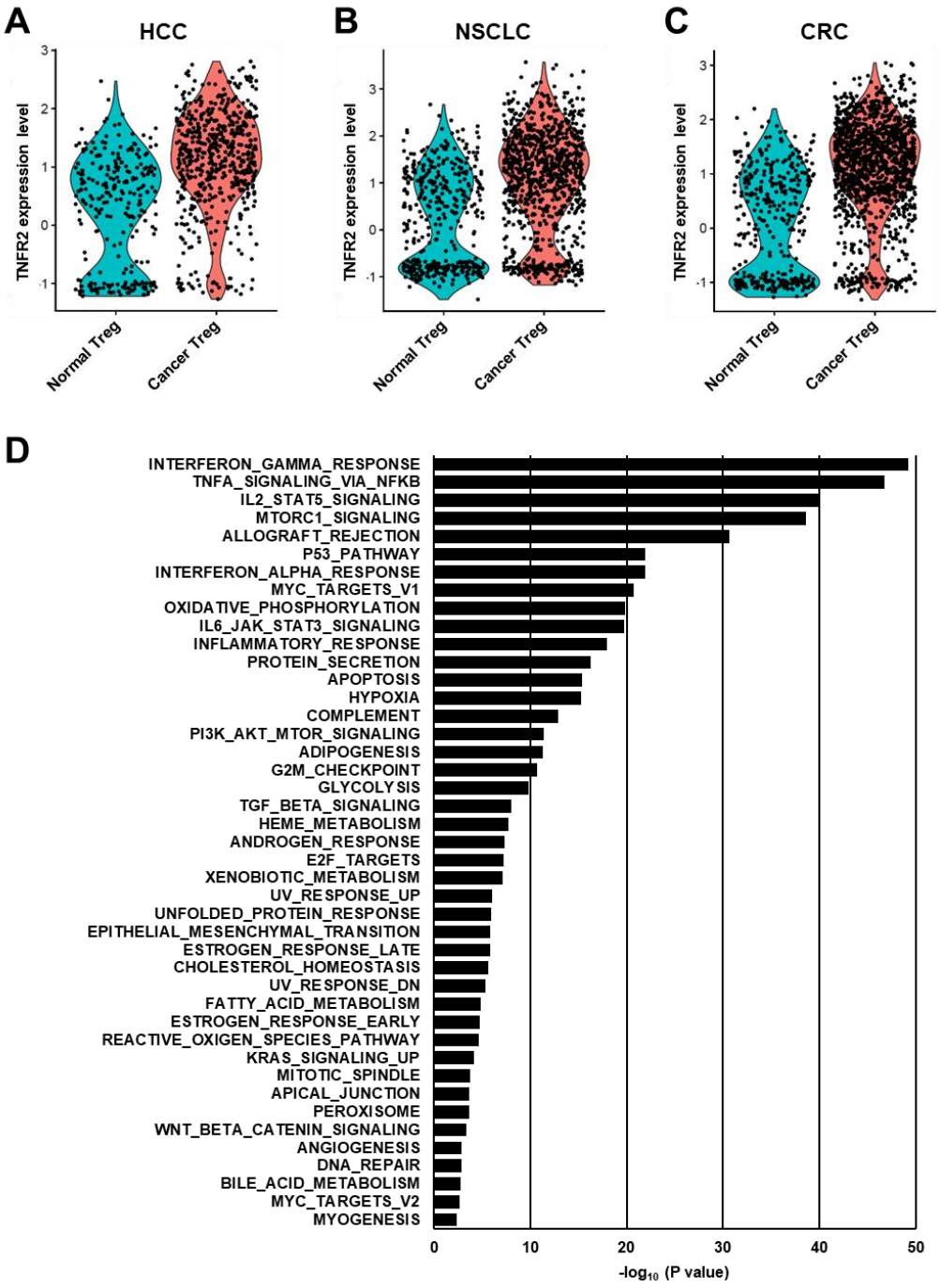

Figure 8. Enhanced *TNFR2* expression and signaling in cancer Tregs

A-C Violin plots showing $\log_e$-normalized expression levels of *TNFR2* in **A** HCC (hepatocellular carcinoma), **B** NSCLC (non-small cell lung cancer), and **C** CRC (colorectal cancer). **D** Pathway enrichment by DEGs between cancer and normal Tregs that were commonly upregulated in the three cancers. Significantly enriched pathways with a P value < 0.01 are shown, and bars indicate the $-\log_{10}$ (P value) for each pathway. The DEGs between cancer and normal Tregs were extracted and commonly upregulated DEGs across three datasets (GSE98638, GSE99254, and GSE108989) were used for pathway enrichment analysis.

General Discussion

The identification of the gene signature that constitute pathologic pathways by comprehensive gene expression analyses allows for new associations of disease and pathologic genes that would be difficult to prove by examining specific genes in past studies.

As concrete examples, in the case of Chapter 1, by comparing the gene signatures after TREM2 activation identified by RNA-seq of iPS-microglia treated with anti-TREM2 agonist antibody and the gene signatures extracted from microglia of AD patients by snRNA-seq, I found for the first time that TREM2 activation was lower in microglia of AD than in microglia of healthy subjects, and was further reduced with disease progression, suggesting that the lower TREM2 activation in microglia of AD patients may allow anti-TREM2 agonist antibodies may be able to control AD progression because TREM2 activation is low in microglia of AD patients. In the case of Chapter 2, My comparisons between (i) the gene signatures of TNFR2-activated Tregs by RNA-seq and scRNA-seq and (ii) those of cancer Tregs revealed that TNFR2 regulates multiple pathways in cancer Tregs that may help cancer cells escape immune surveillance. Combined, I proposed that inhibition of TNFR2 signaling could be a target for anticancer therapy. Although the diseases in the above two cases are completely different, they are considered to be successful cases in which the relationship between the disease-causing genes and the disease was clarified by identifying the gene signatures that constitute the

pathologic pathways using comprehensive gene expression analysis.

In this section, I would like to discuss the commonalities between my two studies and the factors that led me to identify the gene signatures that comprise the pathologic pathways using comprehensive gene expression analysis. First, in both cases, I clearly defined the gene signature, which is controlled by the presence or absence of expression of the gene of interest, by performing in-vitro experiments and exhaustive gene expression analyses that specifically regulate the expression of pathologic genes alone. Next, I unified the cell types used in the experiments with the cell types in which disease-specific gene signatures appear, and extracted the gene signatures regulated by the pathologic genes. This unification of cell types allowed direct comparison of the gene signatures regulated by the pathologic genes and those of the disease, eliminating potential factors unrelated to the phenomena of interest. Furthermore, in the comparison of the gene signatures, I incorporated biological interpretation using pathway and GO enrichment analysis to each gene signature and compared overlaps on pathway and GO levels. This method confirms that biologically important functions in disease were regulated by a pathologic gene. The common factors mentioned above enabled us to identify the gene signatures constituting the pathologic pathways using comprehensive gene expression analysis and even suggested the possibility of drug discovery.

Based on the above discussion, I would like to further discuss some points to be noted in

conducting this research method and promote the effective use of this research method in the future. First, it is important to note that studies using comprehensive gene expression analysis are required to handle a huge number of results, for example, approximately 26,000 genes for human, as many as the number of genes, and the interpretation of the gene signatures obtained from such studies is intensive. Therefore, it is important to have a precise plan in the research planning phase that allows the acquisition of the gene signatures focused only on the specific phenomenon to be elucidated without confounding factors. In addition to basic knowledge of the hypothesis to be proved, the interpretation of the gene signature requires a comprehensive and objective evaluation, integrating expert knowledge of the vast number of genes and their populations, such as pathways, omics, and bioinformatics. Knowledge bias toward a particular gene population or pathway sometimes runs the risk of creating arbitrary bias in the interpretation of the gene signature. To avoid this risk, it is useful to use biological information from mechanical methods such as enrichment analysis using GO and pathway databases and GSEA as a source of interpretation when interpreting the gene signature [64]. On the other hand, those bioinformatic analysis methods calculate importance scores based on gene overlap and ranking, so it is not always clear whether the highlighted pathways contain biologically key genes. Therefore, human curation after analysis is also important. Since it is difficult for one researcher to do all of the

interpretation covering all of the above specialties, it is also said that the ideal research structure for the future is to have various specialists collaborate on the interpretation, since it is difficult for a single researcher to do all of the interpretation covering all of the above specialties [160].

Finally, I would like to describe the significance of this study. I here proposed the method that is based on comprehensive gene expression analyses and allows us to interpret the relationship between the pathologic gene and the disease comprehensively, beyond the extent to which conventional studies have only examined certain aspects of the pathologic gene. This method may increase the speed of identifying the pathogenesis of diseases and the probability of success in drug discovery. In addition, this research approach is applicable to basic biology. When you wish to verify a complex phenomenon in a difficult-to-obtain species, you may first extract the gene signatures that are reliably regulated by the target gene in an in-vitro experiment in a closely related model species, and feedback the data from the model organism to the species of the primary interest.

In conclusion, based on the above considerations, if the identification of the gene signature that constitutes pathologic pathways by comprehensive gene expression analyses can be performed with high accuracy, many new insights into the relationship between disease and pathway genes, which have been difficult to prove by simply examining specific genes, will be realized. I hope that such this method will accelerate

precise drug discovery research directly related to the pathology of diseases.

Acknowledgements

I am most grateful to Professor Yuji Inagaki for being in charge of this dissertation, and for his valuable guidance and encouragement through my doctoral program.Also, I am sincerely grateful to Professors Ryusuke Niwa, Kaori Ishikawa and Yukihiko Toquenaga for guiding my work and valuable discussions.

I also thank Dr. Shuji Sato in Takeda Pharmaceutical Company Limited for his encouragement and helpful guidance in my research work.

Acknowledgements are also made to Dr. Yo Muraki in Takeda Pharmaceutical Company Limited for his kind cooperation and advice in my research work.

Further, I thank Associate Director Shuuichi Miyakawa and Dr. Yusuke Kikukawa, current supervisors in Takeda Pharmaceutical Company Limited, for endorsement of participation in the graduate program.

Finally, I would like to appreciate my family for supporting my life in University of Tsukuba.

References

1. Moraes, F, & Góes, A (2016) A decade of human genome project conclusion: Scientific diffusion about our genome knowledge. *Biochemistry and molecular biology education : a bimonthly publication of the International Union of Biochemistry and Molecular Biology*, 44(3), 215–223.

2. Hue-Roye, K, & Vege, S (2008) Principles of PCR-based assays. *Immunohematology*, 24(4), 170–175.

3. Pareek, CS, Smoczynski, R, & Tretyn, A (2011) Sequencing technologies and genome sequencing. *Journal of applied genetics*, 52(4), 413–435.

4. Jovic, D, Liang, X, Zeng, H, Lin, L, Xu, F, & Luo, Y (2022) Single-cell RNA sequencing technologies and applications: A brief overview. *Clinical and translational medicine*, 12(3), e694.

5. Schneider, MV, & Orchard, S (2011) Omics technologies, data and bioinformatics principles. *Methods in molecular biology (Clifton, N.J.)*, 719, 3–30.

6. Kalucka, J, de Rooij, LPMH, Goveia, J, Rohlenova, K, Dumas, SJ, Meta, E, Conchinha, NV, Taverna, F, Teuwen, LA, Veys, K, García-Caballero, M, Khan, S, Geldhof, V, Sokol, L, Chen, R, Treps, L, Borri, M, de Zeeuw, P, Dubois, C, Karakach, TK, Carmeliet, P (2020) Single-Cell Transcriptome Atlas of Murine Endothelial Cells. *Cell*, 180(4), 764–779.e20.

7. Wang, K, Wang, D, Zheng, X, Qin, A, Zhou, J, Guo, B, Chen, Y, Wen, X, Ye, W, Zhou, Y, & Zhu, Y (2019) Multi-strategic RNA-seq analysis reveals a high-resolution transcriptional landscape in cotton. *Nature communications*, 10(1),

4714.

8. Zhang, TQ, Chen, Y, & Wang, JW (2021) A single-cell analysis of the Arabidopsis vegetative shoot apex. *Developmental cell*, 56(7), 1056–1074.e8.

9. Liu, Y, Morley, M, Brandimarto, J, Hannenhalli, S, Hu, Y, Ashley, EA, Tang, WH, Moravec, CS, Margulies, KB, Cappola, TP, Li, M, & MAGNet consortium (2015) RNA-Seq identifies novel myocardial gene expression signatures of heart failure. *Genomics*, 105(2), 83–89.

10. Sotiriou, C, & Pusztai, L (2009) Gene-expression signatures in breast cancer. *The New England journal of medicine*, 360(8), 790–800.

11. Wang, R, Zheng, X, Wang, J, Wan, S, Song, F, Wong, MH, Leung, KS, & Cheng, L (2022) Improving bulk RNA-seq classification by transferring gene signature from single cells in acute myeloid leukemia. *Briefings in bioinformatics*, 23(2), bbac002.

12. Yu, L, Shen, N, Shi, Y, Shi, X, Fu, X, Li, S, Zhu, B, Yu, W, & Zhang, Y (2022) Characterization of cancer-related fibroblasts (CAF) in hepatocellular carcinoma and construction of CAF-based risk signature based on single-cell RNA-seq and bulk RNA-seq data. *Frontiers in immunology*, 13, 1009789.

13. Bao, X, Shi, R, Zhao, T, Wang, Y, Anastasov, N, Rosemann, M, & Fang, W (2021) Integrated analysis of single-cell RNA-seq and bulk RNA-seq unravels tumour heterogeneity plus M2-like tumour-associated macrophage infiltration and aggressiveness in TNBC. *Cancer immunology, immunotherapy : CII*, 70(1), 189–202.

14. Agatonovic-Kustrin, S, Kettle, C & Morton, DW (2018) A molecular approach in drug development for Alzheimer's disease. *Biomed Pharmacother* 106: 553–565.

15. Jonsson, T, Stefansson, H, Steinberg, S, Jonsdottir, I, Jonsson, PV, Snaedal, J, Bjornsson, S, Huttenlocher, J, Levey, AI, Lah, JJ & Rujescu, D (2013) Variant of TREM2 associated with the risk of Alzheimer's disease. *N Engl J Med* 368: 107–116.

16. Guerreiro, R, Wojtas, A, Bras, J, Carrasquillo, M, Rogaeva, E, Majounie, E, Cruchaga, C, Sassi, C, Kauwe, JS, Younkin, S & Hazrati, L (2013) *TREM2* variants in Alzheimer's disease. *N Engl J Med* 368: 117–127.

17. Corder, EH, Saunders, AM, Strittmatter, WJ, Schmechel, DE, Gaskell, PC, Small, GW, Roses, AD, Haines, JL & Pericak-Vance, MA (1993) Gene dose of apolipoprotein E type 4 allele and the risk of Alzheimer's disease in late onset families. *Science* 261: 921–923.

18. Zhang, B, Gaiteri, C, Bodea, LG, Wang, Z, McElwee, J, Podtelezhnikov, AA, Zhang, C, Xie, T, Tran, L, Dobrin, R & Fluder, E (2013) Integrated systems approach identifies genetic nodes and networks in late-onset Alzheimer's disease. *Cell* 153: 707–720.

19. Wang, Y, Cella, M, Mallinson, K, Ulrich, JD, Young, KL, Robinette, ML, Gilfillan, S, Krishnan, GM, Sudhakar, S, Zinselmeyer, BH & Holtzman, DM (2015) TREM2 lipid sensing sustains the microglial response in an Alzheimer's disease model. *Cell* 160: 1061–1071.

20. Atagi, Y, Liu, CC, Painter, MM, Chen, XF, Verbeeck, C, Zheng, H, Li, X, Rademakers, R, Kang, SS, Xu, H & Younkin, S (2015) Apolipoprotein E is a ligand for triggering receptor expressed on myeloid cells 2 (TREM2). *J Biol Chem* 290: 26043–26050.

21. Bailey, CC, DeVaux, LB & Farzan, M (2015) The triggering receptor expressed on myeloid cells 2 binds apolipoprotein E. *J Biol Chem* 290: 26033–26042.

22. Song, W, Hooli, B, Mullin, K, Jin, SC, Cella, M, Ulland, TK, Wang, Y, Tanzi, RE & Colonna, M (2017) Alzheimer's disease-associated TREM2 variants exhibit either decreased or increased ligand-dependent activation. *Alzheimer's Dement* 13: 381–387.

23. Park, JS, Ji, IJ, An, HJ, Kang, MJ, Kang, SW, Kim, DH & Yoon, SY (2017) Disease-associated mutations of TREM2 alter the processing of N-linked oligosaccharides in the Golgi apparatus. *Traffic* 16: 510–518.

24. Park, JS, Ji, IJ, Kim, DH, An, HJ & Yoon, SY (2017) The Alzheimer's disease-associated R47H variant of TREM2 has an altered glycosylation pattern and protein stability. *Front Neurosci* 10: 618. doi: 10.3389/fnins.2016.00618

25. Luis, EO, Ortega-Cubero, S, Lamet, I, Razquin, C, Cruchaga, C, Benitez, BA, Lorenzo, E, Irigoyen, J, Pastor, MA & Pastor, P (2014) Frontobasal gray matter loss is associated with the *TREM2* p.R47H variant. *Neurobiol Aging* 35: 2681–2690.

26. Roussos, P, Katsel, P, Fam, P, Tan, W, Purohit, DP & Haroutunian, V (2015) The triggering receptor expressed on myeloid cells 2 (*TREM2*) is associated with

enhanced inflammation, neuropathological lesions and increased risk for Alzheimer's dementia. *Alzheimer's Dement* 11: 1163–1170.

27. Rajagopalan, P, Hibar, DP & Thompson, PM (2013) *TREM2* and neurodegenerative disease. *N Engl J Med* 369: 1565–1567.

28. Deming, Y, Li, Z, Benitez, BA & Cruchaga, C (2018) Triggering receptor expressed on myeloid cells 2 (TREM2): a potential therapeutic target for Alzheimer disease? *Expert Opin Ther Targets* 22: 587–598.

29. Jiang, T, Tan, L, Zhu, XC, Zhang, QQ, Cao, L, Tan, MS, Gu, LZ, Wang, HF, Ding, ZZ, Zhang, YD & Yu, JT (2014) Upregulation of TREM2 ameliorates neuropathology and rescues spatial cognitive impairment in a transgenic mouse model of Alzheimer's disease. *Neuropsychopharmacology* 39: 2949–2962.

30. Lee, CYD, Daggett, A, Gu, X, Jiang, LL, Langfelder, P, Li, X, Wang, N, Zhao, Y, Park, CS, Cooper, Y & Ferando, I (2018) Elevated TREM2 gene dosage reprograms microglia responsivity and ameliorates pathological phenotypes in Alzheimer's disease models. *Neuron* 97: 1032–1048.e5.

31. Jiang, T, Zhang, YD, Chen, Q, Gao, Q, Zhu, XC, Zhou, JS, Shi, JQ, Lu, H, Tan, L & Yu, JT (2016) TREM2 modifies microglial phenotype and provides neuroprotection in P301S tau transgenic mice. *Neuropharmacology* 105: 196–206.

32. Schlepckow, K, Monroe, KM, Kleinberger, G, Cantuti-Castelvetri, L, Parhizkar, S, Xia, D, Willem, M, Werner, G, Pettkus, N, Brunner, B & Sülzen, A (2020) Enhancing protective microglial activities with a dual function TREM2 antibody

to the stalk region. *EMBO Mol Med* 12: e11227. doi: 10.15252/emmm.201911227

33. Wang, S, Mustafa, M, Yuede, CM, Salazar, SV, Kong, P, Long, H, Ward, M, Siddiqui, O, Paul, R, Gilfillan, S & Ibrahim, A (2020) Anti-human TREM2 induces microglia proliferation and reduces pathology in an Alzheimer's disease model. *J Exp Med* 217: e20200785. doi: 10.1084/jem.20200785

34. Celarain, N, Sánchez-Ruiz de Gordoa, J, Zelaya, MV, Roldán, M, Larumbe, R, Pulido, L, Echavarri, C & Mendioroz, M (2016) *TREM2* upregulation correlates with 5-hydroxymethycytosine enrichment in Alzheimer's disease hippocampus. *Clin Epigenet* 8: 37. doi: 10.1186/s13148-016-0202-9

35. Perez, SE, Nadeem, M, He, B, Miguel, JC, Malek-Ahmadi, MH, Chen, K & Mufson, EJ (2017) Neocortical and hippocampal TREM2 protein levels during the progression of Alzheimer's disease. *Neurobiol Aging* 54: 133–143.

36. Zhao, Y, Bhattacharjee, S, Jones, BM, Dua, P, Alexandrov, PN, Hill, JM & Lukiw, WJ (2013) Regulation of TREM2 expression by an NF-κB-sensitive miRNA-34a. *Neuroreport* 24: 318–323.

37. Strobel, S, Grünblatt, E, Riederer, P, Heinsen, H, Arzberger, T, Al-Sarraj, S, Troakes, C, Ferrer, I & Monoranu, CM (2015) Changes in the expression of genes related to neuroinflammation over the course of sporadic Alzheimer's disease progression: CX3CL1, TREM2, and PPARγ. *J Neural Transm (Vienna)* 122: 1069–1076.

38. Ma, L, Allen, M, Sakae, N, Ertekin-Taner, N, Graff-Radford, NR, Dickson, DW,

Younkin, SG & Sevlever, D (2016) Expression and processing analyses of wild type and p.R47H TREM2 variant in Alzheimer's disease brains. *Mol Neurodegener* 11: 72. doi: 10.1186/s13024-016-0137-9

39. Lue, LF, Schmitz, CT, Serrano, G, Sue, LI, Beach, TG & Walker, DG (2015) TREM2 protein expression changes correlate with Alzheimer's disease neurodegenerative pathologies in post-mortem temporal cortices. *Brain Pathol* 25: 469–480.

40. Zhou, Y, Song, WM, Andhey, PS, Swain, A, Levy, T, Miller, KR, Poliani, PL, Cominelli, M, Grover, S, Gilfillan, S & Cella, M (2020) Human and mouse single-nucleus transcriptomics reveal TREM2-dependent and TREM2-independent cellular responses in Alzheimer's disease. *Nat Med* 26: 131–142.

41. Kleinberger, G, Yamanishi, Y, Suárez-Calvet, M, Czirr, E, Lohmann, E, Cuyvers, E, Struyfs, H, Pettkus, N, Wenninger-Weinzierl, A, Mazaheri, F & Tahirovic, S (2014) TREM2 mutations implicated in neurodegeneration impair cell surface transport and phagocytosis. *Sci Transl Med* 6: 243ra86. doi: 10.1126/scitranslmed.3009093.

42. Feuerbach, D, Schindler, P, Barske, C, Joller, S, Beng-Louka, E, Worringer, KA, Kommineni, S, Kaykas, A, Ho, DJ, Ye, C & Welzenbach, K (2017) ADAM17 is the main sheddase for the generation of human triggering receptor expressed in myeloid cells (hTREM2) ectodomain and cleaves TREM2 after histidine 157. *Neurosci Lett* 660: 109–114.

43. Gispert, JD, Suárez-Calvet, M, Monté, GC, Tucholka, A, Falcon, C, Rojas, S,

Rami, L, Sanchez-Valle, R, Lladó, A, Kleinberger, G & Haass, C (2016) Cerebrospinal fluid sTREM2 levels are associated with gray matter volume increases and reduced diffusivity in early Alzheimer's disease. *Alzheimer's Dement* 12: 1259–1272.

44. Suárez-Calvet, M, Kleinberger, G, Araque Caballero, MÁ, Brendel, M, Rominger, A, Alcolea, D, Fortea, J, Lleó, A, Blesa, R, Gispert, JD & Sánchez-Valle, R (2016) sTREM2 cerebrospinal fluid levels are a potential biomarker for microglia activity in early-stage Alzheimer's disease and associate with neuronal injury markers. *EMBO Mol Med* 8: 466–476.

45. Suárez-Calvet, M, Araque Caballero, MÁ, Kleinberger, G, Bateman, RJ, Fagan, AM, Morris, JC, Levin, J, Danek, A, Ewers, M & Haass, C (2016) Early changes in CSF sTREM2 in dominantly inherited Alzheimer's disease occur after amyloid deposition and neuronal injury. *Sci Transl Med* 8: 369ra178. doi: 10.1126/scitranslmed.aag1767

46. Wu, K, Byers, DE, Jin, X, Agapov, E, Alexander-Brett, J, Patel, AC, Cella, M, Gilfilan, S, Colonna, M, Kober, DL & Brett, TJ (2015) TREM-2 promotes macrophage survival and lung disease after respiratory viral infection. *J Exp Med* 212: 681–697.

47. Suárez-Calvet, M, Morenas-Rodríguez, E, Kleinberger, G, Schlepckow, K, Araque Caballero, MÁ, Franzmeier, N, Capell, A, Fellerer, K, Nuscher, B, Eren, E & Levin, J (2019) Early increase of CSF sTREM2 in Alzheimer's disease is associated with tau related-neurodegeneration but not with amyloid-β pathology.

Mol Neurodegener 14: 1. doi: 10.1186/s13024-018-0301-5

48. Kennedy, M, D'Souza, SL, Lynch-Kattman, M, Schwantz, S & Keller, G (2007) Development of the hemangioblast defines the onset of hematopoiesis in human ES cell differentiation cultures. *Blood* 109: 2679–2687.

49. Sturgeon, CM, Ditadi, A, Awong, G, Kennedy, M & Keller, G (2014) Wnt signaling controls the specification of definitive and primitive hematopoiesis from human pluripotent stem cells. *Nat Biotechnol* 32: 554–561.

50. Abud, EM, Ramirez, RN, Martinez, ES, Healy, LM, Nguyen, CHH, Newman, SA, Yeromin, AV, Scarfone, VM, Marsh, SE, Fimbres, C & Caraway CA (2017) iPSC-derived human microglia-like cells to study neurological diseases. *Neuron* 94: 278–293.e9.

51. Ihaka, R & Robert, G (1996) R: A language for data analysis and graphics. *J Comp Graph Stat* 5: 299–314. Available via http://www.R-project.org.

52. Robinson, MD, McCarthy, DJ & Smyth, GK (2010) edgeR: a Bioconductor package for differential expression analysis of digital gene expression data. *Bioinformatics* 26: 139–140.

53. McCarthy, DJ, Chen, Y & Smyth, GK (2012) Differential expression analysis of multifactor RNA-Seq experiments with respect to biological variation. *Nucleic Acids Res* 40: 4288–4297.

54. Mathys, H, Davila-Velderrain, J, Peng, Z, Gao, F, Mohammadi, S, Young, JZ, Menon, M, He, L, Abdurrob, F, Jiang, X & Martorell, AJ (2019) Single-cell transcriptomic analysis of Alzheimer's disease. *Nature* 570: 332–337.

55. O'Bryant, SE, Humphreys, JD, Smith, GE, Ivnik, RJ, Graff-Radford, NR, Petersen, RC & Lucas, JA (2008) Detecting dementia with the mini-mental state examination in highly educated individuals. *Arch Neurol* 65: 963–967.

56. Love, MI, Huber, W & Anders, S (2014) Moderated estimation of fold change and dispersion for RNA-seq data with DESeq2. *Genome Biol* 15: 550. doi: 10.1186/s13059-014-0550-8

57. Stuart, T, Butler, A, Hoffman, P, Hafemeister, C, Papalexi, E, Mauck, WM 3rd, Hao, Y, Stoeckius, M, Smibert, P & Satija, R (2019) Comprehensive integration of single-cell data. *Cell* 177: 1888–1902.e21.

58. Hodge, RD, Bakken, TE, Miller, JA, Smith, KA, Barkan, ER, Graybuck, LT, Close, JL, Long, B, Johansen, N, Penn, O & Yao, Z (2019) Conserved cell types with divergent features in human versus mouse cortex. *Nature* 573: 61–68.

59. Satoh, J, Shimamura, Y & Tabunoki, H (2012) Gene expression profile of THP-1 monocytes following knockdown of DAP12, a causative gene for Nasu-Hakola disease. *Cell Mol Neurobiol* 32: 337–343.

60. Bouchon, A, Hernández-Munain, C, Cella, M & Colonna, M (2001) A DAP12-mediated pathway regulates expression of CC chemokine receptor 7 and maturation of human dendritic cells. *J Exp Med* 194: 1111–1122.

61. Hamerman, JA, Jarjoura, JR, Humphrey, MB, Nakamura, MC, Seaman, WE & Lanier, LL (2006) Cutting edge: inhibition of TLR and FcR responses in macrophages by triggering receptor expressed on myeloid cells (TREM)-2 and DAP12. *J Immunol* 177: 2051–2055.

62. Rosales, C (2017) Fcγ receptor heterogeneity in leukocyte functional responses. *Front Immunol* 8: 280. doi: 10.3389/fimmu.2017.00280

63. Mootha, VK, Lindgren, CM, Eriksson, KF, Subramanian, A, Sihag, S, Lehar, J, Puigserver, P, Carlsson, E, Ridderstråle, M, Laurila, E & Houstis, N (2003) PGC-1α-responsive genes involved in oxidative phosphorylation are coordinately downregulated in human diabetes. *Nat Genet* 34: 267–273.

64. Subramanian, A, Tamayo, P, Mootha, VK, Mukherjee, S, Ebert, BL, Gillette, MA, Paulovich, A, Pomeroy, SL, Golub, TR, Lander, ES & Mesirov, JP (2005) Gene set enrichment analysis: a knowledge-based approach for interpreting genome-wide expression profiles. *Proc Natl Acad Sci USA* 102: 15545–15550.

65. Sessa, G, Podini, P, Mariani, M, Meroni, A, Spreafico, R, Sinigaglia, F, Colonna, M, Panina, P & Meldolesi, J (2004) Distribution and signaling of TREM2/DAP12, the receptor system mutated in human polycystic lipomembraneous osteodysplasia with sclerosing leukoencephalopathy dementia. *Eur J Neurosci* 20: 2617–2628.

66. Humphrey, MB, Daws, MR, Spusta, SC, Niemi, EC, Torchia, JA, Lanier, LL, Seaman, WE & Nakamura, MC (2006) TREM2, a DAP12-associated receptor, regulates osteoclast differentiation and function. *J Bone Miner Res* 21: 237–245.

67. Sun, M, Zhu, M, Chen, K, Nie, X, Deng, Q, Hazlett, LD, Wu, Y, Li, M, Wu, M & Huang, X (2013) TREM-2 promotes host resistance against *Pseudomonas aeruginosa* infection by suppressing corneal inflammation via a PI3K/Akt signaling pathway. *Invest Ophthalmol Vis Sci* 54: 3451–3462.

68. Kobayashi, M, Konishi, H, Sayo, A, Takai, T & Kiyama, H (2016) TREM2/DAP12 signal elicits proinflammatory response in microglia and exacerbates neuropathic pain. *J Neurosci* 36: 11138–11150.

69. Varnum, MM, Clayton, KA, Yoshii-Kitahara, A, Yonemoto, G, Koro, L, Ikezu, S & Ikezu, T (2017) A split-luciferase complementation, real-time reporting assay enables monitoring of the disease-associated transmembrane protein TREM2 in live cells. *J Biol Chem* 292: 10651–10663.

70. Cheng, Q, Danao, J, Talreja, S, Wen, P, Yin, J, Sun, N, Li, CM, Chui, D, Tran, D, Koirala, S & Chen, H (2018) TREM2-activating antibodies abrogate the negative pleiotropic effects of the Alzheimer's disease variant *Trem2*^{R47H} on murine myeloid cell function. *J Biol Chem* 293: 12620–12633.

71. Rosciszewski, G, Cadena, V, Murta, V, Lukin, J, Villarreal, A, Roger, T & Ramos, AJ (2018) Toll-like receptor 4 (TLR4) and triggering receptor expressed on myeloid cells-2 (TREM-2) activation balance astrocyte polarization into a proinflammatory phenotype. *Mol Neurobiol* 55: 3875–3888.

72. He, GL, Luo, Z, Shen, TT, Wang, ZZ, Li, P, Luo, X, Yang, J, Tan, YL, Wang, Y, Gao, P & Yang, XS (2020) TREM2 regulates heat acclimation-induced microglial M2 polarization involving the PI3K-Akt pathway following EMF exposure. *Front Cell Neurosci* 13: 591. doi: 10.3389/fncel.2019.00591

73. Szczepanik, AM, Funes, S, Petko, W & Ringheim, GE (2001) IL-4, IL-10 and IL-13 modulate Aβ(1–42)-induced cytokine and chemokine production in primary murine microglia and a human monocyte cell line. *J Neuroimmunol* 113:

49–62.

74. Shimizu, E, Kawahara, K, Kajizono, M, Sawada, M & Nakayama, H (2008) IL-4-induced selective clearance of oligomeric β-amyloid peptide$_{1-42}$ by rat primary type 2 microglia. *J Immunol* 181: 6503–6513.

75. Kawahara, K, Suenobu, M, Yoshida, A, Koga, K, Hyodo, A, Ohtsuka, H, Kuniyasu, A, Tamamaki, N, Sugimoto, Y & Nakayama, H (2012) Intracerebral microinjection of interleukin-4/interleukin-13 reduces β-amyloid accumulation in the ipsilateral side and improves cognitive deficits in young amyloid precursor protein 23 mice. *Neuroscience* 207: 243–260.

76. Yuan, P, Condello, C, Keene, CD, Wang, Y, Bird, TD, Paul, SM, Luo, W, Colonna, M, Baddeley, D & Grutzendler, J (2016) TREM2 haplodeficiency in mice and humans impairs the microglia barrier function leading to decreased amyloid compaction and severe axonal dystrophy. *Neuron* 90: 724–739.

77. Slattery, CF, Beck, JA, Harper, L, Adamson, G, Abdi, Z, Uphill, J, Campbell, T, Druyeh, R, Mahoney, CJ, Rohrer, JD & Kenny J (2014) *R47H TREM2* variant increases risk of typical early-onset Alzheimer's disease but not of prion or frontotemporal dementia. *Alzheimer's Dement* 10: 602–608.e4.

78. Engelman, CD, Darst, BF, Bilgel, M, Vasiljevic, E, Koscik, RL, Jedynak, BM & Johnson, SC (2018) The effect of rare variants in *TREM2* and *PLD3* on longitudinal cognitive function in the Wisconsin Registry for Alzheimer's Prevention. *Neurobiol Aging* 66: 177.e1–e5.

79. Berner, DK, Wessolowski, L, Armbrust, F, Schneppenheim, J, Schlepckow, K &

Koudelka, T (2020) Meprin β cleaves TREM2 and controls its phagocytic activity on macrophages. *FASEB J* 34: 6675–6687.

80. Song, WM, Joshita, S, Zhou, Y, Ulland, TK, Gilfillan, S & Colonna, M (2018) Humanized TREM2 mice reveal microglia-intrinsic and -extrinsic effects of R47H polymorphism. *J Exp Med* 215: 745–760.

81. Wunderlich, P, Glebov, K, Kemmerling, N, Tien, NT, Neumann, H & Walter, J (2013) Sequential proteolytic processing of the triggering receptor expressed on myeloid cells-2 (TREM2) protein by ectodomain shedding and γ-secretase-dependent intramembranous cleavage. *J Biol Chem* 288: 33027–33036.

82. Glebov, K, Wunderlich, P, Karaca, I & Walter, J (2016) Functional involvement of γ-secretase in signaling of the triggering receptor expressed on myeloid cells-2 (TREM2). *J Neuroinflammation* 13: 17. doi: 10.1186/s12974-016-0479-9

83. Perez, SE, Nadeem, M, Malek-Ahmadi, MH, He, B & Mufson, EJ (2017) Frontal cortex and hippocampal γ-secretase activating protein levels in prodromal Alzheimer disease. *Neurodegener Dis* 17: 235–241.

84. Jiang, T, Wan, Y, Zhang, YD, Zhou, JS, Gao, Q, Zhu, XC, Shi, JQ, Lu, H, Tan, L & Yu, JT (2017) TREM2 Overexpression has no improvement on neuropathology and cognitive impairment in aging APPswe/PS1dE9 mice. *Mol Neurobiol* 54: 855–865.

85. Bekris, LM, Khrestian, M, Dyne, E, Shao, Y, Pillai, JA, Rao, SM, Bemiller, SM, Lamb, B, Fernandez, HH & Leverenz, JB (2018) Soluble TREM2 and biomarkers of central and peripheral inflammation in neurodegenerative disease.

J Neuroimmunol 319: 19–27.

86. Shackleton, B, Crawford, F & Bachmeier, C (2017) Apolipoprotein E-mediated modulation of ADAM10 in Alzheimer's disease. *Curr Alzheimer Res* 14: 578–585.

87. Reinhardt, S, Schuck, F, Grösgen, S, Riemenschneider, M, Hartmann, T, Postina, R, Grimm, M & Endres, K (2014) Unfolded protein response signaling by transcription factor XBP-1 regulates ADAM10 and is affected in Alzheimer's disease. *FASEB J* 28: 978–997.

88. Sogorb-Esteve, A, García-Ayllón, MS, Gobom, J, Alom, J, Zetterberg, H, Blennow, K & Sáez-Valero, J (2018) Levels of ADAM10 are reduced in Alzheimer's disease CSF. *J Neuroinflammation* 15: 213. doi: 10.1186/s12974-018-1255-9

89. Morimoto, K, Horio, J, Satoh, H, Sue, L, Beach, T, Arita, S, Tooyama, I & Konishi, Y (2011) Expression profiles of cytokines in the brains of Alzheimer's disease (AD) patients compared to the brains of non-demented patients with and without increasing AD pathology. *J Alzheimer's Dis* 25: 59–76.

90. Li, C, Zhao, B, Lin, C, Gong, Z & An, X (2019) TREM2 inhibits inflammatory responses in mouse microglia by suppressing the PI3K/NF-κB signaling. *Cell Biol Int* 43: 360–372.

91. Nanba, D & Higashiyama, S (2004) Dual intracellular signaling by proteolytic cleavage of membrane-anchored heparin-binding EGF-like growth factor. *Cytokine Growth Factor Rev* 15: 13–19.

92. Martín, R, Cordova, C & Nieto, ML (2012) Secreted phospholipase A_2-IIA-induced a phenotype of activated microglia in BV-2 cells requires epidermal growth factor receptor transactivation and proHB-EGF shedding. *J Neuroinflammation* 9: 154. doi: 10.1186/1742-2094-9-154

93. Jun, GR, Chung, J, Mez, J, Barber, R, Beecham, GW, Bennett, DA, Buxbaum, JD, Byrd, GS, Carrasquillo, MM, Crane, PK & Cruchaga, C (2017) Transethnic genome-wide scan identifies novel Alzheimer's disease loci. *Alzheimer's Dement* 13: 727–738.

94. Maurya, SK, Mishra, J, Abbas, S & Bandyopadhyay, S (2016) Cypermethrin stimulates GSK3β-dependent Aβ and p-tau proteins and cognitive loss in young rats: reduced HB-EGF signaling and downstream neuroinflammation as critical regulators. *Mol Neurobiol* 53: 968–982.

95. Sasaki, K, Omotuyi, OI, Ueda, M, Shinohara, K & Ueda, H (2015) NMDA receptor agonists reverse impaired psychomotor and cognitive functions associated with hippocampal *Hbegf*-deficiency in mice. *Mol Brain* 8: 83. doi: 10.1186/s13041-015-0176-0

96. Lalaoui, N & Vaux, DL (2018) Recent advances in understanding inhibitor of apoptosis proteins. *F1000Res* 7: F1000 Faculty Rev-1889. doi: 10.12688/f1000research.16439.1

97. Kavanagh, E, Rodhe, J, Burguillos, MA, Venero, JL & Joseph, B (2014) Regulation of caspase-3 processing by cIAP2 controls the switch between pro-inflammatory activation and cell death in microglia. *Cell Death Dis* 5: e1565.

doi: 10.1038/cddis.2014.514

98. Twayana, KS, Chaudhari, N & Ravanan, P (2019) Prolonged lipopolysaccharide exposure induces transient immunosuppression in BV2 microglia. *J Cell Physiol* 234: 1889–1903.

99. Matsuda, S, Rouault, J, Magaud, J & Berthet, C (2001) In search of a function for the TIS21/PC3/BTG1/TOB family. *FEBS Lett* 497: 67–72.

100. Lee, H, Cha, S, Lee, MS, Cho, GJ, Choi, WS & Suk, K (2003) Role of antiproliferative B cell translocation gene-1 as an apoptotic sensitizer in activation-induced cell death of brain microglia. *J Immunol* 171: 5802–5811.

101. Martínez-Barriocanal, A & Sayós, J (2006) Molecular and functional characterization of CD300b, a new activating immunoglobulin receptor able to transduce signals through two different pathways. *J Immunol* 177: 2819–2830.

102. Murakami, Y, Tian, L, Voss, OH, Margulies, DH, Krzewski, K & Coligan, JE (2014) CD300b regulates the phagocytosis of apoptotic cells via phosphatidylserine recognition. *Cell Death Differ* 21: 1746–1757.

103. Gebicke-Haerter, PJ, Appel, K, Taylor, GD, Schobert, A, Rich, IN, Northoff, H & Berger, M (1994) Rat microglial interleukin-3. *J Neuroimmunol* 50: 203–214.

104. Bright, JJ, Natarajan, C, Sriram, S & Muthian, G (2004) Signaling through JAK2-STAT5 pathway is essential for IL-3-induced activation of microglia. *Glia* 45: 188–196.

105. Andrae, J, Gallini, R & Betsholtz, C (2008) Role of platelet-derived growth factors in physiology and medicine. *Genes Dev* 22: 1276–1312.

106. Saito, Y, Yamaguchi, A, Nakamura, S, Okuyoshi, H, Shimazawa, M & Hara, H (2020) Contribution of platelet-derived growth factor signaling to retina regeneration in zebrafish. *Neurosci Lett* 727: 134930. doi: 10.1016/j.neulet.2020.134930

107. Hu, N, Tan, MS, Yu, JT, Sun, L, Tan, L, Wang, YL, Jiang, T & Tan L (2014) Increased expression of TREM2 in peripheral blood of Alzheimer's disease patients. *J Alzheimer's Dis* 38: 497–501.

108. Kusdra, L, Rempel, H, Yaffe, K & Pulliam, L (2000) Elevation of $CD69^{+}$ monocyte/macrophages in patients with Alzheimer's disease. *Immunobiology* 202: 26–33.

109. Thome, AD, Faridar, A, Beers, DR, Thonhoff, JR, Zhao, W, Wen, S, Pascual, B, Masdeu, JC & Appel SH (2018) Functional alterations of myeloid cells during the course of Alzheimer's disease. *Mol Neurodegener* 13: 61. doi: 10.1186/s13024-018-0293-1

110. Guerreiro, RJ, Santana, I, Brás, JM, Santiago, B, Paiva, A & Oliveira, C (2007) Peripheral inflammatory cytokines as biomarkers in Alzheimer's disease and mild cognitive impairment. *Neurodegener Dis* 4: 406–412.

111. Shevyrev, D, & Tereshchenko, V (2020) Treg Heterogeneity, Function, and Homeostasis. *Frontiers in immunology*, 10, 3100.

112. Sharabi, A, Tsokos, MG, Ding, Y, Malek, TR, Klatzmann, D, & Tsokos, GC. (2018) Regulatory T cells in the treatment of disease. *Nature reviews. Drug discovery*, 17(11), 823–844.

113. Kim, JH, Kim, BS, & Lee, SK (2020) Regulatory T Cells in Tumor Microenvironment and Approach for Anticancer Immunotherapy. *Immune network*, 20(1), e4.

114. Kumar, P, Bhattacharya, P, & Prabhakar, BS (2018) A comprehensive review on the role of co-signaling receptors and Treg homeostasis in autoimmunity and tumor immunity. *Journal of autoimmunity*, 95, 77–99.

115. Medler, J, & Wajant, H (2019) Tumor necrosis factor receptor-2 (TNFR2): an overview of an emerging drug target. *Expert opinion on therapeutic targets*, 23(4), 295–307.

116. Okubo, Y, Mera, T, Wang, L, & Faustman, DL (2013) Homogeneous expansion of human T-regulatory cells via tumor necrosis factor receptor 2. *Scientific reports*, 3, 3153.

117. Chopra, M, Biehl, M, Steinfatt, T, Brandl, A, Kums, J, Amich, J, Vaeth, M, Kuen, J, Holtappels, R, Podlech, J, Mottok, A, Kraus, S, Jordán-Garrote, AL, Bäuerlein, CA, Brede, C, Ribechini, E, Fick, A, Seher, A, Polz, J, Ottmüller, KJ, Beilhack, A (2016) Exogenous TNFR2 activation protects from acute GvHD via host T reg cell expansion. *The Journal of experimental medicine*, 213(9), 1881–1900.

118. Fischer, R, Marsal, J, Guttà, C, Eisler, SA, Peters, N, Bethea, JR, Pfizenmaier, K, & Kontermann, RE (2017) Novel strategies to mimic transmembrane tumor necrosis factor-dependent activation of tumor necrosis factor receptor 2. *Scientific reports*, 7(1), 6607.

119. Lamontain, V, Schmid, T, Weber-Steffens, D, Zeller, D, Jenei-Lanzl, Z, Wajant, H, Straub, RH, & Männel, DN (2019) Stimulation of TNF receptor type 2 expands regulatory T cells and ameliorates established collagen-induced arthritis in mice. *Cellular & molecular immunology*, 16(1), 65–74.

120. Case, K, Tran, L, Yang, M, Zheng, H, Kuhtreiber, WM, & Faustman, DL (2020) TNFR2 blockade alone or in combination with PD-1 blockade shows therapeutic efficacy in murine cancer models. *Journal of leukocyte biology*, 107(6), 981–991.

121. He, T, Liu, S, Chen, S, Ye, J, Wu, X, Bian, Z, & Chen, X (2018) The p38 MAPK Inhibitor SB203580 Abrogates Tumor Necrosis Factor-Induced Proliferative Expansion of Mouse $CD4^{+}Foxp3^{+}$ Regulatory T Cells. *Frontiers in immunology*, 9, 1556.

122. Urbano, PCM, Koenen, HJPM, Joosten, I, & He, X (2018) An Autocrine TNFα-Tumor Necrosis Factor Receptor 2 Loop Promotes Epigenetic Effects Inducing Human Treg Stability *In Vitro*. *Frontiers in immunology*, 9, 573.

123. Torrey, H, Kühtreiber, WM, Okubo, Y, Tran, L, Case, K, Zheng, H, Vanamee, E, & Faustman, DL (2020) A novel TNFR2 agonist antibody expands highly potent regulatory T cells. *Science signaling*, 13(661), eaba9600.

124. Govindaraj, C, Scalzo-Inguanti, K, Madondo, M, Hallo, J, Flanagan, K, Quinn, M, & Plebanski, M (2013) Impaired Th1 immunity in ovarian cancer patients is mediated by TNFR2+ Tregs within the tumor microenvironment. *Clinical immunology (Orlando, Fla.)*, 149(1), 97–110.

125. Ye, LL, Peng, WB, Niu, YR, Xiang, X, Wei, XS, Wang, ZH, Wang, X, Zhang, SY, Chen, X, & Zhou, Q (2020) Accumulation of TNFR2-expressing regulatory

T cells in malignant pleural effusion of lung cancer patients is associated with poor prognosis. *Annals of translational medicine*, 8(24), 1647.

126. Chen, X, Subleski, JJ, Hamano, R, Howard, OM, Wiltrout, RH, & Oppenheim, JJ (2010) Co-expression of TNFR2 and CD25 identifies more of the functional CD4+FOXP3+ regulatory T cells in human peripheral blood. *European journal of immunology*, 40(4), 1099–1106.

127. Robinson, MD, McCarthy, DJ, & Smyth, GK (2010) edgeR: a Bioconductor package for differential expression analysis of digital gene expression data. *Bioinformatics (Oxford, England)*, 26(1), 139–140.

128. McCarthy, DJ, Chen, Y, & Smyth, GK (2012) Differential expression analysis of multifactor RNA-Seq experiments with respect to biological variation. *Nucleic acids research*, 40(10), 4288–4297.

129. Gu, Z, Eils, R, & Schlesner, M (2016) Complex heatmaps reveal patterns and correlations in multidimensional genomic data. *Bioinformatics (Oxford, England)*, 32(18), 2847–2849.

130. Butler, A, Hoffman, P, Smibert, P, Papalexi, E, & Satija, R (2018) Integrating single-cell transcriptomic data across different conditions, technologies, and species. *Nature biotechnology*, 36(5), 411–420.

131. McGinnis, CS, Murrow, LM, & Gartner, ZJ (2019) DoubletFinder: Doublet Detection in Single-Cell RNA Sequencing Data Using Artificial Nearest Neighbors. *Cell systems*, 8(4), 329–337.e4.

132. Neuwirth E (2014) RColorBrewer: ColorBrewer Palettes. *R package* version 1.1-2; https://CRANR-projectorg/package=RColorBrewer. (21 September 2021, date last accessed)

133. Zheng, C, Zheng, L, Yoo, JK, Guo, H, Zhang, Y, Guo, X, Kang, B, Hu, R, Huang, JY, Zhang, Q, Liu, Z. Dong, M, Hu, X, Ouyang, W, Peng, J, & Zhang, Z (2017) Landscape of Infiltrating T Cells in Liver Cancer Revealed by Single-Cell Sequencing. *Cell*, 169(7), 1342–1356.e16.

134. Guo, X, Zhang, Y, Zheng, L, Zheng, C, Song, J, Zhang, Q, Kang, B, Liu, Z, Jin, L, Xing, R, Gao, R, Zhang, L. Dong, M, Hu, X, Ren, X, Kirchhoff, D, Roider, HG, Yan, T, & Zhang, Z (2018) Global characterization of T cells in non-small-cell lung cancer by single-cell sequencing. *Nature medicine*, 24(7), 978–985.

135. Zhang, L, Yu, X, Zheng, L, Zhang, Y, Li, Y, Fang, Q, Gao, R, Kang, B, Zhang, Q, Huang, JY, Konno, H, Guo, X, Ye, Y, Gao, S, Wang, S, Hu, X, Ren, X, Shen, Z, Ouyang, W, & Zhang, Z (2018) Lineage tracking reveals dynamic relationships of T cells in colorectal cancer. *Nature*, 564(7735), 268–272.

136. Subramanian, A, Tamayo, P, Mootha, VK, Mukherjee, S, Ebert, BL, Gillette, MA, Paulovich, A, Pomeroy, SL, Golub, TR, Lander, ES, & Mesirov, JP (2005) Gene set enrichment analysis: a knowledge-based approach for interpreting genome-wide expression profiles. *Proceedings of the National Academy of Sciences of the United States of America*, 102(43), 15545–15550.

137. Liberzon, A, Subramanian, A, Pinchback, R, Thorvaldsdóttir, H, Tamayo, P, & Mesirov, JP (2011) Molecular signatures database (MSigDB) 3.0. *Bioinformatics (Oxford, England)*, 27(12), 1739–1740.

138. Liberzon, A, Birger, C, Thorvaldsdóttir, H, Ghandi, M, Mesirov, JP, & Tamayo, P (2015) The Molecular Signatures Database (MSigDB) hallmark gene set collection. *Cell systems*, 1(6), 417–425.

139. Bournazos, S, Gupta, A, & Ravetch, JV (2020) The role of IgG Fc receptors in antibody-dependent enhancement. *Nature reviews. Immunology*, 20(10), 633–643.

140. Cao X (2010) Regulatory T cells and immune tolerance to tumors. *Immunologic research*, 46(1-3), 79–93.

141. Lubrano di Ricco, M, Ronin, E, Collares, D, Divoux, J, Grégoire, S, Wajant, H, Gomes, T, Grinberg-Bleyer, Y, Baud, V, Marodon, G, & Salomon, BL (2020) Tumor necrosis factor receptor family costimulation increases regulatory T-cell activation and function via NF-κB. *European journal of immunology*, 50(7), 972–985.

142. Nagar, M, Jacob-Hirsch, J, Vernitsky, H, Berkun, Y, Ben-Horin, S, Amariglio, N, Bank, I, Kloog, Y, Rechavi, G, & Goldstein, I (2010) TNF activates a NF-kappaB-regulated cellular program in human CD45RA- regulatory T cells that modulates their suppressive function. *Journal of immunology (Baltimore, Md. : 1950)*, 184(7), 3570–3581.

143. Wang, J, Ferreira, R, Lu, W, Farrow, S, Downes, K, Jermutus, L, Minter, R, Al-Lamki, RS, Pober, JS, & Bradley, JR (2018) TNFR2 ligation in human T regulatory cells enhances IL2-induced cell proliferation through the non-canonical NF-κB pathway. *Scientific reports*, 8(1), 12079.

144. Sun SC (2011) Non-canonical NF-κB signaling pathway. *Cell research*, 21(1), 71–85.

145. Chen, X, Bäumel, M, Männel, DN, Howard, OM, & Oppenheim, JJ (2007) Interaction of TNF with TNF receptor type 2 promotes expansion and function of mouse CD4+CD25+ T regulatory cells. *Journal of immunology (Baltimore, Md. : 1950)*, 179(1), 154–161.

146. Zorn, E, Nelson, EA, Mohseni, M, Porcheray, F, Kim, H, Litsa, D, Bellucci, R, Raderschall, E, Canning, C, Soiffer, RJ, Frank, DA, & Ritz, J (2006) IL-2 regulates FOXP3 expression in human CD4+CD25+ regulatory T cells through a STAT-dependent mechanism and induces the expansion of these cells in vivo. *Blood*, 108(5), 1571–1579.

147. He, X, Landman, S, Bauland, SC, van den Dolder, J, Koenen, HJ, & Joosten, I (2016) A TNFR2-Agonist Facilitates High Purity Expansion of Human Low Purity Treg Cells. *PloS one*, 11(5), e0156311.

148. So, T, & Croft, M (2013) Regulation of PI-3-Kinase and Akt Signaling in T Lymphocytes and Other Cells by TNFR Family Molecules. *Frontiers in immunology*, 4, 139.

149. Wang, Z, Hong, J, Sun, W, Xu, G, Li, N, Chen, X, Liu, A, Xu, L, Sun, B, & Zhang, JZ (2006) Role of IFN-gamma in induction of Foxp3 and conversion of CD4+ CD25- T cells to CD4+ Tregs. *The Journal of clinical investigation*, 116(9), 2434–2441.

150. Rauch, I, Müller, M, & Decker, T (2013) The regulation of inflammation by interferons and their STATs. *JAK-STAT*, 2(1), e23820.

151. Metidji, A, Rieder, SA, Glass, DD, Cremer, I, Punkosdy, GA, & Shevach, EM (2015) IFN-α/β receptor signaling promotes regulatory T cell development and function under stress conditions. *Journal of immunology (Baltimore, Md. : 1950)*, 194(9), 4265–4276.

152. de Kivit, S, Mensink, M, Hoekstra, AT, Berlin, I, Derks, RJE, Both, D, Aslam, MA, Amsen, D, Berkers, CR, & Borst, J (2020) Stable human regulatory T cells switch to glycolysis following TNF receptor 2 costimulation. *Nature metabolism*, 2(10), 1046–1061.

153. Yan, F, Du, R, Wei, F, Zhao, H, Yu, J, Wang, C, Zhan, Z, Ding, T, Ren, X, Chen, X, & Li, H (2015) Expression of TNFR2 by regulatory T cells in peripheral blood is correlated with clinical pathology of lung cancer patients. *Cancer immunology, immunotherapy : CII*, 64(11), 1475–1485.

154. Li, X, Wang, S, Ren, H, Ma, J, Sun, X, Li, N, Liu, C, Huang, K, Xu, M, & Ming, L (2016) Molecular correlates and prognostic value of tmTNF-α expression in colorectal cancer of 5-Fluorouracil-Based Adjuvant Therapy. *Cancer biology & therapy*, 17(6), 684–692.

155. Hamano, R, Huang, J, Yoshimura, T, Oppenheim, JJ, & Chen, X (2011) TNF optimally activatives regulatory T cells by inducing TNF receptor superfamily members TNFR2, 4-1BB and OX40. *European journal of immunology*, 41(7), 2010–2020.

156. Urbano, PCM, Koenen, HJPM, Joosten, I, & He, X (2018) An Autocrine TNFα-Tumor Necrosis Factor Receptor 2 Loop Promotes Epigenetic Effects Inducing Human Treg Stability *In Vitro*. *Frontiers in immunology*, 9, 573.

157. DuPage, M, Chopra, G, Quiros, J, Rosenthal, WL, Morar, MM, Holohan, D, Zhang, R, Turka, L, Marson, A, & Bluestone, JA (2015) The chromatin-modifying enzyme Ezh2 is critical for the maintenance of regulatory T cell identity after activation. *Immunity*, 42(2), 227–238.

158. Deng, B, Zhang, W, Zhu, Y, Li, Y, Li, D, & Li, B (2022) FOXP3^{+} regulatory T cells and age-related diseases. *The FEBS journal*, 289(2), 319–335.

159. Osman, A, Yan, B, Li, Y, Pavelko, KD, Quandt, J, Saadalla, A, Singh, MP, Kazemian, M, Gounari, F, & Khazaie, K (2021) TCF-1 controls T_{reg} cell functions that regulate inflammation, CD8^{+} T cell cytotoxicity and severity of colon cancer. *Nature immunology*, 22(9), 1152–1162.

160. Davis, MM, Tato, CM, & Furman, D (2017) Systems immunology: just getting started. *Nature immunology*, 18(7), 725–732.